Progress in Materials Science 65 (2014) 1–66

Contents lists available at ScienceDirect

Progress in Materials Science

journal homepage: www.elsevier.com/locate/pmatsci

A review of numerical analysis of friction stir welding

Xiaocong He [a,*], Fengshou Gu [b], Andrew Ball [b]

[a] Innovative Manufacturing Research Centre, Kunming University of Science and Technology, Kunming 650500, PR China
[b] Centre for Efficiency and Performance Engineering, University of Huddersfield, Queensgate, Huddersfield HD1 3DH, UK

ARTICLE INFO

Article history:
Received 2 September 2013
Received in revised form 29 November 2013
Accepted 6 March 2014
Available online 21 March 2014

Keywords:
Friction stir welding
Numerical analysis
Microstructure
Mechanical behavior

ABSTRACT

Friction stir welding is a relatively new solid-state joining technique which is widely adopted in different industry fields to join different metallic alloys that are hard to weld by conventional fusion welding. Friction stir welding is a highly complex process comprising several highly coupled physical phenomena. The complex geometry of some kinds of joints and their three dimensional nature make it difficult to develop an overall system of governing equations for theoretical analyzing the behavior of the friction stir welded joints. The experiments are often time consuming and costly. To overcome these problems, numerical analysis has frequently been used since the 2000s. This paper reviews the latest developments in the numerical analysis of friction stir welding processes, microstructures of friction stir welded joints and the properties of friction stir welded structures. Some important numerical issues such as materials flow modeling, meshing procedure and failure criteria are discussed. Numerical analysis of friction stir welding will allow many different welding processes to be simulated in order to understand the effects of changes in different system parameters before physical testing, which would be time-consuming or prohibitively expensive in practice. The main methods used in numerical analysis of friction stir welding are discussed and illustrated with brief case studies. In addition, several important key problems and issues remain to be addressed about the numerical analysis of friction stir welding and opportunities for further research are identified.

* Corresponding author. Tel.: +86 871 65930928; fax: +86 871 65194243.
E-mail address: hhxxcc@yahoo.co.uk (X. He).

http://dx.doi.org/10.1016/j.pmatsci.2014.03.003
0079-6425/

Contents

1. Introduction

There is an increasing need to design lightweight structures such as those in aircraft panels and vehicle body shells. Advanced joining technology is an integral part of the manufacturing processes of lightweight structures. Considerable effort has been expended to develop various joining processes and assess their suitability for use in lightweight structures [1–5].

Friction stir welding (FSW) is a solid-state joining technique which was invented at The Welding Institute (TWI), UK, in 1991 [6]. The FSW has been found to be effective for joining hard-to-weld metals and for joining plates with different thickness or different materials.

In the FSW process a non-consumable rotating tool with a specially designed pin and shoulder is inserted into the abutting edges of workpieces to be joined and traversed along the line of the joint, as shown in Fig. 1 [7]. As the tool travels, heat is created by the contact friction between the shoulder and the workpiece, and by the plastic deformation of the materials in the stir zone. The high strain and heat energies experienced by the base metal during stirring causes dynamic recrystallization, which is the formation of new grains in the weld zone [6]. Although Fig. 1 shows a butt joint for illustration, other types of joints, as shown in Fig. 2, also can be fabricated by FSW [8].

FSW is often a preferred joining technique not only for aluminum alloys [e.g. 9,10] but also for other difficult-to-weld metals such as magnesium alloys [e.g. 11,12], titanium alloys [e.g. 13,14] and metal-matrix composites [e.g. 15,16], etc. The technique is now widely used in many industrial sectors such as marine, aerospace, railway, land transportation, etc. Some general information on the FSW is available from TWI [17].

FSW is a highly complex process comprising several highly coupled (and non-linear) physical phenomena. These phenomena include large plastic deformation, material flow, mechanical stirring, surface interaction between the tool and the workpiece, dynamic structural evolution and heat

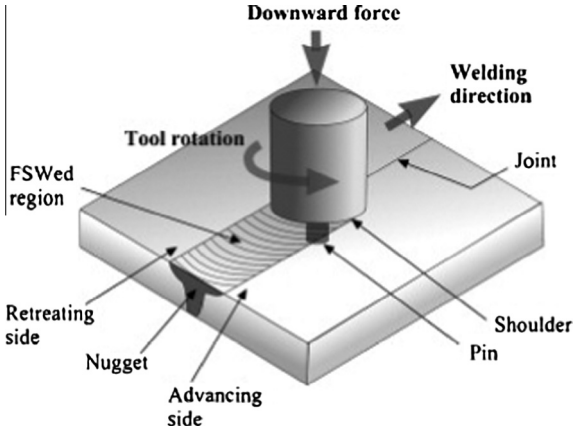

Fig. 1. Schematic drawing of FSW process [7].

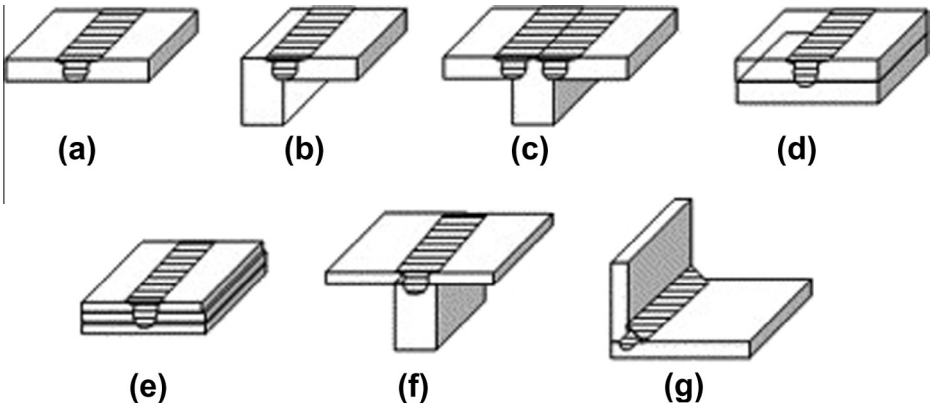

Fig. 2. Joint configurations for FSW: (a) square butt, (b) edge butt, (c) T butt joint, (d) lap joint, (e) multiple lap joint, (f) T lap joint and (g) fillet joint [8].

generation resulting from friction and plastic deformation. Multiple parameters greatly influence the quality of the FSW joints. Consequently, FSW has been the subject of a considerable amount of experimental and numerical study. Mishra and Ma [8] comprehensively reviewed both the FSW and friction stir processes. Nandan et al. [18] give a very comprehensive review on the process, structure and properties of FSW. Threadgill et al. [19] provided an exhaustive overview of the FSW of aluminum alloys and Çam [20] reviewed extensively FSW of other alloys.

The behavior of the FSW joints is not only influenced by the geometry of the tools and the joints but also by different process parameters. The complex geometry of some kinds of joints and their three dimensional nature make it difficult to develop an overall system of governing equations for predicting the behavior of the FSW joints. In addition, material non-linearity due to plastic behavior is difficult to incorporate because the analysis becomes very complex in the mathematical formulation. The experiments are often time consuming and costly. To overcome these problems, numerical analysis has frequently been used since the 2000s.

Some exciting developments in the numerical study of FSW have been accompanied by scientific research such as that at the University of South Carolina (United States) [e.g. 21-25], the University of Palermo (Italy) [e.g. 26-30], the Dalian University of Technology (China) [e.g. 31-35], and the Sharif

University of Technology (Iran) [e.g. 36-40], etc. Numerical analysis has found widespread applications in FSW. Significant progress has been made in the fundamental understanding of both the FSW process and the properties of the resulting welded joints. However, no comprehensive review on numerical analysis of FSW has been reported so far.

Recent progress in numerical analysis of FSW is reviewed in this paper, including the welding processes and the microstructure and properties of the resulting joints. Important issues such as material flow modeling, meshing procedure and failure criteria are discussed. Numerical simulation of FSW enables many different welding processes to be simulated in order to select different system parameters. Without this, physical testing would be time-consuming or prohibitively expensive. The main methods used in numerical investigation of FSW are discussed and illustrated with brief case studies.

2. FSW process

The properties and performance of the FSW joints are dictated by the microstructure, which in turn is determined by the FSW process. The FSW process can normally be varied by changing the welding parameters. Therefore welding parameters must be selected that give the best possible microstructure. Furthermore an accurate knowledge of the FSW process is a prerequisite for reliable prediction of the weld dimensions, final microstructure and mechanical properties of the FSW joints. Due to the complexity of the FSW process, it is very difficult to gain insight into the joint during the actual forming process. Numerical simulation helps overcome this problem by providing an effective way of analyzing the formation of FSW joints [41].

2.1. Process modeling techniques

Simulating the FSW process is a complex problem which involves physical couplings between mechanics and heat transfer, very large deformations and strain rates in the stirring zone around the pin. Numerical simulation of the FSW processes enables estimation of different process parameters such as tool geometry and speeds etc. Simulation is not an easy task, however, since it involves the interaction of thermal and mechanical phenomena. Some established numerical modeling techniques have been developed that can explain and predict important features of the process physics involved in the FSW [e.g. 42,43]. The FSW models cover a broad range of complexity, from the simple conduction heat transfer models [e.g. 44,45], to the metal flow models [e.g. 46-49], to the fully coupled models [e.g. 50-52] in which the viscoplastic flow and the heat transfer are modeled for predicting temperature and residual stress distributions.

Several simplified numerical models were designed to elucidate various aspects of the complex thermomechanical phenomena associated with FSW. Scaling methods provided a balance of simplicity and accuracy. Scaling methods are based on the proper identification of the dominant parameters and their correct numerical description. The following phenomena were investigated in separate numerical models: (i) coupled friction heat generation; (ii) plastic flow slip zone development: and (iii) 3D heat and material flow. A simplified 3D heat and material flow model, based on the observations from the coupled friction heat generation model, was used to establish some initial insight regarding the heat and material flow [53]. The results, from the three subproblem areas were then generalized in the form of a simple parametric relationship between welding variables (i.e. travel and rotating speeds) and weld formation conditions. The findings from the study not only illuminate some of the important weld formation mechanisms in FSW, but also provide an effective framework for more focused investigations into some of the fundamental phenomena identified in the three subproblem areas. Clegrove and Shercliff [54–56] used scaling methods to propose timescales and developed a scaling law for heat input.

The FSW processes involve multiple coupled physical phenomena, the determination of the dominant phenomena from the governing equations can involve up to several thousand iterations. Scaling laws based on the governing equations of transport phenomena provide closed form mathematical expressions that capture the essence of a welding process explicitly. Despite the simplicity of the scaling models, they are capable of capturing correct trends and the order of magnitude of the unknown

estimations in a problem. Moreover, they are capable of determining the dominant forces that act on the process studied. The range of validity of the scaling laws can be established based on a rigorous description of the limits of the asymptotic regimes. The scaling analysis can be applied into multiphysics and multicoupled problems related to FSW processes. A set of scaling laws for the coupled thermomechanical problem of FSW was introduced and compared with published data [57–59]. The maximum temperature was estimated using scaling analysis and compared with experimental and numerical results reported in the literature. A coupled phenomenological model of heat transfer and plastic flow around the pin in FSW was presented [60]. The approach is analogous to the boundary layer analysis in fluid mechanics, and is based on the methodology of scaling. The results are a set of novel closed-form expressions for the maximum temperature reached in the process, the thickness of the shear layer, the shear stress around the pin, the torque and the thermal effect of the shoulder. The ultimate purpose of this model is to provide simple and accurate expressions useful for providing a temperature and strain rate context for the metallurgical analysis of FSW and for the selection of process parameters when using FSW to join novel alloys.

The scaling expressions for the peak temperature in FSW can also be obtained by dimensional analysis. A dimensionless correlation has been developed based on Buckingham's pi-theorem [61]. The relationship can also be used for the selection of welding conditions to prevent melting of the workpiece during FSW. The correlation includes thermal properties of the material and the tool, the area of the tool shoulder and the rotational and translation speeds of the tool. The peak temperatures reported in the literature during FSW of various materials and welding conditions were found to be in fair agreement with the proposed correlation. Reynolds et al. [62] proposed weld pitch (a scaling law based on basic process parameters) as a single expression capturing most of the physics of FSW. An asymptotic analysis was performed to obtain power laws characterizing the flow around the tool [63].

Understanding the physical phenomena and predicting what will happen at the tool/workpiece interface during high shear processing can be achieved in different ways. The concept of combining the latest FE and discrete element (DE) multiscale numerical technologies for modeling the tool/workpiece interface during high shear processing was described [64,65]. Linking of the modeling scales is based on transferring the corresponding boundary conditions from the macro model to the representative cell, considered as the meso-level model. The transfer processes were described by the system of diffusion and motion equations including contact detection and interaction solutions for particles integrated over time. Modeling of the tool/workpiece interface included both the mixing of the oxide particles into the subsurface layer during hot rolling of aluminum and heat generation during FSW. The effect of the mass scaling factor on the temperature field during the plunge stage in FSW was studied [66]. The optimization of 3D explicit FE analysis of FSW was obtained. The mass scaling factor has a significant influence on the computation time and the displacement of the tool. A reasonable temperature field can be obtained with less computation time when the mass scaling factor is 10^6. Avettand-Fènoël et al.'s study [67] presented three kinds of FSW beads between pure copper and 6082 aluminum alloys. Their structure was characterized at a multi-scale level by using a number of techniques. The tool placement was shown to govern the microstructure and the ensuing mechanical behavior of the weld.

The investigation of the plunge stage of the tool during FSW enables an understanding of the nature of FSW, which is especially important for friction stir spot welding (FSSW). A basic platform in the form of a physical-based, coupled, thermo-mechanical model was developed and used to investigate thermo-mechanical behavior during the FSSW of AA6082-T6 [68]. To cope with high calculation time and distortion of the mesh, built-in features of the code, mass scaling, ALE (Arbitrary Lagrangian Eulerian) and mesh re-mapping were used. With the help of this model, the effects of process parameters on the temperature-displacement behavior of the workpiece were studied. The role of interacting conditions at the tool-workpiece interface was emphasized and a simplified conceptual mechanism for the effects of process variables on the physical phenomena was presented. An advanced FE model can encapsulate complex FSW behavior and present various detailed aspects associated with the FE model such as contact modeling, material model and meshing techniques [69]. The numerical model is continuum solid mechanics-based, fully thermo-mechanically coupled and has successfully simulated the FSW process including plunging, dwelling and welding stages. Several field variables

are quantified by the model including temperature, stress and strain. The equivalent load method based on the inherent strain approach was suggested as an efficient welding deformation and residual stress analysis method for large scale FSW structures of aluminum alloy Al6061-T6 sheet metal [70]. The results show fairly good agreements with those of existing FE analysis as well as the FSW experiments.

The information that can be obtained from a well-tested analysis model of FSW includes: materials flow, peak temperatures, torque, and weld properties. The torque, power requirement and stir zone geometry during FSW of AA2524 aluminum alloy were modeled by Arora et al. [71] by solving the equations of conservation of mass, momentum and energy. The model predictions agreed well with the corresponding measured values for a wide range of welding speeds and tool rotational speeds when the heat transfer coefficient and the friction coefficient values were adjusted. In a later work, an approximate analytical technique for calculating the 3D material flow during FSW was proposed. This involved considering the motion of an incompressible fluid induced by a solid rotating disk [72]. For the estimation of peak temperatures, the accuracy of an existing dimensionless correlation was improved using a large volume of recently published data. It was shown that the torque can be calculated analytically from the yield stress using estimated peak temperatures.

In the FE technology based on a three-field mixed formulation, the use of an independent nodal variable for the pressure field allows for an ad hoc treatment of the incompressibility constraint. This is a mandatory requirement due to the isochoric nature of the plastic strain in metal forming processes. The highly non-linear stress field typically encountered in the FSW process was used as an example to show the performance of this new FE technology [73]. The numerical simulation of the FSW process was tackled by means of an Arbitrary–Lagrangian–Eulerian (ALE) formulation. A fully coupled thermo-mechanical analysis was introduced showing the heat fluxes generated by the plastic dissipation in the stir-zone (Sheppard rigid-viscoplastic constitutive model) as well as the frictional heat dissipation at the contact interface (Norton frictional contact model). Tracers were used to show the material flow around the pin allowing a better understanding of the welding mechanism.

In Uyyuru and Kallas's article [74], the available literature on modeling of FSW was reviewed, followed by details of an attempt to understand the interaction between process parameters from a simulation study. The distributions of temperature, residual stress, strain, and strain rates were analyzed across various regions of the weld apart from material flow as a means of evaluating process efficiency and the quality of the weld. The distribution of process parameters is important in predicting the occurrence of welding defects, and locating areas of concern for the metallurgist. It was found that the lack of detailed material constitutive information and other thermal and physical properties in conditions such as very high strain rates and elevated temperatures seems to be the limiting factor while modeling the FSW process. A simple but robust moving mesh technique based on Eulerian formalism was proposed recently for the numerical modeling of the FSW process [75]. The mesh is composed of 2 parts: the first one called Ω_1 which is fixed around the stirring zone and the second one called Ω_2 which includes the base material in contact with the tool, as shown in Fig. 3(a). The second part Ω_2 is circular with a radius $R_{\Omega 2}$ and moves with a rotational solid motion corresponding to the tool's velocity. The usefulness of this approach is that it involves no distortion of the mesh and the Eulerian formalism leads to satisfactory computation times. To ensure the consistency of the discretization, the mesh of the boundary common to Ω_1 and Ω_2 is the same and it is periodic as shown in Fig. 3(b). Fig. 3(c) shows the temperature distributions through the thickness of the sheets and Fig. 3(d) shows the velocity distributions around the pin. The example clearly evidences the efficiency and robustness of the moving mesh technique proposed for a 3D complex geometry of the tool.

A sliding mesh, rotating together with the pin (ALE formulation), can be used to avoid the extremely large distortions of the mesh around the tool in the so called stirring zone while the rest of the mesh of the sheet was fixed (Eulerian formulation) [76]. The orthogonal subgrid scale (OSS) technique was used to stabilize the mixed velocity–pressure formulation adopted to solve the Stokes problem. This stabilized formulation can deal with the incompressible behavior of the material allowing for equal linear interpolation for both the velocity and the pressure fields. The material behavior was characterized either by Norton-Hoff or Sheppard-Wright rigid thermo-visco-plastic constitutive models. Heat convection and heat radiation models were used to dissipate the heat through the boundaries. Both the streamline-upwind/Petrov–Galerkin (SUPG) formulation and the OSS stabilization

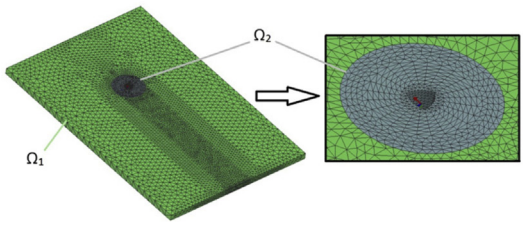

(a) Partition of the mesh

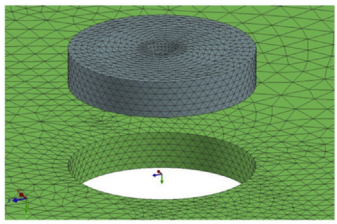

(b) Example of mesh between Ω_1 and Ω_2

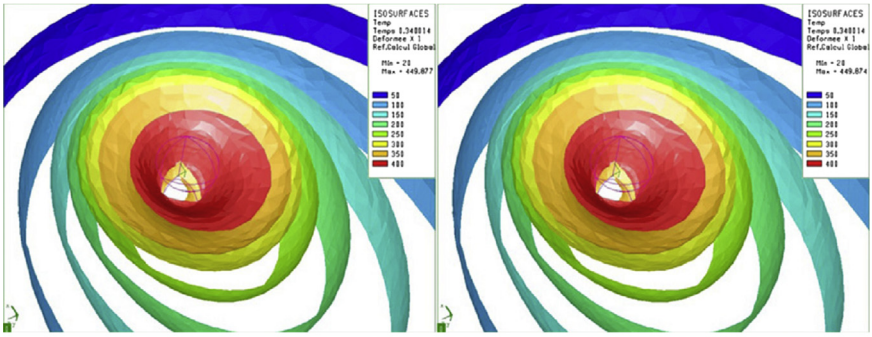

(c) Temperature distributions (^{o}C) for $R_{\Omega 2}$=12mm (left) and $R_{\Omega 2}$=15mm (right)

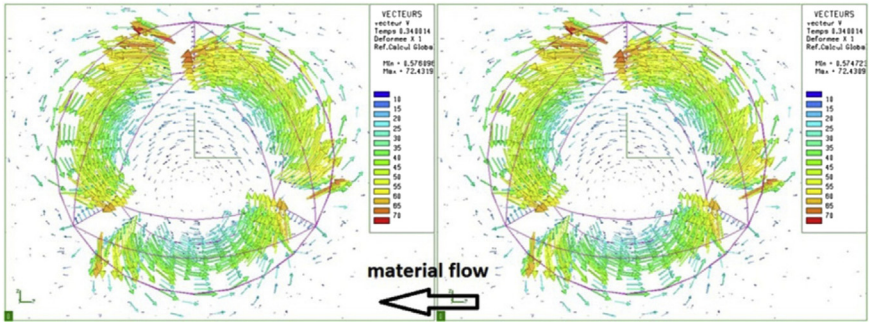

(d) Velocity distributions around the pin (ms^{-1}) for $R_{\Omega 2}$=12mm (left) and $R_{\Omega 2}$=15mm (right)

Fig. 3. Moving mesh technique for the FE simulation of FSW [75].

technique were implemented to stabilize the convective term in the energy balance equation. The numerical simulations presented are intended to show the accuracy of the proposed methodology and its capability to aid the study of real FSW processes where a non-circular pin is often used. The local adaptive mesh method was used for simulating the FSW process [77]. Based on the numerical result, the distribution of temperature, strain, stress and metal flow state of the specimen were obtained and the defects were forecast for the FSW process. The results showed that the temperature distribution of the workpiece is asymmetrical; strain distribution is not uniform throughout the thickness of the specimen, and severe plastic deformation exists in the welding zone.

Some finite element (FE) models use adjustable parameters that control the heat loss to the backing bar, as well as the heat input to the weld. Wang et al. described a method for determining these parameters by using a hybrid artificial neural network (ANN) coupled thermal flow process model of the FSW process [78]. The method successfully determined temperature dependent boundary condition parameters for a series of FSW in 3·2 mm thick 7449 aluminum alloy. The success of the

technique depended on the method used to input thermal data into the ANN and the ANN topology. Using this technique to obtain the adjustable parameters of a model is more efficient than the conventional trial and error approach, especially where complex boundary conditions are implemented. Shojaeefard et al.'s paper [79] focused on the microstructural and mechanical properties of the FSW of AA7075-o to AA5083-o aluminum alloys. An ANN model was developed to simulate the correlation between the FSW parameters and mechanical properties. Performance of the ANN model was excellent and the model was employed to predict the ultimate tensile strength and hardness of butt joint of AA7075–AA5083 as functions of weld and rotational speeds. The multi-objective particle swarm optimization was used to obtain the pareto-optimal set. An apropos kinematic setting for different zones of the computational domain was introduced and an efficient coupling strategy was proposed for simulating the FSW process [80]. Heat generation via viscous dissipation as well as frictional heating was considered. The results of the simulation using the proposed model were compared with the experimental evidence. The effect of slip and stick condition on non-circular pin shapes was analyzed.

Unlike traditional grid-based methods, Lagrangian particle methods such as SPH can simulate the dynamics of interfaces, large material deformations, and the material's strain and temperature history without employing complex tracking schemes. A new smoothed particle hydrodynamics (SPH) model for FSW was proposed recently [81]. 3D simulations of FSW on AZ31 Mg alloy were performed. The temperature history and distribution, grain size, micro-hardness as well as the evolution of texture were presented. Numerical results were found to be in good agreement with experimental observations. FSW of stainless steel was modeled using a steady-state, Eulerian formula that considers coupled viscoplastic flow and heat transfer in three dimensions [82,83]. The model equations were solved using the FE method to determine the velocity field and temperature distribution, with a modified Petrov–Galerkin formula employed to stabilize the temperature distribution. Strain hardening is incorporated using a scalar state variable for the isotropic strength that evolves with deformation as material moves along streamlines of the flow field. The influence of pin threads on the friction between the tool and the workpiece was modeled by supplementing the tangential tractions along the pin interface with axial tractions that depend on the pitch of the threads. An axis-symmetric 2D FE model with an adaptive re-meshing algorithm was proposed [84]. By using the proposed model, temperature distribution, the joining shape of the transverse section including toe flash on the surface and hook on the joining interface, can be simulated. The simulated results agree well with those of the experiment. Furthermore, the effects of clamp position and stirring direction on material flow and joining shape were investigated.

The FE method was used to study the selection of the constitutive models, the frictional coefficients, the contact models and the physical parameters [85]. The shape of the shoulder can affect the material flow obviously and a total of about 54.3% energy can be transformed into heat in FSW. When the physical parameters are further considered to be functions of temperature, the predicted temperature is lower than the one in which the physical parameters are constant. When the strain-hardening effect is considered, the equivalent plastic strain is decreased and the corresponding energy dissipated by plastic deformation is decreased. The effect of the frictional coefficient in predicting the temperature field in FSW/FSP is small for minor changes in the frictional coefficient. The computational costs in the simulation of FSW are affected by the mesh sizes, wave speed and also by the mesh distortions. Thus mesh distortions should be minimized in the numerical modeling of FSW to reduce the computational costs. A friction model was proposed for simulation of the FSW process [86]. The main feature of this approach is that it accurately computes the contact and frictional surface between the plate and the tool. FSW trials were conducted on an Al 6061 aluminum plate with an unthreaded concave tool. Forces and tool temperatures were accurately recorded at steady welding state, for different welding speeds. A first study using Norton's friction model showed the great sensitivity of welding forces and tool temperatures to friction coefficients, the need to take into account the changes brought to the contact surface by slight friction variations, the possibility of getting very accurate calibrations on forces, and the impossibility of properly rendering the temperature profile of the tool. On the other hand, the use of Coulomb's friction model enables realistic temperature profiles to be obtained and therefore a friction coefficient that offers an excellent agreement with experiments.

In material forming or cutting, the contact zone between the tool and the working piece is often very difficult to analyze because of diverse local phenomena. In the special case of FSW, a specific

difficulty is the study of material mixing. The Discrete Element Method (DEM) was applied as a tool to understand/propose/confirm physical scenarios involved in the FSW process [87]. A simple micro-behavior law that takes into account thermal, mechanical and material aspects was proposed and a 2D simulation based on this law is presented. The results showed qualitatively good agreement with observations on real nuggets. One of the main advantages of the DEM approach is the simplicity of the local input law compared with laws proposed at the continuous media mechanics level. Nevertheless, numerical aspects must be improved in order to carry out 3D simulations with reasonable calculation times. An innovative methodology for the semi-analytical calculation of the total heat generated during the FSW process was proposed [88]. The methodology includes a simple and straightforward procedure for the determining the heat produced during the stirring of the material. It combines the advantages of the conventional moving heat approach with those of alternative modeling approaches, (i.e. computational fluid dynamics or arbitrary Lagrangian Eulerian), while, simultaneously overcoming some of their main limitations. Moreover, the predicted FSW heat energy was introduced in a global 3D FE thermal model, which predicts the spatial temperature history developing in the welded parts during the process. The proposed methodology can be easily modified and used in FSW applications involving variable welded plate geometry, FSW tool type, joint type and process parameters.

The post-welding stress state, the strain history and the material conditions of FSW joints are often strongly idealized when used in subsequent modeling analyses, typically by neglecting one or more of the features above. But, it is obvious that the conditions after welding do influence the weld performance. The objective of Hattel et al.'s studies [89,90] was to discuss some of the main conflicts that arise when taking both the post-welding material conditions and stress–strain state into account in a subsequent structural analysis. The numerical model of the FSW joint, employed a step-wise modeling approach to combine an in situ weld simulation with a post-welding failure analysis. Using the commercial software ANSYS, a thermo-mechanical model was employed to predict the thermally induced stresses and strains during welding, while an in-house FE code was used to study the plastic flow localization and failure in a subsequent structural analysis. The coupling between the two models was made by mapping the post-welding stress–strain conditions predicted in ANSYS to those produced by the in-house code, using re-meshing techniques. A multi-scale simulation methodology was presented for the study of texture and the development of residual strain in the deformation of FSW material and includes a coordinated experimental program for model initialization and verification [91]. Based on elastoviscoplastic polycrystal plasticity implemented in a FE framework, the simulation methodology involves detailed tracking of selected elements in a relatively coarse macroscopic model followed by highly resolved simulations of the selected elements at the microscopic level. The results were compared with neutron diffraction data obtained by subjecting FSW specimens to a program of in situ loadings and unloadings.

D'Urso et al.'s systematic investigation [92–94] deals with the FE model for the simulation of the FSW process whose results are correlated with the experimental observations carried out when joining AA6060-T6 aluminum alloy. The information obtained from the model helped in the understanding of the welding phenomena. The behaviors of aluminum alloys and stainless steel during FSW were overviewed using 2D Eulerian formulations coupling viscoplastic flow and heat transfer [95]. The plastic behaviors of the materials were complicated and the flow stresses depended on the deformation rate, the temperature and the deformation histories. Constitutive equations considering both strain hardening from the accumulation of crystal defects and softening from recovery or recrystallization were used to model the materials. Strength evolutions have a Voce-like saturation limit because of the severe plastic deformation during FSW process. The model equations for kinematics and temperature were solved using the standard FE method. The strength and temperature distribution vary with process conditions and constitutive equations. Stainless steel and AA6061 have different strengthening mechanisms. Modified constitutive equations were applied to reflect the microstructural features of each material. A modified FSSW process, with a spiral circular movement given to the tool after the sinking stage, was proposed [96]. In this research, a continuum-based numerical model for FSSW process was developed that is 2D Lagrangian implicit, coupled and rigid-viscoplastic. This model can be used to investigate the distribution of the main field variables, namely temperature, strain and strain rate, as well as the Zener–Hollomon parameter which, in turn, strongly affects the Continuous Dynamic Recrystallization (CDRX) process that takes place in the weld nugget.

The forming behavior of tailor welded blanks (TWBs) has been widely studied since its development. In the numerical simulation studies, the TWBs are modeled as blanks composed of two different materials, and often, the presence of the weld bead is neglected in its FE discretization. The influence of the weld bead shape on the formability of FSW TWBs has been analyzed [97]. Several FE meshes were constructed in order to represent different weld bead geometries and numerical simulations of the cylindrical cup drawing were performed. Strong influence of the weld bead shape on the formability of the TWBs was observed when the weld was in overmatch relatively to the base material, and little influence when the weld was in under-match condition. An integrated model was utilized to predict thermo-mechanical behavior during the FSW of an aluminum alloy [36]. A FE code, ABAQUS, was employed to solve the governing equations of heat conduction and plastic deformation, while a rigid-viscoplastic material behavior was utilized and the effects of different thermal and mechanical boundary conditions were considered in the simulation. A fully coupled thermo-mechanical 3D FE model was developed in ABAQUS/Explicit to analyze the primary conditions under which the cavity behind the tool was filled [98]. The model accounted for compressibility by including the elastic response of the aluminum matrix. The different thermo-mechanical states in the colder, stiffer far-field matrix and the hotter, softer near-field matrix resulted in contact at the tool/matrix interface, thus no void formation was observed. Alfaro et al.'s paper [99] addressed the problem of numerically simulating the FSW process. Due to the special characteristics of the FSW (e.g. the high speed of the rotating pin, very large deformations, etc.), FE methods encounter several difficulties. Meshless methods somewhat alleviate these problems, allowing for an updated Lagrangian framework in the simulation. In particular, the accuracy will not be affected by mesh distortion. Some examples were shown on the performance of the Meshless methods.

The Johnson–Cook material strength model is frequently used in FE analyses of various manufacturing processes involving plastic deformation of metallic materials. However, this model displays serious shortcomings when used in the engineering analyses of various hot-working processes. An attempt was made to combine the basic physical-metallurgical principles with the associated kinetics to properly modify the Johnson–Cook material model, so that the model can be used in the analyses of metal hot-working and joining processes [100]. The model was next used to help establish relationships between process parameters, material microstructure and properties in FSW joints of AA5083 alloy. In Buffa et al.'s paper [14] an ANN was properly trained and linked to an existing 3D FE model for the FSW of Ti–6Al–4V titanium alloy, with the aim of predicting both the micro-hardness values and the microstructure of the friction stir butt welding (FSBW) joints while varying the main process parameters. A good agreement was found between experimental values and calculated results.

In Chenot and Massoni's paper [101], some important numerical issues were discussed, including meshing, remeshing and adaptivity, parallel computing and coupling between work-piece and tools. Five example applications of FE models to new processes were presented: the FSW, hot stamping of quenchable steels, tube hydroforming, thixoforming and self-piercing riveting. It was concluded that many new forming processes can be designed and optimized much more effectively using the numerical simulation technology. An approach for modeling the innovative joining process of composite extruded profiles by FSW was presented [102]. This approach aimed to predict the structural behavior and improve the geometrical quality of joined light weight components after welding. Van Der Stelt et al. [103] presented a numerical problem with contacting solid metal flows and solved with an arbitrary Lagrangian–Eulerian (ALE) FE method. For this simulation a new free surface boundary condition was implemented for remeshing the boundary elements. It uses explicitly, that the integral of the convective velocity along a boundary element remains zero. The new remeshing option for the free surface was tested on a cladding problem employing FSW. The problem describes two elastoviscoplastic aluminum material flows which interact mechanically. Numerical models based on the commercial code DEFORM were developed to provide a better understanding of the FSW process [104]. A DEFORM 2D model was used to simulate the material flow pattern and the initial plunge force during the FSW of Aluminum 1100-O, assuming the material deformed plastically. A thermo-mechanically coupled, rigid-viscoplastic DEFORM 3D analysis was performed to predict the forces, stresses, strains, strain rates and temperatures occurring during the FSW of 4.89 mm thick sheets of Aluminum 2024-T3. The main findings of the work suggested that the DEFORM package was able to effectively model

the large deformations encountered during the FSW process but did not have the capability to generate the expected high temperatures at the end of the plunging process.

In numerical analysis of FSW, the most frequently used method is the FE method or finite difference (FD) method. However, by employing these methods, it is difficult or troublesome to calculate the advective term for both momentum and temperature. It is also difficult to calculate large deformations of the material. Moreover, a complex process is required to analyze dissimilar joining, particularly with respect to substance transfer. To avoid these difficulties or troublesome processes, a particle method was adopted for simulating FSW involving dissimilar materials [105]. In the particle method, advective term, substance transfer and surface deformation are calculated automatically mainly because the Lagrangian approach is used. The effectiveness of this method was verified by some case studies. A 3D FSW process model for 2014 aluminum alloy was developed based on fluid mechanics [106]. The material transport in the FSW process was regarded as a laminar, viscous and non-Newtonian liquid flow passing a rotating pin. The results of the simulation showed that the material in the middle part of the weld flows vertically. In the retreating side, the material is pushed up and in the advancing side the material is pushed down. Visualization experiments of material flow employing marker insert technology were used to validate the simulation results. Under higher welding speeds, material separated motion can be seen in the shoulder-pin transition part, and an actual welding void defect was observed at the same position in the weld seam.

Two contact models, the classical Coulomb contact model and the modified Coulomb contact model, were used in a fully coupled thermo-mechanical numerical model of the FSW and the suitabilities of the two models to simulate the FSW process were analyzed [107]. There is little difference between the numerical results of the two contact models for the FSW at low rotating speeds. In high rotating speed, the classical Coulomb contact model fails because the shear stress at the interface is not limited, but the modified Coulomb contact model may be used. A semi-analytical thermal model for the FSW was proposed [108]. The formulation of heat flow during the FSW process is based on generic solutions of the differential equation for heat conduction in a solid body, formulated for a point heat source with constant linear velocity. The heat generation was considered as a function of the tool-matrix interface temperature, which is calculated by means of a numerical routine written in MATLAB code. A comparison with the experimental measurements taken from the literature showed that the results from the present semi-analytical model are in good agreement with the test data.

In the FSW joints some defects may arise that are very sensitive to small variations in some process parameters. Moreover, the results from computational modeling of the FSW are only valid for non-defective welds. In order for modeling of the process to contribute to the industrial consolidation of the FSW process, the experimental implementation results need to be supported by a reliable, Non-Destructive Testing (NDT) system. Santos et al.'s work [109] addressed an integrated scheme of two computational tools which enables the support of a faster establishment of process parameters, addressing the material flow analysis, with numerical coupling between fluid dynamics and solid mechanics; using the analytical iSTIR code; and a new, NDT, eddy currents probe, able to detect the typical FSW root imperfections. A FSW numerical simulation tool, based on Forge® F.E software, was developed [110]. Its main features are an Arbitrary Lagrangian Eulerian (ALE) formulation and an adaptive remeshing procedure based on error estimation. A 3D FSW simulation based on friction models calibration was presented using Eulerian and ALE formulation. Two friction models, namely Norton's and Coulomb's, were used to model friction in the tool-plate interface in aluminum alloy 6061-T6. Comparisons with experimental results considering various travel speed have been performed.

Many numerical models have been used to calculate the thermal field, distortion and residual stress in welded components but some modeling parameters such as the film coefficient and the thermal radiation of the work pieces may be technically difficult and/or expensive to measure experimentally. It is important to establish a systematic procedure to identify FSW process parameters. A simplified FE model for the analysis of a FSW thermal progress was proposed in which two parameters, tool heat input rate and heat loss through the backing plate, are identified as parameters to be optimized by the application of a generic algorithm [111]. A generic algorithm was used to evaluate the two thermal parameters. By comparing the FEM numerical results with experimental results, the FSW process thermal parameters have been successfully identified. This automatic parameter

characterization procedure could be used to optimize the FSW process. A quasi-steady approach to FSW heat transfer modeling was proposed and implemented using FLUENT [112]. An idealized model of the mechanical dissipation heating in FSW was employed. Selected numerical predictions based on the model were shown to capture most of the features of corresponding experimental data available in literature. It can be concluded that the quasi-steady formula is an attractive alternative to more computationally intensive unsteady approaches to FSW modeling under some circumstances. A temperature function method based on a line-gauss heat source model has been reported [113]. The heat source control variable in the line-gauss model was changed from heat input to welding temperature. This led to more consistency between the simulated welding temperature field and experimental results in the width and thickness direction of model. This new high-efficiency simulation method was validated by a model of the FSW on Al alloy sheet.

2.2. Tool design

The success of the FSW process depends on the design of the welding tool. The welding tool consists of two features, a pin and the shoulder. Several pin geometries have been proposed, for example a threaded cylinder, a threaded cylinder with flattened sides, etc. Fig. 4 shows a selection of tools designed at TWI [17]. The rotating pin forces the materials to flow around the pin and to mix. The shoulder applies a pressure to the material to constrain the plasticized material around the pin and generates heat through friction and plastic deformation in a relatively thin layer under the shoulder surface. Tool geometry significantly affects the energy input, deformation pattern, plunge force, microstructures, and mechanical properties of FSW joints. Rai et al. [114] reviewed and critically examined several important aspects of FSW tools such as tool material selection, geometry and load bearing ability, mechanisms of tool degradation and process economics.

The FSW process for tailored blanks of aluminum alloy was investigated by Buffa et al. [115] through a FE model developed by the authors. In particular FSW for sheets with different thicknesses was studied. For each setup a different welding tool was designed, an extra nuting angle was considered, and numerical simulations were performed in order to predict the feasibility of the process, the final shape of the welding blank, and the distribution of the main process variables. As shown in Fig. 5, a quite large range of different thicknesses can be successfully welded with good nugget integrity.

The most important geometric parameter in the FSW tool design is the shoulder diameter, which is currently designed by trial and error methods. The influences of shoulder diameter on thermal cycles, peak temperatures, power requirements, and torque during FSW processes are complex and remain to

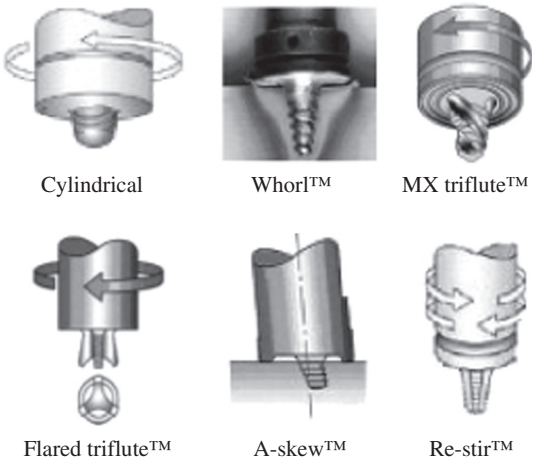

Fig. 4. A selection of tools designed at TWI [17].

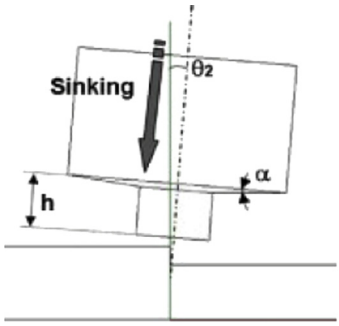

(a) Sketch of the utilized tool and geometrical parameters

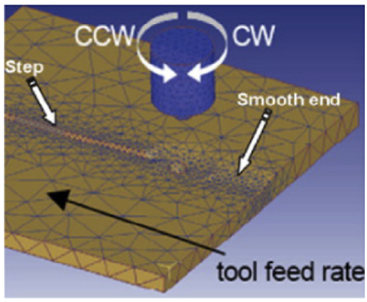

(b) The utilized FEM model.

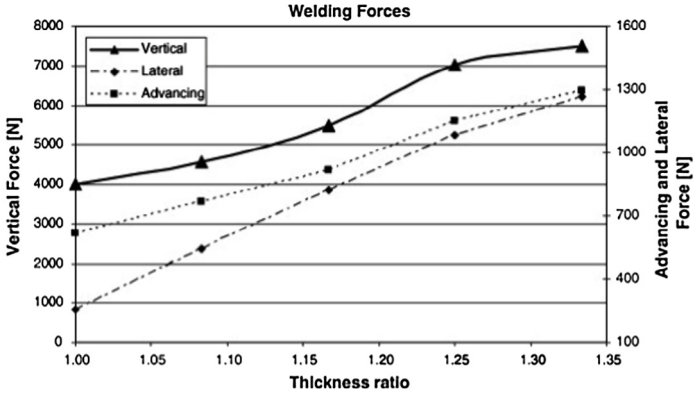

(c) Welding force components vs. thickness ratio.

Fig. 5. FSW for sheets with different thicknesses [115].

be fully understood. A criterion for the design of a tool shoulder diameter based on the principle of maximum utilization of supplied torque for traction was proposed and tested [116]. The optimum tool shoulder diameter computed from this principle using a numerical heat transfer and material flow model resulted in best weld metal strength in independent tests and peak temperatures that are well within the commonly encountered range. An optimum tool shoulder diameter was identified using a 3D, heat transfer and materials flow model [117]. The predictive capability of the model was tested by comparing the computed values of peak temperature, spindle power, and torque requirements for various shoulder diameters against the corresponding experimental data. The change in the values of these variables with shoulder diameter was correctly predicted by the model. The model was then used to identify the optimum tool shoulder diameter that facilitates maximal use of the supplied torque in overcoming interfacial sticking.

In the plunge stage, the larger the pin radius, the higher force and torque the tool experiences and the greater the amount of heat generated. The effect of changing the tool geometry parameters on thermo-mechanical behavior in FSW of AA5086 aluminum alloy was investigated numerically and experimentally by Jamshidi Aval et al. [37,39]. The conical tool with the shoulder angle of 2° has been found to produce a larger deformation region as well as higher mechanical properties compared with the cylindrical tools employed in this research. The ratio of heat generation from plastic deformation to friction dissipation in the conical threaded pin is 44% more than with a cylindrical pin of similar shoulder diameter. A 3D FE transient thermal analysis of FSW was presented for different tool geometries and process parameters [118]. Thermal history of FSW of 6-mm thick AA1100 plates for

different tool geometries was calculated and tool geometry with a concave shoulder and conical pin was found to be preferable for the FSW of AA 1100. It is preferable to keep the tool pin diameter as small as possible to avoid occurrence of a wormhole defect. The effects of variation in tool geometry parameters, such as the tool shoulder surface angle etc., on the FSW process on AA2024 aluminum alloy were also investigated numerically [119].

Buffa et al. [120] presented an experimental and numerical investigation on the lap joining of AA2198-T4 aluminum alloy blanks by FSW. The joints strength and metallurgical properties were investigated by varying the joint configuration and the tool geometry and rotational speed. It was found that using cylindrical-conical pin tools and the correct choice of the relative sheet positioning increased the welded nugget extension and integrity, thereby improving the mechanical performance of the joints. Experimental and numerical analyses were carried out on FSW magnesium alloy thin sheets using "pin" and "pinless" tools [121]. The effect of the different tool configurations and sizes, and welding parameters on mechanical properties of the joints was analyzed in detail. The results shown that the pin tool configuration, with a shoulder diameter of 8 mm, results in strength and ductility values higher than those provided by the "pinless" tool. A strong beneficial effect is obtained by increasing the shoulder diameter from 8 to 19 mm using the "pinless" configuration, whilst the FSW with the pin tool is critically affected by the welding conditions. Experimental and numerical campaigns were conducted to study the effect of the tool geometry and welding parameters on the properties of FSW joints of AZ31 magnesium alloy sheets [122,123]. The results, presented in terms of tensile strength, ductility, micro-hardness values and the distribution of numerical field variables enable a deeper understanding of the behavior of FSW joints of this relatively new material, and can be used for a full optimization of the joints.

Tool and workpiece temperatures, torque, traverse force and stresses on the tools are affected by the FSW variables such as plate thickness, welding speed, tool rotational speed, shoulder and pin diameters, pin length and tool material. The large number of these variables makes the experimental determination of their effects intractable. A set of five neural networks were developed to calculate the peak temperature, torque, traverse force and bending and equivalent stresses on the tool pin for the FSW of an aluminum alloy [124]. The neural networks were trained and tested with the results from a well tested, comprehensive, 3D heat and material flow model. The predictions of peak temperature and torque were also compared with appropriate experimental data for various values of shoulder radius and tool revolutions per minute. The models can be used even beyond the range of training with predictable levels of uncertainty. In Debroy et al's work [125], an ANN was trained and tested with results from a phenomenological model and was then used to generate tool durability maps that show the ratio of the shear strength of the tool material to the maximum shear stress on the tool pin for various combinations of welding variables. These maps show how the thicker plates and faster welding speeds adversely affect tool durability and how that can be optimized.

Fully coupled thermo-mechanical models were adopted to study the effect of tool shapes on the temperature distribution and the material deformations in the FSW process [126,127]. Numerical results indicated that the stirring zone can be enlarged by the increase of the shoulder size. The temperature variation is the main factor for controlling the grain growth near the welding line. But, when the strain and the strain rate become smaller near the border of the stirring zone, the recrystallization process is dominated by the material deformations instead of the temperature variation. The conventional tool design employs a cylindrical shoulder with a single profiled pin. Mukherjee and Ghosh [128] designed a new process that uses a two-pin tool under the same shoulder to increase shear deformation within the workpiece. This configuration can enhance local heating where joining occurs. The design employs two closely spaced pins rotating in the same direction within the workpiece under a separately controlled shoulder. Prior to gathering considerable experimental data with the new equipment, a fully coupled thermo-mechanical 3D FE model was developed to compare the existing single-pin technology with the new technology of friction driven stitch welding. The results of this study indicated that the two-pin tool design with a separate shoulder, with the same direction of pin rotation, can be a superior design compared with the conventional single-pin FSW tool and could minimize damage to the tool material.

In FSSW processes, instead of moving along the weld seam, the tool only indents two overlapped parts. In some applications, this technology can be considered as a valid alternative for single point

joining processes like resistance spot welding (RSW) and riveting processes. In the FSSW process a specially designed tool is brought into rotation and plunged straight down. Heat is generated as a result of friction between the tool and materials. Numerical simulation of the Al 6061-T6 FSSW process was carried out with the ADINA System [129]. The calculations were carried out for different tool stem radii and different angles of abutment. The influences of tool geometry parameters on the temperature field and the temperature gradient in the welded materials were analyzed. An experimental and numerical study of the FSSW process for the lap-joining of thin aluminum sheets was carried out [130]. An experimental campaign was conducted on AA6060 T6 aluminum sheets having a thickness equal to 2 mm. The FSSW process was applied on pairs of overlapped sheets by varying the tool rotational speed, and by keeping fixed the other process parameters, such as axial feed rate, indentation depth, and dwell time. Preliminary tensile tests and metallurgical analyses were also performed to evaluate the quality of the joints as function of the chosen process parameters. A numerical model of the FSSW process was developed and implemented using the commercial FE code Deform 3D. The model parameters were set according to the experimental evidence.

The principal detraction of the FSSW process is the keyhole left by pin extraction, which can be detrimental to the weld strength. A pinless tool can be used to eliminate the keyhole. However, this approach is limited to joining thin sheet (<1 mm). A rotating anvil with the pinless FSSW process permits the joining of thicker cross sections, decreases the cycle time and reduces the reaction forces and torques acting on the spot welding frame. The objective of Cox et al.'s work [131] was to establish the ideal conditions for creating mechanically sound spot welds. Tensile shear tests, macrosection analysis and a numerical model of the process were used to evaluate the spot welds. Macrosection and numerical analysis revealed that the material flow between the pinless tool and rotating anvil is complex and unique to this process. It was found that the use of a rotating anvil for FSSW is a viable means to repeatably create quality spot welds in thicker weldments.

A new idea was proposed for the FSW of the thin plate of AI alloy by using a rotational tool without a pin [132,133]. Experiments were carried out using tools with an inner-concave-flute shoulder, a concentric-circles-flute shoulder and a three-spiral-flute shoulder, respectively. The grain size in the weld nugget zone attained by the tool with three-spiral-flute shoulder is nearly the same while the grain sizes decrease with the decrease of welding velocity. The displacement of material flow in the heat-mechanical affected zone by the tool with three-spiral-flute shoulder is much greater than for tools with an inner-concave-flute shoulder or a concentric-circles-flute shoulder. An Arbitrary Lagrangian Eulerian (ALE) formulation was developed to simulate the different stages of the FSW process with the FORGE3® F. E. software [134]. Friction parameters were identified for an Eulerian steady state simulation by comparison with experimental results. Simulation of the transient plunge and welding phases helps to better understand the deposition process that occurs at the trailing edge of the probe, and in particular the possible formation of voids. The flexibility and robustness of the model allows investigation of the influence of threads and tooling designs.

2.3. Welding parameters

The main welding parameters, which can be controlled in the FSW process for a given tool, are the rotational speed and the traverse speed, the axial force of the tool shoulder on the workpiece, and the angle of the contact between the tool and workpiece. The tool rotation results in stirring and mixing of material around the rotating pin. The rotation of the tool moves the stirred material from the front to the back of the pin. Higher tool rotation rates generate higher temperatures because of greater frictional heating and result in more intense stirring and mixing of the material. These two parameters have considerable importance and must be chosen with care to ensure a successful and efficient FSW cycle. Except for the initial and the final periods of welding, heat is generated at a constant rate (assuming that the tool rotates and moves forward at a constant speed).

A thermo-mechanical fully coupled 3D FE analysis was carried out in a study of the effect of tool geometry and advancing speed on the FSW of AA7075 aluminum alloy [135]. A significant refinement in the grain size was observed when advancing speed was increased from 50 mm/min to 100 mm/min and that increasing the pin angle enlarges both the heat-affected zone and the thermal mechanical zone, resulting in a bigger weld nugget. The results enable the optimal tool geometry and advancing

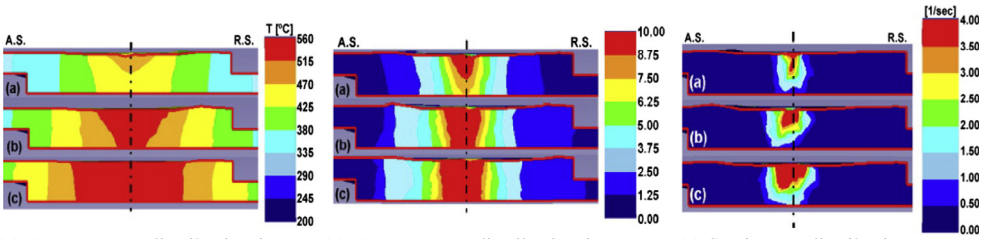

(a) Temperature distribution in a transverse section

(a) Temperature distribution in a transverse section

(c) Strain rate distribution in a transverse section

Fig. 6. Effect of the rotating tool speed ((a) R = 500 rpm, (b) R = 700 rpm and (c) R = 1000 rpm) on temperature, strain and strain rate distributions [135].

speed to be chosen so as to improve the nugget integrity of aluminum alloys. Fig. 6 shows the effect of the rotating tool speed on temperature, strain and strain rate distributions. A 3D FE model of FSW process was established to study the effect of the variations of process parameters on the mechanical features in FSW processes [136]. The comparisons of numerical and experimental results showed that the equivalent plastic strain can approximately correlate with the microstructural evolution. It was found from both the numerical model and the experiments that the quality of the FSW can be improved when the angular velocity of the pin is increased or the welding speed is decreased. With the increase of the angular velocity of the pin, the equivalent plastic strain is increased. The equivalent plastic strain is decreased with the increase of the translational velocity of the pin.

The FSW superplastic forming of AA6061-T6 sheet was investigated by means of physical experiments and mathematical simulations [137]. A selected range of tool rotating speeds of 500, 1000 and 2000 rpm was used for FSW. At a constant temperature of 550 °C and a constant pressure of 0.4 MPa, superplastic forming experiments were performed using a free forming die for the FSW joints. The proposed FE model was validated by comparison with experimental data. The effect of constant pressure, coefficient of friction, strain-rate and strain-rate sensitivity has been studied using the proposed FE model. The plunge stage of FSW was examined numerically by a dynamic explicit FE method with more attention to the temperature evolution [138]. The high temperature region around the stirred zone extended with increasing rotation speed. The range of the stirred zone changed little with variations of rotation speed and insertion time. The simulation result on the temperature field was in general agreement with the experimental one. A thermal model was developed to simulate FSW of pure copper plates with the thickness of 4 mm in the constant traverse speed of 25 mm/min and with five different tool rotation speeds [139]. A moving coordinate system was used for modeling the tool movement during the FSW process. The generated heat was used to model the grain growth in the copper plates, and the resulting mechanical properties of the copper plates. An analysis of metallographic images showed that increasing the speed of rotation results in an increase in grain size in the nugget zone. This confirmed the numerical results from the model.

Michopoulos et al.'s paper [140] presented the results of a sensitivity analysis that determines the effects of FSW processing parameters, such as the rotation speed and the traveling speed, on the resulting residual strain fields. The problem was modeled as a thermostructurally coupled problem via FE analysis of an elastoplastic workpiece under the influence of heat generated from the FSW process and taking into account the temperature dependent yield strength of the material. A coupled thermal viscoplastic model was used for the FE simulation of the FSW process of non-similar aluminum–copper sheets [141]. Tool speeds and temperature distribution were coupled and solved together using this method. The relationship between the tool speeds and the heat input during FSW was obtained by numerical analysis, and the stress contour relative to the temperature field and tool force was surveyed. A thermo-mechanical model was developed to predict the material deformations and temperature histories in the FSW process [142]. Numerical results indicated that the material particles on the top surface do not enter into the wake and just pile up at the border of the wake on the retreating side and this is the reason for the formation of the weld fash in FSW.

Both increasing the rotating speed and decreasing the traverse speed can lead to an increase in the stirring effect of the welding tool, which can improve the quality of the FSW. When the traverse speed becomes higher, the rotating speed must also be increased to avoid any possible welding defects such as voids. Simultaneously increasing the rotation and translating speeds of the welding tool can lead to an increase in the residual stress.

A FE analysis program-WELDSIM was developed specifically for 3D nonlinear thermal and thermo-mechanical numerical simulations of the FSW process for 304L stainless steel [24]. Two cases with tool rotation speeds of 300 and 500 rpm were analyzed. Based on the experimental records of transient temperature at several specific locations during the FSW process for the 304L stainless steel, an inverse analysis method for thermal numerical simulation was developed. After the transient temperature field was determined, the residual stresses in the FSW plate were then calculated using a 3D elastic–plastic thermo-mechanical simulation. A comparison with the residual stress fields measured by the neutron diffraction technique showed that the results from the numerical simulation agreed well with the physical test data. A thermal history and distribution analysis of the preheating period of FSW of AZ31 magnesium alloy using FE method was presented [143]. Temperature history and distributions at different plunge speeds and rotation speeds were simulated and measured to determine the appropriate preheating parameters. When a rotating speed of 600 r/min and a plunge speed of 3 mm/min is used, the maximum preheating temperature can reach about 450 °C, showing that the heat generated by the pin cannot be neglected during FSW. The proportion of heat generated by the pin was found to be about 15% of the total heat generated by the welding tool (including generated by the shoulder and the pin).

Empirical models relating the process parameters (i.e., plunge depth, rotation speed and travel speed) to the process variables (i.e., axial, path, and normal forces) were developed to understand their dynamic relationships [144]. The steady-state relationships between the process parameters and the process variables were constructed, and the relative importance of each process parameter on each process variable was determined. The results indicated that the steady-state relationship between the process parameters and the process variables can be well characterized by a nonlinear power relationship, and the dynamic responses can be well characterized by low-order linear equations. Experiments were conducted that validated the developed FSW dynamic models. The solid state bonding conditions obtained in FSW of AA5754–H111 butt joints were analyzed, considering the so-called zig-zag line in the transverse section of the joints [145]. A wide range of experiments were carried out varying both the travel and rotation speeds of the tool. The effects of the process parameters on the mechanical properties of the joint were highlighted and micro-and macro-observations were used in order to explain the reasons for the enhanced mechanical properties found for the welded material. Numerical results derived from a FE model previously developed by the authors were utilized to point out the different mechanical and metallurgical behavior of the joints obtained. The microstructural aspects in AA2024-T3 friction stir butt welds were numerically and experimentally investigated [146]. A 3D CFD model was implemented to simulate temperature field, material flow, and microstructural aspects in an Eulerian framework. Recrystallized grain size was numerically predicted taking into account the Zener–Holloman parameter and experimentally measured by means of conventional metallographic techniques.

The FE modeling of material flow was used to understand the physical phenomena occurring during the dwell phase of FSW using thin sheets of 7075 aluminum alloy [7]. Numerical results were compared with reference experimental data including torque measurements and metallographic observations made at different tool rotation speeds. A comparison between the experimental and calculated torques shows that the contact condition depends on tool rotation speed. This result is supported by the differences between nugget grain size and nugget shape evolutions obtained with different tool rotation speeds. The effect of process parameters on the temperature distribution and the mechanical properties of aluminum alloy AA2014 FSW joints was investigated [147]. A 3D transient thermal model using ANSYS FE code was developed and experimentally validated to quantify the thermal history. Nine experiments based on full factorial design were performed to systematically study the influence of input parameters, such as tool rotational and traverse speed. Analysis of variance (ANOVA) was used to investigate the effect of varying input parameters on the thermal history and mechanical properties of the joints. The analysis indicated that the temperature under the tool

was more strongly dependent on the tool rotational speed than the traverse speed. The results also indicated that the traverse speed had the greatest influence on mechanical properties. In Gök and Aydin's recent study [148], a DEFORM 3D FE model was developed for simulating the FSW process on AZ31 magnesium alloy. The simulation was carried out with different rotational and traverse speeds. The proposed FE model has been validated against experimental data.

The thermo-mechanical responses during FSW of dissimilar aluminum alloys were evaluated using a 3D ABAQUS FE model [40]. FSW experiments were conducted under different working conditions. The temperature variations during and after welding and the residual stresses in various positions in the welded samples were measured using a hole-drilling technique. It was found that tool rotation speed significantly affects the amount of residual tensile stress while varying the traverse speed mainly affects the distribution of residual transverse stresses. Also, both experimental and simulated results indicate that welding fixtures significantly affect the residual stress profiles as well as their magnitudes. A FE model using an adaptive re-meshing technique was used to investigate tool forces in FSW processes [149]. Results indicated that forces in the tool were greatest at the start of the translational stage. Of the three directional forces, the axial force is the most significant and the force perpendicular to the welding line is the minimum. The tool forces in the three directions are all increased with the increase in transverse speed and decreased with the increase in angular velocity. Veljic et al.'s paper [150] deals with the heat generation in Al2024-T3 plate under different tool rotating speeds and plunge speeds during the plunge stage of the FSW processes. A 3-D FE model was developed in the commercial code ABAQUS/Explicit using the arbitrary Lagrangian–Eulerian formulation, the Johnson–Cook material law, and Coulomb's Law of friction. Numerical results obtained in this work indicate a more prominent influence from the friction-generated heat. The slip rate of the tool relative to the workpiece material is related to this portion of heat. The material velocity, on the other hand, is related to the heat generated by plastic deformation.

A sequentially coupled FE model was used to study the residual stresses caused by the thermal cycling induced by FSW [151]. The predicted longitudinal stresses peaked at 300 MPa and had a "W" profile with tensile stress peaks in the weld and compressive stresses outside the weld. The application of 'hot' welding conditions, i.e. low welding speed and high rotational speed, increased the residual stresses significantly, mainly in the transverse direction. Conversely, 'cold' welding conditions resulted in lower residual stresses. The magnitude and distribution of the residual stresses predicted by the FE model were validated by neutron diffraction. Roy et al. [152] proposed a 3D thermal pseudo mechanical model formulated in an Eulerian frame considering a quasi-steady state approach to modeling FSW of AA6061 Aluminum alloy. The model was implemented using nonlinear FE code in Comsol Multiphysics v 4.1. The effect of different operating parameters on the FSW process was analyzed. The material flow was found to be enhanced by an increase in the traverse speed and the angular velocity of the pin, with a pronounced swirl on the advancing side. The distribution of equivalent plastic strain and dynamic viscosity was found to correlate with the distribution of the microstructure zones in the weld. The objective of Zhang et al.'s work [153] was to develop an understanding of FSW applied to thin plates so as to improve welding quality and increase production efficiency. The study was conducted by using FE modeling and temperature field analysis to obtain optimization parameters, and to monitor the force of the stirring spindle by using virtual instrument, multi-sensor data fusion.

Tube-sheet joints are critical in some applications, where contact between the shell and tube side fluids is not tolerable. FSW was used for tube-sheet seal joints and simulated using a 3D thermo-mechanical FE model [154]. The model included the thermal effect of the tool-workpiece interaction along with axial load but ignoring the metal flow around the tool. The objectives of the model were to evaluate the temperature distribution and residual stress in the workpiece resulting from the thermal cycle and axial load during welding for various process parameters, and to study how residual stresses in adjacent roller expanded tubes are affected during FSW. An experimental setup was designed and manufactured to show the feasibility of the process in constrained size joints and to validate the numerical results. The response to temperature and force during the FSW of Invar 36 alloy was investigated numerically and experimentally [155]. Results indicated that increasing rotational speed results in increasing temperature and decreasing axial force. Rotational speed was found to have no obvious influence on the longitudinal force. Increasing the traveling speed produces increasing axial force and longitudinal force and a decreased trend of temperature out of the center of the stir zone.

Material stirring and heat generation in the FSW processes induce significant alterations to microstructure and material properties. The influence of rotating and welding speed on microstructure, mechanical properties, and joint quality in AA2024-T3 FSBW joints were reported by Carlone and Palazzo [156]. Experimental data were presented and discussed, considering numerically computed temperature and strain rate distributions. The data provide useful information for setting parameters. A 3D numerical model for the FSW was developed using ABAQUS software to investigate the heat of plastic deformation [157,158]. The effects of rotation and welding speeds on the temperature field when welding 2024-T3 aluminum alloy were systematically investigated. Temperatures were measured to validate the reliability of the model. Results showed that increasing the welding speed has a significant effect on the time to reach the peak temperature but the value of the peak temperature changes little. The temperature field during the welding of the overlap joint in a stringer and skin structure was studied for 7A04 Al alloy [159]. The results of numerical simulation showed that the welding temperature field is greatly influenced by the resting time of the rotating tool at the insertion position after the inserting process is finished. A simplified heat input numerical model was used to simulate the transient temperature field distribution and the feature points of thermal cycle curve of 4 mm Q235A steel FSW butt joints [160]. The heat input model and the simulation method were verified by comparing the simulation results and the feature point temperature curve measured by the thermocouple.

Although the mechanical loads have been considered in FSW simulation by some researchers, the loads are greatly simplified and the analysis is only localized in the asymmetric distribution of residual stress. In Yan et al.'s paper [161,162], numerical simulations were carried out to investigate the functions of mechanical loads during the FSW process. Based on experiments of FSW aluminum alloy sheets, three simulation models were established with different conditions, considering thermal load only, considering both thermal load and down force, and considering thermal load, down force and working torque together. The results showed that the down force significantly reduces residual stress and the torque leads to the asymmetrical distribution of residual stress. On the other hand, mechanical loads absolutely change the residual distortion pattern from saddle state into anti-saddle state. Dissimilar intermixing during FSSW of Al 5754 and Al 6111 sheets was investigated both experimentally and numerically [163,164]. It was proposed that dissimilar intermixing during the dwell period in FSSW results from the incorporation of upper (Al 5754) and lower (Al 6111) sheet materials at the top of the thread on the rotating pin. A ribbon of contiguous Al 5754 and Al 6111 lamella is moved downward via the pin thread as the tool rotates during the dwell period in the FSSW. A helical vertical rotational flow is created during the dwell period in the FSSW because the ribbon of contiguous Al 5754 and Al 6111 lamellae discharged from the bottom of the pin thread moves outward and upward before moving back toward the tool periphery and downward again.

A detailed design of a reluctance position sensor for determining the penetration of the welding tool in a FSW machine was proposed [165]. It functions by sensing the variations of the inductance of a coil due to the changes in the gap of the magnetic circuit created by the welding tool and the working bench. Intensive FE simulations were performed to decide the best configuration, including the geometry of the sensor, the winding of the coil and the properties of the magnetic materials. Static measurements in a functional prototype demonstrated the validity of the method and the design.

2.4. Tool wear

As mentioned above, the geometry of the tool significantly affects the energy input, deformation pattern, plunge force, microstructures, and mechanical properties of FSW joints. Excessive tool wear during the FSW process is hindering the application of FSW to hard materials such as steel and titanium alloys. Most of the tool wear occurs during the plunge stage.

A better understanding of the plunge phase is extremely important with the growing role of FSSW and also for understanding tool wear in case of FSW of harder materials. A 3D ABAQUS FE analysis model was developed to study the thermo-mechanical processes involved during the plunge stage [166,167]. The strain rate and temperature dependent Johnson–Cook material law was used as the constitutive law. The heat source incorporated in the model included friction between the material, the probe and the shoulder and also the heat generated during plastic deformation. A good correlation

was found between the results from the ABAQUS model and the experimental data. The FSW of L80 steel was investigated with experiments and modeling [168]. Severe tool deformation and some wear were observed when commercial pure tungsten was used. The temperature histories in the weld region and tool forces were measured and supplied to a FE model. The simulated pin deformation matched the experimental observation. Using this model and optimization techniques, the yield strength required of the pin material is estimated to be 400 MPa at 1000 °C to avoid mushrooming.

A FE model implementing the Johnson–Cook material constitutive law was used by Rice et al. [169] to investigate the shear stress and axial force experienced by the tool during the plunge phase of FSW into AISI 1045. The model in this research consisted of a deformable work-piece, deformable donor material, and a rigid tool. The numerical simulation data supports the concept of using a donor material to reduce tool wear and the need to implement this concept to experimental work for verification. Further research involving initial donor material experiments with Cu/Al were conducted by the same authors [170] to confirm the feasibility of applying this method to the FSW process. Images obtained by scanning electron microscopy (SEM) and energy dispersive X-ray spectroscopy (EDX) of the donor material showed no mixing of Cu with Al at the interface of the Al plate during the plunge. The images showed the formation of columnar grains and recrystallization of grains at the interface.

Although FSW is now widely used for the welding of aluminum and other soft alloys, premature tool failure limits its application to hard alloys such as steels and titanium alloys. The tool pin experiences severe stresses at high temperatures due to both the bending moment and torsion. It is shown that the optimum tool pin geometry can be determined from its load bearing capacity for a given set of welding variables, tool and work-piece materials. The traverse force and torque during FSW were computed using a 3D heat transfer and viscoplastic material flow model, considering the temperature and strain rate-dependent flow stress of the work-piece material [171]. These computed values were used to determine the maximum shear stress experienced by the tool pin due to the bending moment and torsion for various welding variables and tool pin dimensions. The proposed methodology was used to explain the failure and deformation of the tool pin in independent experiments for the welding of both L80 steel and AA7075 alloy. The results demonstrated that the short tool life in a typical FSW of steels is contributed to by low values for safety factors in an environment of high temperature and severe stress. An experimental study of tool life in the FSW of titanium alloys sheets provided useful insights [172]. Numerical simulation provided important information for the fixture design and analysis of experimental results. Tungsten and Rhenium alloy W25Re tools were found to be the most reliable among those considered. Scutelnicu et al.'s paper [173] addressed a comparative study on FSW and Tungsten Inert Gas (TIG) assisted FSW of copper. The base materials were preheated by an additional heat source and some remarkable advantages were obtained. These included as: faster and better plasticization of the base material, reduced FSW tool wear and clamping forces, faster welding speed and improved joint quality. The aim of the investigation was to develop two FE models, simulating the welding of copper by FSW and TIG-assisted FSW procedures. These are useful in predicting the temperature distribution, the peak temperature of the process and temperature changes in the cross section of the welded joints.

Preheating has the potential to enable higher welding speeds and reduced tool wear particularly when welding alloys with higher melting temperatures. A transient 3D FE heat transfer model of workpieces was developed to predict the influence of preheating on the temperature distribution and heat flux within the workpieces [174]. The energy deposited by the laser in the top plate does not penetrate into the bottom plate ahead of the tool due to the contact resistance between the plates. Hence, the thermal contact resistance, inherent in lap welds, controls the effectiveness of preheating. The effect of preheating on FSW of aluminum was investigated by varying the laser power and workpiece material while maintaining constant tool geometry and material. It was also found that the total power consumed in the process, defined as the sum of tool power and absorbed laser power, can decrease with preheating. Mandal et al. [175] proposed recently the "donor material" concept for reducing tool wear in the plunge phase. This works by providing localized preheating at the plunge area and using a softer material as a "donor." The process generates heat in a relatively soft "donor" material and the heat is transferred to the much harder workpiece material by conduction. This research includes several numerical simulations of the donor material concept with different donor materials and plain carbon steel as the workpiece. A Significant reduction in both axial force and

contact pressure were needed when a donor material was used in the plunge area. The decreases in both axial force and contact pressure are very likely to contribute to decreasing tool's wear.

2.5. Material flow

Material flow plays a fundamental role in the FSW since it determines the effectiveness of the joints. Most of the material flow occurs through the retreating side and the transport of the plasticized material behind the tool forms the FSW joint. The material flow around the tool is very complex depending on the tool geometry, process parameters and material to be welded [176]. Thus it is very important to understand the material flow characteristics for optimal tool design and process parameter combinations. Several models of FSW processes have been developed for the calculation of heat transfer and materals flow [177–181].

The objective of Tutunchilar et al.'s paper [182] was to develop a 3D Lagrangian incremental FE method simulation of friction stir processing using DEFORM-3D software. This simulation method can also be used for predicting the material flow of the FSW. The 3D results of the material flow patterns in the center, advancing and retreating sides were extracted using point tracking. Fig. 7 shows the tunneling cavity formation and the slot formation behind the pin. The results reveal that the main part of the material flow occurs near the top surface and at the advancing side (AS). Material near the top surface was stretched to the advancing side resulting in a non-symmetrical shape of the stir zone. Fig. 8 shows comparison of simulated and experimental stir zone shape.

Studies of material flow can provide valuable information about the material mixture and enable improvements in tool design and the selection of process parameters. Colegrove et al's systematic papers [183–187] described the application of the computational fluid dynamics (CFD) code, FLUENT,

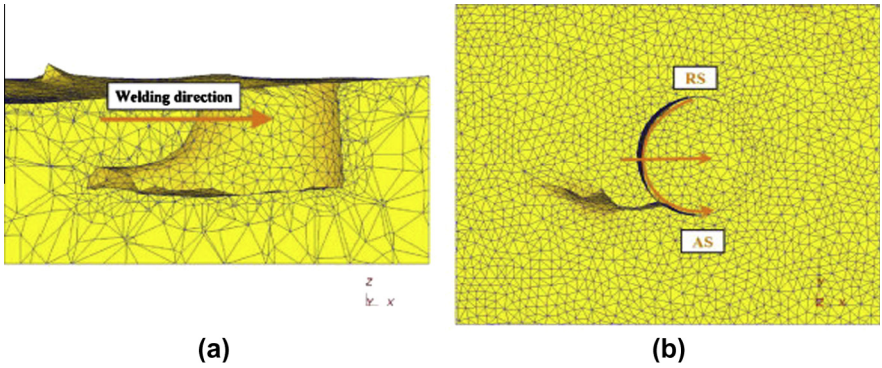

Fig. 7. (a) Tunneling cavity formation at the behind of the pin and (b) slot formation at advancing side behind the pin [182].

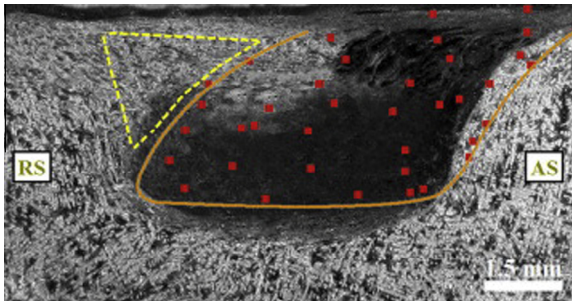

Fig. 8. Comparison of simulated and experimental stir zone shape [182].

to modeling 2D or 3D metal flow in FSW processes. A standard threaded tool profile was used for the analysis and features such as the tool rake angle, heat generation and heat flow were included. The primary goal was to gain a better understanding of the material flow around a complex FSW tool and to demonstrate the effect of the tool rake angle, and weld and rotation speed. The papers also demonstrated several novel modeling techniques. The first was the slip boundary condition in three dimensions, where a limiting shear stress was applied at the surface and the material was allowed to slip against the tool. The second involved adjusting the limiting shear stress so that the weld power of the model matched that obtained experimentally. The final technique was the inclusion of the temperature profile by interpolating the result from a thermal model. This obviated the need to solve the thermal profile in conjunction with the flow model. A CFD model of an aluminum-steel dissimilar butt weld was implemented using the FE software Comsol v4.3 [188]. The model assumed a viscoplastic material behavior and was calibrated using temperature measurements for two different tool offsets (+0.5 and +1.5 mm) with respect to the joint line. The model can reproduce the maximum measured temperatures and heat input, but the cooling rates are higher than the experimental ones. The simulated material flow is laminar and it is dependent on the tool geometry. The model can also provide information on the principal mechanism of heat generation for each material: friction in the steel and plastic deformation in the aluminum.

FE models based on solid mechanics were developed to study the flow patterns and the residual stresses in FSW processes [189,190]. The flow of metal during FSW was investigated using tracer particles. It was shown that the flows on the advancing side and retreating side are different. After several rotations the material rotating around the nib sloughs off in the wake of the pin, primarily on the advancing side. A 3D numerical model was presented for the study of material flow in the FSW process [191]. Results indicated that the material in front of the pin moves upwards due to the extrusion effect of the pin and rotates with the pin. Behind the rotating tool, the material starts to move downwards and deposit in the wake. Most of the material flow in the FSW process is tangential. There is a swirl on the advancing side and with the increase of the translational velocity the inverse material flow on the advancing side becomes faster. The shoulder can increase the velocity of material flow in both radial direction and tangent direction near the top surface. The FSW process was modeled using a general purpose FE based program to produce a material thermal map and a corresponding mass flow [192]. Numerical thermal results were compared against experimental thermo-graphic maps and the numerical material flow results were compared using material flow visualization techniques, with acceptable agreement.

Transient-heat transfer models for both the tool and the workpiece in FSW processes were presented [193–195]. A moving coordinate was introduced to reduce the difficulty of modeling the heat generation due to the movement of the tool pin. The finite difference method was used in solving the energy equations. A non-uniform grid mesh was generated for the calculation in order to improve the temperature resolution near the tool. Material flow in FSW under different process parameters was simulated using the FE technique based on nonlinear continuum mechanics [196–198]. The distribution of the equivalent plastic strain correlates well with the distribution of the microstructure zones in the weld. The material flow can be accelerated with an increase in the translational velocity and angular velocity of the pin. The 3D material flow pattern can be compared with the 2D case to show that the material flow obtained in a 2D numerical simulation corresponds with the ones near the bottom surface obtained in a 3D simulation [199]. The equivalent plastic strain distribution also shows that the shoulder can affect the material flow behavior near the top surface and that the effect of the shoulder becomes weaker near the bottom surface. This demonstrated that the 2D case corresponds with the flow near the bottom surface in the 3D case.

The evolution of texture during the FSW of stainless steel was investigated using a poly-crystal plasticity model [200,201]. The influence of frictional conditions with the tool pin and shoulder on the flow in the through-thickness direction was examined in terms of their impact on the evolving crystallographic texture. Trends in the strengthening and weakening of the texture were discussed in relation to the relative magnitudes of the deformation rate and spin. The computed textures were compared to electron backscatter diffraction measurements and discussed with respect to their distribution along the orientation of the fibers and also with respect to the dominant texture components along the fibers. In a systematic study, a fully coupled thermo-mechanical model of the FSW process

was developed [202,203]. Results indicated that the rotation of the shoulder can accelerate the material flow near the top surface. The material deformation and the temperature field can also be related to the evolution of the microstructure. The texture and appearance of the FSW joints can correlate well with the equivalent plastic strain distributions on the top surface. The temperature field in the FSW process is approximately symmetrical around the welding line. The flows vary with differing thicknesses of material.

A study on the AA2024-T3 FSW process with different thicknesses of material was carried out [204]. The computed results showed that the material flow on the retreating and the front sides are higher. It follows that the slipping rates on the retreating and the front sides are lower than on the trailing and advancing sides. This is the reason why the heat fluxes on the trailing and the advancing sides are higher, which leads to higher temperatures in this region for both thin and thick plates. The energy entering the welding plate accounts for over 50% of the total energy and about 85% in the energy comes from the frictional heat in FSW of AA2024-T3. The balance of the heat is generated by mechanical effects. The FE method was used to model the material flow of alloy Al 6061-T6 in the FSW process and to establish the relationship between the flow of material and the angular velocity of the pin [205–207]. With an increase in the angular velocity, the material flow becomes faster. The material in front of the pin moves around in the direction of rotation and upward due to the extrusion effect of the pin. The material behind the pin is forced downward, during the continuous FSW process.

The direction of material flow during the FSW of transparent poly-vinyl chloride (PVC) was investigated using a high speed video camera [208]. The aim was to simulate the flows in aluminum alloys. At the same time, the velocity of material flow was measured by particle image velocimetry (PIV). The material flow was also numerically simulated using the DEFORM-3D FE software. Results indicated that the material flows in different directions at the advancing and retreating sides. Materil velocities ranged from about 2 to 20 mm/s at the advancing side and from 1 to 5 mm/s at the retreating side. The material behavior and the mechanical features in non-line welding were studied to help an understanding of the mechanism of FSW [209]. Results indicate that the material flow around the pin on the retreating side is much faster than that on the advancing side. Also the material near the top surface flows fastest. Moving the pin to the advancing side increases the material flow velocity around the pin. Varying the translational direction of the pin changes the distributions law of material flow.

The material flow in the FSW of aluminum alloy T-joints was investigated by Fratini et al. [210]. They varied the most relevant technological and geometrical parameters in both numerical simulations and experiments. Their research investigated the metal flow, a wide range of experimental tests and observations. They used a thin brass foil as marker, placed at the interface of the two blanks to be welded. Some relevant conclusions on the process mechanics and on the actual material flow determining the material bonding are outlined, permitting an insight into the FSW of T-joints. A 3D elastic–plastic and coupled thermo-mechanical FE model for FSW of 7075 aluminum alloy plate was developed based on the dynamic explicit code ABAQUS/explicit [211]. The FSW process of 7075 aluminum alloy plate was simulated and the material flow behavior was analyzed. The results showed that in the horizontal direction of the plate, two patterns of material migration are produced: (1) the material rotates with the tool and finally deposits the tentative cavity behind the pin; (2) the material transfers in the mode of laminar flow. A coupled thermo-mechanical viscoplastic FE model based on the character of FSSW was presented by Gao et al. [212]. The model was calibrated by comparing the temperature history obtained from the simulation with experimental data and subsequently used to investigate the effective strain distribution in the weld zone as well as the material flow and the shape of the stir zone. A coupled thermal/material flow model of the FSW process was developed and applied to the joining of Sc-modified aluminum alloy (7042-T6) extrusions [213]. The model revealed that surface material is pulled from the retreating side into the weld zone where it is interleaved with in situ material. Due to frictional contact with the shoulder, the surface material is hotter than the in situ material, so that the final weld microstructure is composed of bands of material with different temperature histories. Based on the numerical simulation and on thermal analysis data from differential scanning calorimetry, a mechanism for the formation of onion rings within the weld zone was presented.

Workpiece material flow and stirring/mixing during the FSW were investigated computationally by Grujicic et al. [214]. The FSW tool was treated as a Lagrangian component, while the workpiece

material was treated as an Eulerian component. The employed coupled Eulerian/Lagrangian computational analysis of the FSW process was of a two-way thermo-mechanical character, while temperature was allowed to affect mechanical aspects of the model through temperature-dependent material properties. The workpiece material was represented using a modified version of the classical Johnson–Cook model while the FSW tool material was modeled as an isotropic linear-elastic material. The results pertaining to the material flow during FSW were compared with their experimental counterparts. A finite volume model of the FSW was established on basis of the ANSYS FLUENT software and used to consider the practical geometry of the rotational tool and the relationship between the material parameters and temperature [215,216]. The effect of shoulder geometry and pin geometry on material plastic flow behavior was studied. The results showed that the flow velocity of material inside the weld is increased by reducing the cone angle of the pin or by decreasing the width of the screw groove. When a rotational tool with a left screw pin rotates clockwise, the flow direction of material near the pin is downward while the flow direction near the thermal–mechanical affected zone is upward, which is opposite to that for a right screw pin.

In previous simulation studies, the contact conditions occurring in the FSW are generally described as stick and/or slip, according to different methodologies but these descriptions have their limitations. A new combination method was presented for characterizing the contact conditions that occur during FSW processes [217]. The thermal and mechanical outcomes from models with prescribed stick and slip conditions were compared to identify the results and drawbacks of assuming different contact conditions. This new method yields more reasonable estimates of heat generation, as validated by the experimental thermal measurements. Thermo-mechanical simulations of the FSBW and FSSW processes were performed for AA5083-H18 sheets utilizing commercial FVM code [218,219]. Simulations were based on the Eulerian formulation. For the FSBW process, the computational fluid dynamics code, STAR-CCM+, was utilized under a steady state condition. It was found that by including the appropriate thermal properties of the backing plate (anvil), the accuracy of the simulation results increased significantly. For the FSSW process, the computational fluid dynamics code, STAR-CD, was utilized under non-steady conditions in order to understand the effect of pin geometry on material flow and weld strength.

A 3D viscous-plastic FE model can be established based on computational fluid mechanics. The material during the welding process is considered as non-Newtonian fluid abided by Norton–Hoff constitutive law, and viscous dissipation is assumed as the unique heat source. The model was used to numerically simulate the material flow and heat transfer in FSW processes [220]. The velocity field was used to calculate streamlines of material flow. 3D viscoplastic flow and heat transfer during the FSW of mild steel were investigated experimentally and theoretically by Nandan et al. [221]. The equations involving conservation of mass, momentum and energy were solved in 3D using spatially variable thermo-physical properties and a methodology adapted from previous, well-established work in fusion welding. Non-Newtonian viscosity for the metal flow was calculated, considering temperature and strain rate dependent flow stress. The computed results showed significant viscoplastic flow near the tool surface, and convection was found to be the primary mechanism for heat transfer in this region. 3D material flows under different process parameters in the FSW process of 1018 steel were studied using a rate-dependent constitutive model [222]. Numerical results indicated that the border of the shoulder can affect the material flow near the shoulder-plate interface. The mixture of the material in the lower half of the FSW can benefit from the increase in the angular velocity or the decrease in the welding speed. But flaws may occur when the angular velocity is very high or the translational velocity is very small.

2.6. Temperature distribution

In the FSW process, heat is generated by friction between the tool and the workpiece. Temperature measurements within the stirred zone are very difficult to make because of the intense plastic deformation produced by the rotation and translation of the tool. Therefore, it is important to obtain information about the temperature distribution during the FSW process by numerical analysis. Thermo-mechanical simulation of the FSW process can predict the transient temperature field, maximum temperatures, active stress forces and may be extended to determine the residual stress

in the joint [223–227]. A comprehensive 3D thermal FE model was proposed to enable the prediction of temperature distribution during an overlap FSW process [228]. The model accounts for moving heat generation caused by the rotation and linear traverse of the shoulder and pin as well as the convective/diffusive heat transfer caused by the plastic material flow in the vicinity of the shoulder and the pin. The contact pressure distribution and consequently the surface conductance at the contact surface between the sheets were modeled as varying, with the highest pressure being applied directly underneath the shoulder area. Temperature dependent properties of the weld-material have been used for numerical modeling. Ulysse presented an attempt [229] to describe the FSW process using 3D visco-plastic FE modeling. Parametric studies were conducted to determine the effect of various tool speeds on plate temperatures and to validate the model predictions using available measurements. The model can be useful in designing welding tools which will yield the desired thermal gradients. The FE mesh and the temperature distribution are showed in Fig. 9.

Transient thermal FE analyses were performed recently to obtain the temperature distribution in the welded aluminum plate during the FSW operation [230]. A moving heat source with a heat distribution simulating the heat generated by the friction between the tool shoulder and the work piece was used in the heat transfer analysis. The 3D modeling was carried out using the commercial ANSYS and HyperXtrude software. APDL (ANSYS Parametric Design Language) code was developed to model a moving heat source and to change the boundary conditions. Chao et al. [231] formulated the heat transfer of the FSW process into two boundary value problems (BVP) – a steady state BVP for the tool and a transient BVP for the workpiece. To quantify the physical values of the process, the temperatures in the workpiece and the tool were measured during FSW. Using the measured transient temperature fields, FE numerical analyses were performed to determine the heat flux generated by the friction

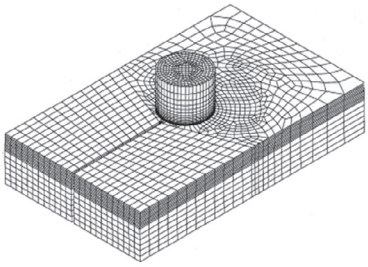

(a) FE mesh of the FSW model.

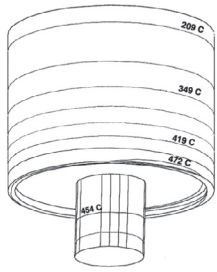

(b) Predicted isotherms (in °C) on an enlarged view of the stir-welding tool.

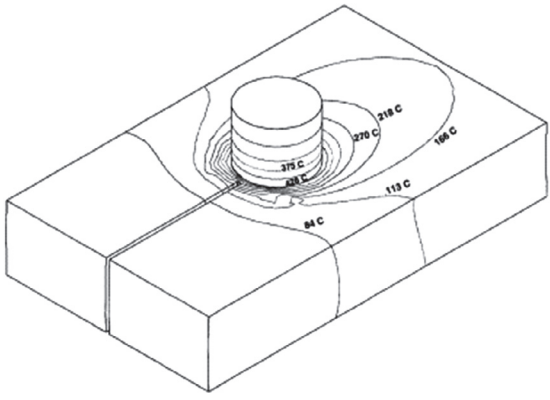

(c) Temperature contours (in °C) on the tool and workpiece surfaces.

Fig. 9. FE mesh and the temperature distribution in the FSW process [229].

between the workpiece and the tool. The results showed that (1) about 95% of the heat generated by friction is transferred into the workpiece and only 5% flows into the tool and (2) the fraction of the rate of plastic work dissipated as heat is about 80%. 3D FE analyses were performed to study the thermal and heat transfer phenomena of FSW of aluminum 6061-T6 plates with a thickness of 37.6 mm [232]. Two welds, one with a long pin and the other with a very short pin (to approximate the no-pin condition), were investigated. A simple model to estimate the heat generated from the tool shoulder as well as the pin was proposed. Issues regarding the effect of thermal contact conductance at the workpiece/back-plate interface and the effect of the length of the pin on the welding thermal profiles were investigated.

The FE software COMSOL, was used by Yin et al. [233] to develop a temperature field numerical model of FSW, including the heat generated by friction and by the plastic deformation of the material. The model was then used to calculate the temperature field of FSW in a quasi-steady-state for 1100 aluminum alloy, with the tool rotating at 750 r/min and traversing at 300 mm/s. The results showed a reasonably good match between the simulated temperature profiles and the experimental data. Inverse modeling has been used by Larsen et al. [234] to determine the magnitude and spatial distribution of the heat transfer coefficient between the workpiece and the backing plate in the FSW process. The objective was to minimize the difference between the experimentally measured temperature and the temperature obtained using a 3D FE model. It was found that the heat transfer coefficient between the workpiece and the backing plate is non-uniform and takes its maximum value in a region below the welding tool. This was the first study using a gradient based optimization method and a non-uniform parameterization of the heat transfer coefficient in an inverse modeling approach to determine the heat transfer coefficient in FSW. A FE simulation model was developed with improved capability to predict temperature evolution in stainless steel [235]. The simulation model was tested with existing experimental results on 304L stainless steel. The peak temperature obtained was 1057 °C, which was much less than the melting point of 304L steel (1450 °C). A fully-coupled thermal–mechanical FE model based on the arbitrary Lagrangian–Eulerian (ALE) method was used to numerically simulate FSW with the inelastic heat generation included in the model [236,237]. The temperature fields during FSW were simulated with rotational speeds of 600 and 800 r/min. The results showed that the numerical model can accurately simulate the temperature distribution of the FSW process.

Muci-Küchler et al.'s paper [238] presented a fully coupled thermo-mechanical FE model of the plunge phase of a modified refill FSSW. The model was developed in Abaqus/Explicit and the simulation results included the temperature, deformation, stress, and the strain distribution in the plates being joined. The simulation results were in good agreement with the temperature measured in the experiment. Also, the model was able to predict in a reasonable fashion, the stresses and plastic strains in the joints. The temperature distribution of the FSW process on 14 mm thick 2219 aluminum alloy was calculated by means of a 3D heat FE mathematical model and the ANSYS software [239]. In the stable welding stage, the temperature gradient presents a different distribution along the thickness direction of the plate, which is wide and high at the top but narrow and low at the bottom. The peak temperature can be increased by increasing the speed of rotation of the tool. A continuum-based FE model for the FSW of steels was proposed, which is 3D Lagrangian implicit, coupled and rigid viscoplastic [240]. The model can be used to predict temperature, strain and the strain rate distribution, together with thermal and mechanical loads on the welding tool, at varying main process variables. Xu et al.'s paper [241] summarized an experimental and numerical study of heat generation and dissipation during the FSW process. The work was aimed at optimizing the design of the welding tool and the selection of process parameters in manufacturing combat vehicle structures. An infrared camera and embedded thermocouples were employed to study the evolution of the temperature distribution during the FSW of 1-in. thick aluminum magnesium alloy 5083-H116 plate. The collected temperature–time data enabled a detailed quantitative analysis of the thermal process in FSW. The heat generation due to the tool-workpiece interaction, the heat loss through the tool and the anvil, and the temperature history in the weld stir zone were determined using FE analysis. The FSW sequence for aluminum alloy sheets with holes was studied using a coupled thermo-mechanical FE model [242]. The curve of 495–500 temperature variation and transient stress variation were obtained under different weld sequence during the FSW process. Good agreement between the FE simulations and the tests has been found.

High speed railway (HSR) manufacturing uses hollow aluminum extrusions as a new material and FSW is an innovative solid phase welding method for constructing carriages. A variety of weld joint designs were realized, which satisfy the features of FSW for a double skinned extruded aluminum alloy structure [243]. Simulations of moving heat sources using ANSYS-APDL were carried out and the temperature field during the FSW process was obtained. The calculated results are in good agreement with experimental data, which indicates the model's feasibility and accuracy. A 3D FE coupled thermal-stress model of the FSSW process was developed using Abaqus/Explicit code [244]. A rate-dependent Johnson–Cook material model was used for elastic–plastic work deformations. Temperature profile and energy dissipation history of the FE model were analyzed. The transient temperature distribution in 2024-T4 Al FSW joints was simulated using the thermal elastic–plastic FE model [245]. The temperature distribution of the weld gradually decreases toward the periphery in a radiate format, whose center is the probe, and the highest temperature in the weld can reach about 400 °C. Thermo-mechanical simulation of the FSBW process was performed for AA5083-H18 sheets, utilizing STAR-CCM+ (a commercial finite volume method (FVM) code) [246]. Distributions of temperature and strain rate histories were calculated under a steady state condition and simulated temperature distributions (profiles and peak values) were compared with experimental results. It was found that including a proper thermal boundary condition for the backing plate (anvil) is critical for accurate simulation results.

The influence of welding parameters such as the angular velocity of the pin, the radius of the pin, the radius of the shoulder, the cone angle, the screw-thread angle, etc., were studied in detail [247]. The results showed that the maximum temperature can be increased by increasing the angular velocity and the radius of the pin within the permitted limits of FSW. The results also showed that when the cone angle and screw-thread angle are increased, the maximum temperature is decreased. Rajesh et al.'s work [248] covered the FSW of A16061 and its thermal distribution based on an asymmetrical analytical model for the heat input into the matrix of Al plates from the FSW tool, due to the combined effect of the translation and rotational motion of the tool pin and shoulder. The heat distribution at the FSW joint in A1 6061 plate was plotted using a 3D FE heat transfer analysis program. The work concluded that the heat distribution obtained from the FE analysis was in reasonable agreement with experimentally measured values. Velocity fields and the initial plunge temperature profile were introduced in the steady state calculation of the temperature field during FSW [249]. The non-adiabatic heat transfer conditions between the tool, the work piece, and the backing plate were also applied to the model. A FE model of the FSW process used to make radar cooling boards was developed in ANSYS software. The model was based on an instantaneous relative linear velocity heat source and the distributions of temperature over time and space were analyzed [250]. The results showed that the temperatures change at each point throughout the FSW process.

A 3D computational fluid dynamic (CFD) model was used to simulate the control of the temperature of a FSW tool during the joining process [251]. The CFD software package FLUENT was used to create the numerical model. The simulation was executed in a small cluster computing environment to shorten the runtimes of the model. Within the model the temperature of the FSW tool was elevated and maintained at a temperature higher than temperatures normally experienced during the FSW process. The FSW tool temperature in the model was optimized to reduce the axial force experienced by the tool during joining. Computational results from the AL6061-T6 aluminum alloy FSW process showed that a region with lower plastic strain can be found behind the welding tool near the bottom surface. The region is formed as a result of the special material flow patterns in the FSW [252]. The distribution of the plastic strain on the top surfaces is similar to onion textures observed in the appearance of the FSW. Numerical investigations of the temperature distribution in the FSW plates were carried out using FE analysis, by Rangel et al. [253,254]. Their model includes friction between the workpiece and the fixed component, as well as the heat dissipation resulting from plastic deformation of the material. The model was found appropriate for estimating important welding characteristics, such as the heat-affected zone (HAZ), and the sensitivity to various welding parameters. The effect of backplate diffusivity on the temperature field of the workpiece was systematically investigated based on the numerical analysis [255]. The results showed that the backplate diffusivity has a significant influence not only on the peak temperature but also the final temperature distribution. With

increasing backplate diffusivity, the peak temperature decreases gradually while the average cooling rate increases at first and then decreases slightly.

FSW has a big potential in the casting industry, especially in high-pressure die casting (HPDC). FSW joints can be made between dissimilar materials such as aluminum casting alloys and technically pure aluminum. This kind of joint can be used to make an assembly from castings with different material properties or to join castings to make an assembly with inner cavities. The temperature distribution of the FSW joint of a cast aluminum alloy (AA413.0) and technically pure aluminum (AA1050) was investigated [256]. In the experimental work several FSW parameters were tested. During joining the temperature was measured with a thermocouple and the temperature distribution in steady state was calculated with the FE program SYSWELD. The microstructure and mechanical properties of the joint were investigated.

3. Microstructure of the FSW joints

Three distinct zones have been identified based on a microstructural characterization of grains and precipitates. These zones are a stirred (nugget) zone, a thermo-mechanically affected zone (TMAZ), and a heat-affected zone (HAZ) as shown in Fig. 10. The microstructural changes in the zones have significant effects on post-weld mechanical properties. Therefore, the evolution of the microstructure during FSW has been studied by a number of investigators [e.g. 8,257]. Murr's review [258] covered 18 reference FSW systems using the same materials and 25 FSW systems using dissimilar materials. The FSW of dissimilar materials systems differed from the systems using the same materials by the formation of complex, intercalated vortex, and related flow patterns. These intercalated, lamellar-like patterns represent solid-state flow by dynamic recrystallization (DRX) which facilitates unrecrystallized, block flow in the DRX regime. A detailed characterization of representative systems involving optical and transmission electron microscopy (TEM) was also presented. Residual microindentation hardness or other hardness measured across the weld face provides comparative performance signatures for the same material FSW systems in contrast to the dissimilar FSW systems. Hardness fluctuations or complex spikes occurring in the dissimilar systems were skewed from the weld centerline and were shifted when the tool rotation direction changed or the advancing side was reversed.

The properties of FSW joints can be characterized using optical micrographs, X-ray diffraction, and TEM. The shape, size, and distribution of precipitates in weld zones, and the strength and ductility of welds were seen to correlate directly with peak temperatures in weld nuggets and heat affected zones. FSBW in 6063-T4 aluminum alloy were obtained using square and two tapered tool pin profiles [259,260]. In tensile strength tests on transverse weld specimens tunnel defects were apparent at higher weld speeds using tapered pin profiles. These defects resulted in mechanical instabilities, i.e. sharp drops in load–displacement curves, well before macroscopic necking occured. Hardness contours in the weld cross-section suggest that loss in ductility is due to significant softening in the heat-affected zone on the retreating side. TEM images demonstrated that while recovery and overaging are responsible for softening in the heat affected zone, grain size refinement from dynamic recrystallization is responsible for strengthening of the weld nugget zone. X-ray diffraction studies in the three weld zones: weld nugget zone, heat-affected zone, and the base metal, corroborate these findings. A weld zone model, for use in forming simulations on FSW plates of naturally aged aluminum alloys, was proposed based on mechanical characterization tests.

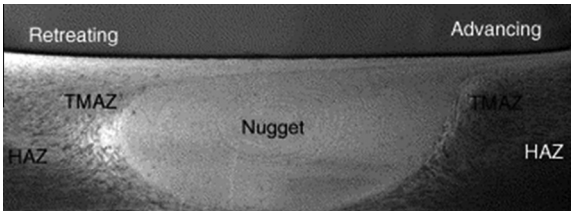

Fig. 10. Typical macrograph showing various micro-structural zones in FSP 7075Al-T651 (standard threaded pin, 400 rpm and 51 mm/min) [8].

3.1. Grain size

During the FSW process, the workpieces are welded together in a solid-state joining process at a temperature below the melting point of the workpiece material by a combination of extrusion and forging. Significant evolution of the microstructure takes place during FSW. In particular the continuous dynamic recrystallization (CDRX) phenomena result in a highly refined grain structure in the weld nugget and strongly affect the final joint resistance. In Fratini et al.'s systematic studies [26,30,261–264], some different analytical models aimed to determine the average grain size due to CDRX in the FSW processes of aluminum alloys. The models were implemented in a 3D FE model and numerical analyses of the welding processes were performed to verify their effectiveness. In particular, the models used, take into account the local effects of strain, strain rate and temperature. An inverse identification approach, based on a linear regression procedure, was utilized in order to develop the proper material characterization. Fig. 11. shows the material microstructures and grain size in a typical joint section [26]. The microstructural phenomena in terms of average grain size occurring in FSW processes were studied [262–264]. In order to predict the average grain size, a properly trained neural network was linked to the FE model of the process. The neural net took as inputs the local values of strain, strain rate, and temperature and was trained by starting with experimental data and numerical results. The results obtained showed the capability of the artificial intelligence (AI) technique in conjunction with the FE tool to predict the final microstructure in the joint section.

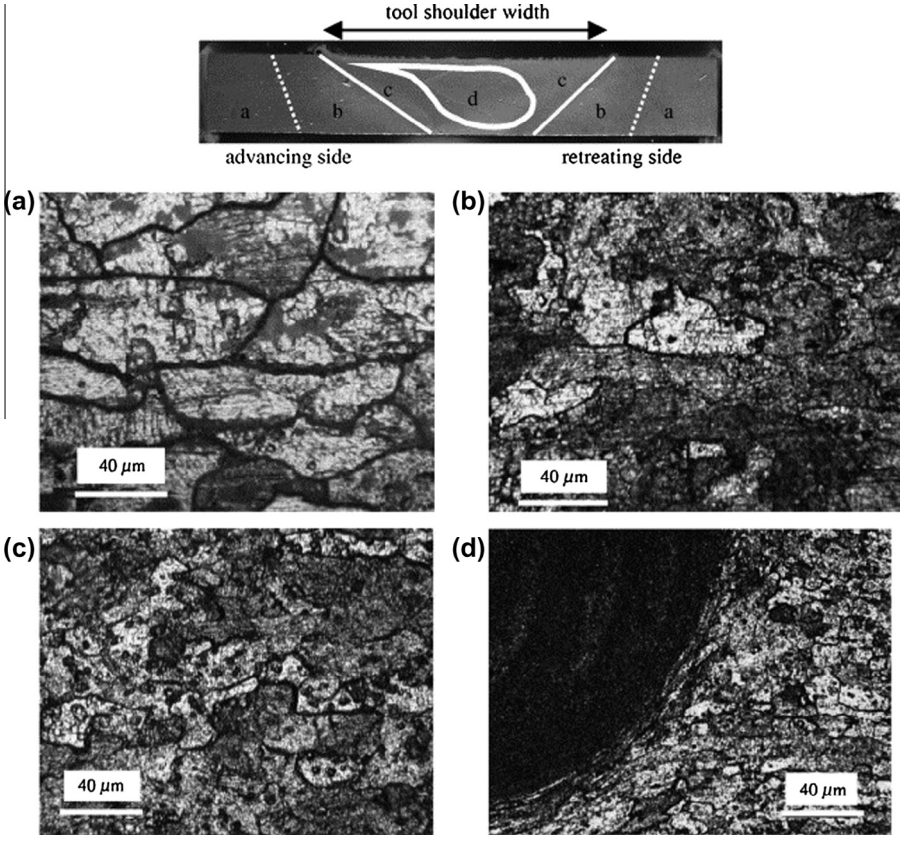

Fig. 11. Material microstructures and grain size in a typical joint section (AA 6082-T6). (a) Parent material. (b) Heat affected zone. (c) Ther mo-mechanically affected zone. (d) The nugget transition zone [26].

A cellular automata coupled finite element (CAFE) model can be used to predict the grain size distribution during FSW and to predict the influence of weld defects on the forming of FSW sheets. The FSW process was simulated by applying thermal and strain-rate analytical models to the elements constituting the FSW blanks, using the ABAQUS6.8 FE code with the help of the DFLUX sub-routine [265]. The final grain size and yield strength were predicted by generating transition rules, relating them to temperature, strain-rate and strain evolved during FSW. Predictions of the grain size and yield strength distribution from the CAFE model agreed well with the experimental results for all the FSW conditions. The true stress–strain behavior of a FSW blank obtained from the CA model (containing grain size and strength history after FSW) coincides well with the stress–strain behavior predicted from FE simulations. A cellular automata, finite element-artificial neural network (CAFE-ANN) hybrid model was developed recently to predict the evolution of grain size and yield strength during FSW [266]. It was demonstrated that a CAFE-ANN hybrid model can be used as a 'virtual machine' to predict and analyze the effect of parameters on the grain size and the evolution of yield strength. Thermo-mechanical behavior and microstructural evolution in the FSW of the dissimilar materials AA6061-T6 and AA5086-O were investigated [38]. Firstly, the thermo-mechanical behavior of materials during similar and dissimilar FSW operations were predicted using ABAQUS 3D FE software and then the mechanical properties and the developed microstructures within the welded samples were studied with the aid of experimental observations and model predictions. It was found that different strengthening mechanisms in AA5086 and AA6061 result in complex behaviors with respect to the hardness of the welded cross section. The hardness variation in similar AA5086-O joints mainly depends on recrystallization and generation of fine grains in weld nugget. However, the hardness variations in the weld zone of AA6061/AA6061 and AA6061/AA5086 joints are affected by subsequent aging phenomena.

Ultra-thin wall tubes were produced using a hybrid process combining FSW and spinning [267]. To evaluate the formability of the tubes, a relationship between the microstructure and the plastic deformation was examined, and hydraulic bulge performances were analyzed by FE simulation. The experiment results showed that fine-equiaxed grains are generated both in the weld nugget and base material during tube forming. The simulation results suggested that large circumferential stresses occur in the regions near and opposite the weld nugget. These lead to a great thinning of the tube at the final stage of hydraulic bulging. This thinning was also observed in the experiment. The mechanical properties of thick (>25 mm) aluminum alloy AA 2139-T8 FSW plates were studied numerically and experimentally [268]. A micro-hardness map of the weld was used to determine the geometry of individual weld zones. Micro-tension specimens of each weld zone were individually tested to develop constitutive models which were validated with a tension experiment on the entire weld. In particular, the failure mechanisms through the thickness of the weld and their relation to the microstructural zones that were formed during the FSW process were examined.

A numerical model based on the Kampmann and Wagner method was developed to predict the evolution of precipitate distribution during the FSW of the aerospace aluminum alloy, AA7449 [269,270]. The model considers both metastable and equilibrium precipitate phases and the transition between them. It also predicts the evolution of grain boundary precipitates and their effect on the size of the precipitate free zone. The model was calibrated against results from isothermal and quenching experiments. Subsequent predictions for welds showed good qualitative agreement between the model and observations. The microstructure of 6082 T6 alloy FSSW joints was extensively examined and a new modeling procedure that enables correct evaluation of the mechanical behavior of the joints was also developed [271]. The base metal had a mean grain size of 27 μm. In the nugget the grain size is not homogeneous and dislocation structures tend to form sub-boundaries of about 100–200 nm and; a distribution of fine and coarse precipitates. Tensile strength tests were carried out on tensile-shear specimens with a unique FSSW joint and on standard probes of the base metal. The elaboration of experimental results provides an information database for creating a numerical model of high complexity, with a high number of parameters. This should make it possible to simulate faithfully the experimental tests in both geometric and technological terms.

An investigation of the banded microstructure observed on horizontal transverse cross-sections in AA2024-T351 and AA2524-T351 aluminum FSW joints was carried out [272]. The results indicated the presence of periodic variations in (a) the size of equiaxed grains, (b) micro-hardness, and (c)

concentration of the base metal impurities that correlate with the observed band spacing. The latter trend is more distinct in AA2024-T351, which has a higher volume fraction of constituent particles resulting in easily recognizable, particle rich regions on horizontal cross-sections near the mid-thickness of the joint and well-defined variations in hardness. Results from numerical simulations of the FSW process enable interpretation of the trends in grain size along the weld centerline in terms of the time–temperature cycle experienced by the material. Texture patterns on transverse, longitudinal and horizontal cross-sections in the FSW were studied experimentally and numerically [273]. Numerical simulations of the FSW process were carried out to understand the texture patterns. Results suggested that the texture patterns are complex but a dominant theme is the appearance of bands, which occur in the advancing-side material. The texture patterns are found to correlate well with equivalent plastic strain contours from simulations of the corresponding FSW process, suggesting that the texture patterns may be formed because periodically spaced material regions experience very different levels of plastic deformation during the FSW process. FSW lap joints of Ti–6Al–4V were produced and the effect of the main process parameters was studied through macro and micro investigations highlighting mechanical resistance, microhardness profiles, grain size and phase distributions [274]. A dedicated numerical model was used to link the input process parameters to distributions of temperature and strain and to the final microstructure in the welded joint. It can be seen that the strain produced in the stir zone by the proper combination of process parameters plays a fundamental role in the final microstructure and mechanical properties of joints.

3.2. Nugget zone

The Gleeble hot compression tests can be used to study the material constitutive behavior and microstructure of aluminum alloys. The novel aspect of the work is that the testing was done at high strain-rates and at temperatures within 5 K of the solidus. The strength can be maintained up to near solidus temperatures, with no dramatic reduction in strength being observed [275]. The averaged grain size can be calculated for comparison with FSW nuggets. The materials mixing on both sides of the welding line in the nugget zone and in the thermo-mechanical zone was studied by means of the research on the equivalent plastic strain distributions under different process parameters [276]. Results indicated that the materials mixing can be improved when the angular velocity of the pin is increased or the welding speed is decreased, but some flaws may occur when the angular velocity of the tool is too high. The effect of process parameters on the CDRX and hardness in the nugget zone was studied in detail [32]. The distributions of microhardness on the top surface are different from those on the bottom surface of the FSW joints. The grain size near the bottom surface in the nugget zone is smaller than in the middle of the joint. The size of the grain in the nugget zone becomes more homogeneous with the increase of the angular velocity of the pin.

A prototypical solution strengthened and strain hardened aluminum alloy, AA5083-H131, was modeled using a fully coupled thermo-mechanical FE procedure [277]. Particular attention was given to the proper modeling of the material behavior of the work-piece during the FSW process. Competition and interactions between plastic deformation and dynamic recrystallization processes were considered to properly account for the evolution of the material microstructure in the weld nugget zone. The proper modeling of the material behavior under conditions of high-temperature and severe-plastic-deformation significantly improved agreement between the computed and measured post-FSW residual stress and the distribution of material strength. A 3D heat transfer FE model was employed to show the thermal history of the whole process and the temperature distributions for any position in the nugget zone [278]. Boundary conditions and material properties in thermal modeling of FSW which play a vital role in the final temperature profile were assumed as a realistic model. The variation of peak temperature with respect to thermal conductivity and specific heat was obtained. Using a moving heat source technique was proved to be a reliable method for simulating the FSW process. This new technique can be used to analyze stress and strain in this process.

The effect of axial load on the FSW process was studied using a fully coupled thermo-mechanical model [279]. Results indicated that insufficient axial load results in the failure of the FSW. The material deformation on the top surface is affected by the rotation of both the welding pin and the shoulder, which causes a larger material deformation on the top surface than near the bottom. The

asymmetry of the material deformation can be reduced by increasing the axial load. The temperature field near the welding tool in the nugget zone can become more homogeneous when the axial load is increased. The 3D material flows and mechanical features under different process parameters were presented by using the FE method, based on solid mechanics [35]. The distribution of the equivalent plastic strain can correlate well with the microstructure zones. The material in the nugget zone can be more fully mixed by increasing the angular velocity of the pin. Greater mixing improves the quality of joint between the two welded plates.

The weld nugget zone created by the FSW process for joining dissimilar materials was modeled using the novel approach of a time-varying Functionally Graded Material (FGM) concept [280,281]. In the real FSW process the weld nugget zone increases in size with time as the tool head travels along weld line of the specimens. This phenomenon was simulated by increasing the size of the FGM area while the welding tool was moving forward. The rate of growth of the FGM region was estimated from the rotational and forward velocities of the tool. For a 3D FSW model, time-varying material field simulations and corresponding thermal analysis were performed using ABAQUS®. The heat generated between the welding tool and the specimens' surfaces was modeled as a moving heat source. The user-defined subroutine DFLUX was used to model the moving heat source load. Thin copper sheets were embedded in the weld path in 2024 aluminum alloy plates as a marker and their final positions after the FSW was examined using metallographic techniques [282]. Referring to the visualized material flow patterns, a 3D model was developed to conduct the numerical simulation of the temperature profile and plastic material flow in the FSW process. The calculated velocity contour of plastic flow in close proximity to the tool is generally consistent with the visualized results. The predicted shape and size of the weld nugget zone match with the experimentally measured ones.

The dry sliding wear properties of the nugget zone of the FSW composites were analyzed using a pin-on-disc wear testing machine [283]. The presence of B4C particulates and fine grain in the weld nugget improved the wear properties. The relationships between the wear rate of AMCs and the FSW process parameters were established using a regression model. The developed regression model was optimized to minimize the wear rate using the Generalised Reduced Gradient (GRG) method. Numerous pits, grooves and wear tracks were observed in the microstructure.

3.3. Thermo-mechanically affected zone

The relationship between the microstructures of TMAZ and heat input in the FSW of 5086 aluminum alloy was investigated [284]. Welding heat input was predicted using a 3D FE analysis. Welding experiments were carried out under annealed and work-hardened conditions to study the resulting microstructures and mechanical properties of the welded metal. The results showed that the microstructures are strongly affected by the heat input, while grain size within the TMAZ decreases with decreasing heat input per unit length. In a similar study, thermo-mechanical responses, the developed microstructure, and the mechanical properties in FSW of artificially aged AA2017 plates were investigated [285]. A FE model was first employed to evaluate the hot deformation behavior of the alloy during welding. Also, hardness, yield strength, and the microstructure of the welded alloy were examined using the results from the model and from experimental testing. Considerable grain refinement was observed in the stir zone where recrystallized grains in the range of 3–8 μm were formed. Natural aging, particularly within the stir zone, also takes place after welding, while subsequent aging increases the yield stress by about 40 MPa in the stir zone. Steady-state FSW of 2014 A1 alloy was modeled using an Eulerian formulation that considers coupled viscoplastic flow and heat transfer in the vicinity of the tool [286]. The model equations were solved using the FE method to determine the velocity field and temperature distribution. With the result of velocity field and viscosity field, a criterion to divide the weld zone has been given.

The thermo-mechanical history of different regions of an HSLA-65 FSW was simulated to better understand the relationships between processing, structure, and properties [287]. The simulations consisted of both computational and Gleeble® studies. The computational modeling was conducted using an Eulerian FE formulation for coupled steady-state viscoplastic flow and heat transfer to determine the velocity field and temperature distribution in the process zone around the tool, including the thermo-mechanical history characteristic of the TMAZ in HSLA-65. The experimental simulations

involved taking the computational results and programming the Gleeble to deform specimens according to the calculated thermo-mechanical histories. The simulated microstructures and microhardnesses were compared with those in an actual FSW weld to validate the Gleeble simulation results and the Eulerian model results. Fratini et al's paper [288] presented the results of a combined experimental and numerical investigation focused on the effects of an in-process water cooling treatment aimed at improving the final quality of FSW butt joints in terms of mechanical resistance and metallurgy of the processed material. Micro and macro observations, together with the evolution of an already developed FE tool, were used to analyze specimens obtained under different process conditions. Water cooling was found to enhance joint strength, reducing the material softening usually observed in the TMAZ area, with no detrimental effect on nugget integrity.

A FE pseudo-steady state thermal model was developed taking the mechanical power as an input data [289]. The total power input is distributed between surface and volume heat sources. Based on the shape of the TMAZ, a simple model for the material flow around the tool was developed in order to take heat convection into account. Special attention was given to the type of contact at the tool-workpiece interface i.e. sliding, sticking or both. A small value of the material circumferential velocity at the tool interface compared to the tool rotating velocity is shown to give good prediction of the temperature difference between the advancing and retreating sides. A 3D thermo-mechanical simulation of ferritic stainless steel FSW processes was carried out utilizing an Eulerian finite volume method under the steady state condition [290]. Based on a viscoplastic self-consistent approach, the texture development in the FSWed material was determined from the velocity gradients along the streamlines in the material flow field. The heat is generated mainly near the interface between the tool and the workpiece. The viscosity changes drastically in the vicinity of the boundary between the stir zone and the TMAZ.

The 3D visco-plastic flow of metals and the temperature fields in the FSW were modeled by Nandan et al. [291] based on thermo-mechanical processing of metals. The equations of conservation of mass, momentum, and energy were solved in 3D using spatially variable thermo-physical properties and non-Newtonian viscosity. Non-Newtonian viscosity for the metal flow was calculated considering strain rate, temperature, and temperature-dependent material properties. The computed profiles of strain rate and viscosity were examined in light of the existing literature on thermo-mechanical processing. Significant asymmetry of heat and mass flow, which increased with welding speed and rotational speed, was observed. The numerically simulated temperature fields, cooling rates, and the geometry of the TMAZ agreed well with independently determined experimental values. The compression response of extruded aluminum 6061-T6 corrugated core sandwich columns was investigated [292]. Analytical equations that predict the collapse load were used to generate failure mechanism maps. From these maps dominant failure mechanisms can be identified as a function of various geometric parameters and material properties. To create longer columns the extruded panels are joined together using the FSW. Studies of the TMAZ showed that the hardness within these regions drops by approximately 50%. This significantly influences the observed failure load and failure mechanism and hence heat treatment post welding is required to ensure uniformity of properties.

3.4. Heat affected zone

A microstructure evolution model was developed and parameterized for the Ti–6Al–4V material residing in the HAZ [293]. Specifically, this model addresses the problem of the evolution of the globular a-phase particles located within prior β-phase grains (the dominant microstructural parameter in the HAZ) during the FSW process. Next this model is combined with the well-established property versus microstructure correlations in Ti–6Al–4V in order to predict the overall structural performance of the weld. The results suggested that the present computational approach may be used to guide the selection of FSW process parameters in order to optimize the structural performance of FSW joints (at least while they are controlled by the HAZ-material microstructure/properties). A continuum based FE model for the FSW process was proposed that is 3D Lagrangian implicit, coupled and rigid-viscoplastic [294]. The model was calibrated by comparing the output with experimental results of force and temperature distribution, and was then used to investigate the distribution of temperature and strain in the heat affect zone (HAZ) and the weld nugget. The model correctly predicts the non-symmetric

nature of the FSW process, and the relationships between the tool forces and the variation in the process parameters.

A 3D-analytical model of the stir zone around the FSW tool pin was developed [295]. In this model, the friction force during a steady state FSW process has been neglected as the material in this zone is plasticized and it has undergone plastic deformation rather than inducing friction at the tool pin boundary. The 3D-analytical model was used for FE analysis to predict heat distribution and based on this thermal history the residual stress distribution in the stir zone, HAZ and the base metal (Al6061-T6) were predicted and found in reasonable agreement with the experimentally measured values. Image-based FE simulations were used to investigate the variation of FSW mechanical properties with weld geometry in AA5456 [296]. FE meshes were generated based upon microhardness maps of the transverse cross-section. The mechanical response was calculated using parameters interpolated from the measured data. Multiple simulations were performed to determine the influence of the size and shape of the weld and HAZ on the distribution of stresses and strains in the weld and in simulated joints.

The heat inputs, temperatures, material flow distributions and the resulting local and overall tensile properties were compared for FSW in similar and dissimilar combinations of 2017-T6 and 6005A-T6 aluminum alloys [297]. Predictions of a 3D FE model of the tensile test transverse to the weldline were assessed towards local deformation fields measured by digital image correlation. Deformation systematically localizes on the weakest HAZ, which is on the 6005A side in joints with 2017-T6. The use of FSW on plastics has had very limited success due to their thermal and viscoelastic properties. Viblade is a new variant of FSW for plastics; this welding process heats the workpiece material by a blade and a shoulder which vibrate in a linear reciprocating motion parallel to the joint line. Design of Experiments (DoE) was used to investigate the influence of the process parameters and blade geometry on the width of HAZ and on the mechanical resistance of the joint [298]. Furthermore, a 2D FE thermal analysis was developed to analyze the thermal phenomena involved in the process. A new nonlinear time reversal technique was presented for the detection and localization of a scattered zone (damage) in a multi-material medium [299]. In particular, numerical findings on FSWed aluminum plate-like structure were reported. Damage was introduced in the HAZ and modeled using a multi-scale material constitutive model (Preisach–Mayergoyz space). Studies were conducted for two different transducer configurations. Particular attention was devoted to find the optimum time-reversed window to be re-emitted in the structures. The methodology was compared with traditional time-reversal acoustics (TRA), showing significant improvements.

Integrally Stiffened Panels (ISP) structures are composed of a base plate and one (or several) longitudinal stiffness sections of simple or complex shape. Three algorithms were studied and compared in the cross-section optimization of ISP for aeronautical applications [300]. Simulation models were introduced for panels with different stiffener cross sections. The presence of a FSW joining ISPs was also taken into account. This enables certain inferences to be drawn about the influence of a HAZ on the overall stability of the structure, under compressive buckling loads within the elasto-plastic regimen. Results showed that using the proposed optimization algorithm is a viable option, giving an added insight into the buckling resistance and mechanical design in nonlinear material and various geometric scenarios.

4. Properties of FSW joints

Academic and industrial interest is focused on the characteristics of the joined part in terms of mechanical resistance and fatigue resistance which are heavily related to the process parameters. Numerical analysis of process and mechanical tests of the FSW can add very useful information in defining how the process parameters influence the joint behavior [301,302].

4.1. Residual stress

Significant amounts of residual stress are often generated during the FSW process, resulting in critical degradation of the structural integrity and performance of components. Both tensile and

compressive residual stresses exist within the FSW joints. The maximum residual stresses are located in the HAZ, and the minimum compressive residual stresses are located on the advancing side just beyond the weld zone [8]. The ability to accurately predict residual stresses and resultant distortions is a key product from simulations of assembly processes.

A 3D FE model with general validity for different joint configurations was used by Buffa et al. [303] to simulate the FSW process of butt joints through a single block approach. The model is able to predict the residual stresses by considering thermal actions only, thanks to a new time efficient approach. A good agreement between calculated and experimentally measured data was found. The effectiveness of the presented numerical procedure was evaluated by comparing the calculation times of the proposed method with the ones of already known FE approaches. Figs. 12 and 13 show the configurations and the residual stress distribution simulation of the FSW joint separately.

In the FSW process the plates are heated, plasticized and jointed locally by the plunged probe and shoulder moving along the joint line. The residual stress due to the thermo-mechanical performance of the material and the constraint of the welded plates by the fixture are one of main concerns for this process. A prediction of the clamping force applied on the plates during FSW is expected to be helpful in controlling the residual stress and joint quality. Furthermore, the prediction of the force history in FSW process will be beneficial to understand the mechanics of the process and to provide valid models for controlling the process, especially in the case of robotic FSW. A 3D FE model can be used to study the thermal history and evolution of stress in the FSW process and subsequently, to compute mechanical forces in the longitudinal, lateral and vertical directions [304–306]. The relationship between the calculated residual stress of the weld and the process parameters such as the tool traverse and rotational speeds, and the fixture release were investigated and presented.

The ability to accurately predict residual stress and resultant distortions is a key product from simulations of assembly processes. These simulations necessarily consider large structural components potentially making the simulations computationally expensive. The objective of McCune et al.'s paper [307] was to develop greater understanding of the influence of the FSW process idealization on the prediction of residual stress and distortion and thus determine the minimum required modeling fidelity for future airframe assembly simulations. The combined computational and experimental results highlight the importance of accurately representing the welding forging force and the process speed. A 2D model of FSW was used to study the distributions of the longitudinal residual stress and the material flow under different process parameters [308]. The maximum longitudinal residual stress occurs on the boundary of HAZ and the longitudinal residual stress is positive near the welding line but negative near the boundaries of welded plate. The maximum longitudinal residual stress can be increased with the argument of the translational velocity of pin. But the change of the angular velocity of pin does not affect the longitudinal residual stress significantly. The scale effect of the pin size on the FSW process was investigated [309]. The flow of the material in the tangential direction is the main contributor to the movement of the material in the FSW process. A fluidized bed of material flow comes into being around the pin. With the increase of the pin's diameter, the laminar flow becomes

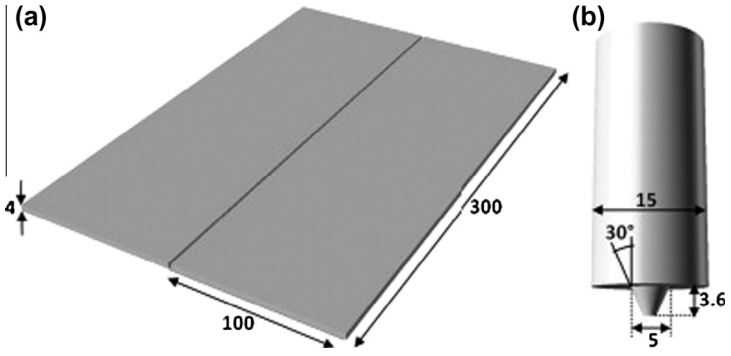

Fig. 12. Sketch of the used (a) joint and (b) tool geometries [303].

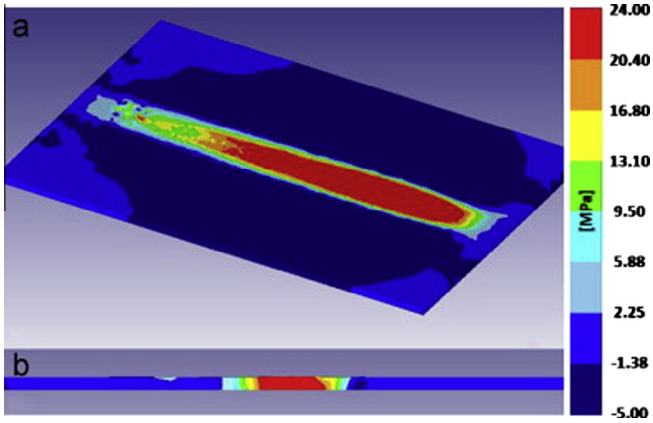

Fig. 13. Longitudinal residual stress distribution (a) on the top surface and (b) in a transverse section of the joint—500 rpm and 225 mm/min case study [303].

much easier to observe. The maximum longitudinal residual stress occurs in the boundary of the HAZ. The double peak feature of the longitudinal residual stress can be found.

Thermo-mechanical simulation of FSW can predict the transient temperature field, active stresses developed and the forces in all the three dimensions and may be extended to determine the residual stress. A FE thermo-mechanical model with mechanical tool loading was developed using a uniform value for the contact conductance [310]. The model was used for predicting the stress at the workpiece and backplate interface. Pressure distribution contours were used to define the non-uniform adaptive contact conductance used in the thermal model for predicting the thermal history in the workpiece. The thermo-mechanical model was then used to predict the development of stresses in FSW. FSW processes can introduce undesirable residual stress and distortions in the final fabricated components, as well as localized loss of mechanical properties at the weld joints. The aim of Murphy et al.'s research [311] was to determine and characterize the key process effects of FSW assembly methods on the static strength of stiffened panels. Utilizing experimentally validated FE modeling methods, it was demonstrated that FSW induced residual stresses have a significant influence, and that collapse behavior is less sensitive to advanced process effects and process effect magnitudes than initial buckling behavior in the panel.

FSW processes used to build large stiffened structures are responsible for introducing geometrical imperfections, changing the material properties and adding residual stresses. These factors can affect the panel's structural behavior when subjected to compressive loads. The longitudinal residual stresses that arise from FSW processes were measured by means of the contour method [312]. These residual stresses were then introduced into a numerical simulation model based on FEM, and their effect on the buckling collapse load was assessed. The sensitivity of the models to initial geometrical imperfections was also analyzed. It could be inferred that the collapse loads showed no relevant sensitivity to the inclusion of the residual stresses in the tested model, being nevertheless affected by small variations of the initial geometrical imperfection magnitude. In order to reduce the residual stress and distortions of large aluminum alloy sheets after FSW, a general method adopted is incoporate stiffeners into the sheet before FSW. The process of FSW of structures (sheet with stiffeners) was numerically simulated [313]. The distortion pattern is convex in the longitudinal direction and concave in the transverse direction after FSW. The distortion shape of structure is similar to that of sheet, but the amount of distortion is much smaller for structured material. A comparison of simulation results showed that the residual plastic strain generated by FSW on the sheet and the structure is nearly the same. The longitudinal distributions of residual stress in FSW joints were investigated for butt and skin-stringer geometries, including lap and T configurations [314]. To measure residual stress, the cut-compliance and the inverse weight-function methodologies were adapted for skin-stringer

FSW geometries via FE analysis. The effects of most relevant process parameters as well as the cooling following the FSW process were investigated to better understand the welding residual stresses. The FSW of complex skin-stringer geometries produces higher residual stress than those of butt joints, and cooling with water reduces the magnitude of the residual stress. Changes of process parameters did not affect markedly the residual stress distribution.

The internal longitudinal stresses in 4 mm and 8 mm thick AA6061-T6 aluminum alloy FSW specimens were measured using a contour method [315]. The longitudinal residual stresses throughout the cut plane for the two joints were mapped, and the through-thickness longitudinal stresses of the two FSW joints were also analyzed. The longitudinal stress distribution in the present study is not an apparent M-shaped distribution in the transverse direction. The peak tensile longitudinal stresses for both joints reached 168 MPa (amount to 61% of the yield strength of AA6061-T6 alloy at room temperature), and appeared at a depth of 62.5% thickness at the edge of the tool shoulder on the advancing side of the weld. A FE analysis was used to develop three innovative rolling methods that reduce residual stress and distortion in FSW [316]. Of the three methods, post-weld direct rolling where a single roller is applied to roll the top surface of the weld after the weld metal has cooled to room temperature proved the most effective. The effectiveness of using post-weld direct rolling was illustrated with an industrial example of a large integrally stiffened panel, where the distortion was virtually eliminated.

In an attempt to map the residual stress distributions after the FSW of copper canisters, a 3D thermo-mechanical model was formulated by Jin and Sandström [317] coupling heat transfer and elasto-plasticity analyses. The simulation showed that the residual stress distribution in a thick-walled copper canister is sensitive to the circumferential angle and asymmetrical to the weld line. Both tensile and compressive stresses emerge along the weld line and its vicinity. The maximum tensile stress, whether it is predicted by the FE method or measured by the hole-drilling technique and the X-ray diffraction method, does not exceed 50 MPa in general. A sequentially coupled FE model of the FSW process was used to study the residual stress caused by the thermal cycles during the FSW of metals [25]. This is a two steps simulation process. In the first step, the thermal history is predicted from an input torque based thermal model. The temperature history generated by the thermal model is then sequentially coupled to a mechanical model that predicts the residual thermal stresses. The model does not deal with the severe plastic deformations within the weld nugget and the TMAZ, a fact that may cause modeled results to deviate from experimentally measured residual stress. The model is 3D and uses temperature dependent material and thermo-physical properties. Three different materials, AA-2024, AA-6061 and SS 304 L, have been studied.

The effect of active cooling on the development of welding stresses during FSW was investigated [318]. The primary aim was to see if cooling as currently attainable using liquid CO_2 cooling systems applied in practically feasible locations could bring about a significant reduction in residual stress. The simulations revealed that a large reduction in residual stress can be obtained, particularly at the weld line, depending on the size, power and positioning of the cooling sinks. All the approaches tended to reduce the weld centerline stress more effectively than those at the HAZ/TMAZ boundary (i.e. below the edge of the tool shoulder). The laser-ultrasonic technique was investigated as a means for defect detection and sizing as well as for residual stress measurement in joints obtained by FSW [319]. When combined with the Fourier domain synthetic aperture focusing technique, very good performances are achieved for detecting lack of penetration in butt joints, the detection limit coinciding with the conditions of reduced mechanical properties. Also, the detection of kissing bonds seems to be possible in lap joints when probing with ultrasonic frequencies up to 200 MHz. Residual stresses induced by the FSW process can also be probed by laser ultrasonics. The residual stress profile measured across the weld line is in good agreement with results from a FE model and from strain gauge measurements.

An analytical framework was presented for predicting the residual stresses that result from the laser shock peening of a FSW 2195 aluminum alloy sample, using the FE software LS-DYNA [320]. The pressures resulting from the laser peening were directly applied in an explicit transient analysis as forces. At the completion of the transient analysis, an implicit spring-back analysis was performed to determine the final residual stresses. To validate the analytical framework, a comparison of residual stresses between analysis and a test specimen was made using laser-peened base material which was not friction stir-welded. In this work, the varying material properties and regions were simplified and

defined as discrete, separate materials. The residual stresses resulting from the welding were introduced directly as initial conditions in the peening transient analysis and were combined within the analysis with the residual stresses from the peening. Analysis of the laser shock peening of FSW had not been accomplished previously. The blind-hole method was used to study the residual stresses of FSW Al alloy LY12 plates with different welding parameters [321]. The strain releasing coefficients A and B were corrected based on the energy parameter which was obtained by the FE analysis results. The results showed that longitudinal residual stresses were asymmetrically distributed at different sides of the weld center and were high at the advancing side and relatively low at the retreating side. The transverse residual stresses were about 12.7% of base metal.

Combining moire interferometry to obtain the relaxed whole-field displacement data with a hole-drilling technique can be used to solve non-uniform residual stress problems, both in-depth and in-plane. The theory of moire interferometry and incremental hole-drilling for non-uniform residual stress measurement was introduced [322]. A 3D FE model was constructed using ABAQUS, to obtain the coefficients for the residual stress calculation. An experimental system including real-time measurement, automatic data processing and residual stress calculation was established. The applications for non-uniform in-depth residual stress of surface nanocrystalline material and non-uniform in-plane residual stress of FSW were presented. A steady-state simulation of FSW was carried out by Bastier et al. [323]. The simulation included two main steps. The first one uses an Eulerian description of the thermo-mechanical problem: a 3D-mixed FE Model based on a Computational Fluid Dynamics package was used to establish the material flow and the temperature field during the process. In the second step, a steady-state algorithm based on an elastoviscoplastic constitutive law was used to estimate the residual state induced by the process. It was observed that the longitudinal residual stress field had a two peaks profile: these two peaks are situated in the zone with a steep gradient of dissolved precipitates. The parametric study showed that the higher the welding speed and the lower the rotational speed, the lower the temperatures and residual distortions.

The general principles behind the global mechanical tensioning technique for controlling weld residual stress were examined by using a FE model to follow the evolution of stresses throughout the welding process [324]. For aluminum alloy FSW joints, the maximum longitudinal weld stresses have been reported to fall approximately linearly to zero under mechanical tensioning to a level around 40% of the yield stress. Under larger tensioning levels, the weld stress becomes increasingly compressive. This behavior is explained in terms of the reduction in compressive plastic straining ahead, and an increase in tensile plastic straining behind, the heat source as the tensioning level is increased. Finally, it was shown that tensioning during FSW is much more effective than post-weld tensioning. In Sonne et al.'s paper [10], a numerical model consisting of a heat transfer analysis based on the Thermal Pseudo Mechanical (TPM) model for heat generation, and a sequentially coupled quasi-static stress analysis with a built-in metallurgical softening model was implemented in ABAQUS. Both isotropic and kinematic rules of hardening were used in order to study the effect of the hardening law on the residual stress as well as on the final yield stress. The comparisons between simulations and experiments showed good agreement with respect to temperatures. However, the residual stress comparisons indicated different sensitivities for the cold and hot welding conditions in the choice of hardening rules and especially whether to include the softening model or not.

An equilibrium-based, weighted least-squares algorithm was developed to reconstruct the complete residual stress field tensor throughout the specimen volume using a limited set of residual stress measurements and a priori boundary conditions [325]. A set of residual stress data acquired by neutron diffraction over a limited region of an AA2024-T351 FSW specimen, was used to reconstruct the complete residual stress tensor field. 3D numerical simulations were carried out to investigate the residual stresses generated by FSW [326]. The modeling was carried out using two FE commercial programs (SYSWELD and MARC). The thermal stage of the process was simulated by using two different numerical heat sources (a 2D and a 3D source, one with each program). The numerical heat inputs were calibrated with the help of experimental results obtained by using thermocouples and infra-red cameras. The mechanical characteristics of all the re-crystallized materials involved were determined notably by micro-tensile tests and then used in the calculations. Finally, experimental measurements of FSW residual stresses made by neutrons diffraction were compared with the numerical residual stresses calculated using both programs. An FE model was used to examine the

effectiveness of the mechanical tensioning technique for controlling residual stresses in FSWs. This was done by studying the trends resulting from changes to the welding parameters [327]. Comparisons between different geometries, traverse speeds, and welding off-axis angle all produced consistent results, and showed that the peak stresses are most strongly influenced by both the local tensioning and heat input, and not by the more global welding conditions. The results also showed a progressive decrease in the residual stresses for increasing tensioning levels and, although affected by the heat input, a relatively low sensitivity to the welding variables.

The influence of alloy type and welding parameters on the magnitude and distribution of residual stresses across the FSW was investigated [328]. The magnitude of stresses is far below the room temperature yield strength of the base material. A distribution with an "M-shape" was always found on age hardenable structural alloys (albeit more pronounced in 6082-T6 alloy than in 2024-T3 alloy), while a "plateau" was found in the case of the strain hardenable 5754 H111 alloy. The low magnitude and the differences in distribution of the longitudinal residual stress are attributed mainly to the microstructural changes in the weld center. A 3D numerical simulation of the FSW was carried out to study the impact of tool traverse speed in relation to heat distribution and residual stress [329]. Material characteristics were introduced into the proposed model as temperature-dependent parameters. The resulting residual stresses indicated that heat distribution along thickness varies and is distinctly asymmetrical. In predicting the resulting residual stress, only the heat impact was studied. This was recognized as the main element causing minor differences in results obtained for simulation compared with experimental results.

The innovative production methods Composite Extrusion and FSW were used to manufacture lightweight frame structures made of steel reinforced aluminum [330]. In order to optimize the processes themselves and the manufacturing of frame structures both processes were analyzed in a structural simulation. The results showed that it is possible to chain the simulations of different manufacturing processes. The chaining was realized by modeling a cooling step as a representation of the extrusion process and by using a model for the FSW as the second analysis step. This second step included a heat and force source. The simulation results were compared with measurements of the residual stresses by means of neutron scattering. The mechanical behaviors of 6056-T6 Al alloy FSW panels were studied [331]. A numerical model was established to simulate the distortion, temperature field and stress fields. The panel bent down along welding direction and maximum distortion reached 6.3 mm. In die transverse direction, the panel bent up relatively to the longitudinal sides and the maximum displacement was 4.5 mm.

Ultrasonic measurements can be used to quantify through-thickness residual stresses in FSW of aluminum plates. The ultrasonic measurement technique is based on an acoustoelasticity law which describes the relation between the acoustic waves and the stress of the material. The ultrasonic stress measurement is accomplished by using longitudinal critically refracted (LCR) waves which are propagated parallel to the surface within an effective depth. The distribution of through-thickness longitudinal residual stresses can be evaluated using the LCR waves produced by four different frequencies (1 MHz, 2 MHz, 4 MHz and 5 MHz) of ultrasonic transducers. Utilizing the FE analysis along with the LCR method (known as FELCR method), the through-thickness longitudinal residual stress distribution of the FSW 5086 aluminum plates was achieved [332]. The comparison between ultrasonic measurement and FE simulation results showed an acceptable level of agreement. Hence the FELCR method could be successfully applied to the FSW plates.

4.2. Damage modeling

The numerous material and gauge combinations pose a major challenge in characterizing and understanding the mechanical behavior of the FSW joints. Damage modeling is being increasingly used to simulate fracture processes in the FSW joints. Since the weld zone dimensions have minimal discrepancy along the welding direction, 2D plane strain FE models are frequently used to simulate the elastic–plastic behavior of the FSW joints.

The evolution of voids (damage) in FSW processes was simulated using a void growth model that incorporates viscoplastic flow and strain hardening of incompressible materials during plastic deformation [333]. The void growth rate is expressed as a function of the void volume fraction, the effective

deformation rate, and the ratio of the mean stress to the strength of the material. A steady-state Eulerian FE formulation was employed to calculate the flow and thermal fields in three dimensions, and the evolution of the strength and damage was evaluated by integrating the evolution equations along the streamlines obtained in the Eulerian configuration. The effects of pin geometry and operational parameters such as tool rotational and travel speeds on the evolution of damage were also examined. Borino et al.'s paper [334] analyzed mechanical response by a FE method up to decohesion failure in fracture mode I for joints of FSW of an aluminum alloy. It first described experimental investigations on specimens with FSW embedded, subjected to uniform traction and local punch tests used to characterize local elastic and plastic material parameters. The heterogeneity of the mechanical properties induced by the FSW process was taken into account for the elastic–plastic FE simulation. The growing damage and the opening failure of the welding zone were described by the adoption of a cohesive interface model with specific mechanical properties.

The development of ductile damage in a FSW aluminum joint subjected to tension was analyzed numerically using FE method based on a total Lagrangian formulation [335]. An elastic-viscoplastic constitutive relation that accounts for nucleation and the growth of microvoids was applied. The main focus in the paper was on the interaction between changes in the material parameters in different regions of the weld, the development of damage and the position of the final fracture. Changes in the yield stress profile transverse to the weld-line were examined especially, since some process parameters have been shown experimentally to affect this. It was found that the development of damage is highly influenced by changes in the yield stress profile and a shift in the final failure was shown for comparable yield stress in the TMAZ and the nugget zone. A coupled thermo-mechanical 3D FE model was developed for FSW using ABAQUS, including the Johnson–Cook material law and the Johnson–Cook failure model [336]. The temperature evolution during the plunge, dwell and moving stages of a FSW 7050 aluminum alloy and the effect of heat conduction by the back plate were investigated. Results showed that the temperature distributes almost symmetrically across the plate cross-section, and the temperature contour in the weld nugget zone (NZ) presents a V type shape after the plunge stage. Moreover, it was shown that the heat conduction through the back plate has a significant effect on the temperature field. Fratini et al. [337] presented an improved continuum FE model for the simulation of FSW processes to produce T joints, made of a stringer in AA7175-T73511 and a skin in AA2024-T4. The model, taking into account the thermo-mechanical behaviors of the two different materials was used to study the material flow and the residual stress state. Numerical results were compared with experimental observations: the model is able to predict the material flow, obtaining important information on the joint failure mode.

Force measurement in FSW provides a significant insight into the process in terms of machine and tool limitations and design. The tool forces were investigated experimentally by using a rotating component dynamometer and a FE model [338]. The model correlated well with the observed temperatures and tool forces and was capable of predicting tool forces for different welding parameters, predicting regions were tool failure is likely to occur and identifying tool pin designs which can process the workpiece more efficiently. The effects of the implementation details of the weld on the accuracy of the failure prediction, strain distribution, and springback behavior of FSW Tailor-welded blanks (TWB) were studied for two benchmark problems, namely the limiting dome height (LDH) test and the S-rail problem [339,340]. The effects of the weld detail implementation on the simulation time were also considered. The Marciniak–Kuczynski (MK) theory was used to predict the forming limits diagrams (FLDs) of the different zones of the studied FSW TWBs. The MK imperfection parameters were obtained by fitting the theoretical FLDs to the experimental tensile test failure limits.

The failure loads for a spot FSW joint of two aluminum alloy 6061-T6 sheets under specific loading cases were predicted using the FE method [341]. The detailed modeling technique of a spot FSW joint using available experimental data was presented in this paper. The mechanical properties calculated from a relation between the measured hardness values and the corresponding strengths for each zone were then applied to the failure prediction model. In this model the ESI-Wilkins-Kamoulakos (EWK) rupture model of the PAM-CRASH commercial software was employed to verify the case of the lap-shear tension test. The failure load obtained in this model showed a good agreement with the experimental value in the reference. The failure prediction for the other loading cases (peel-tension test and cross-tension test) was then conducted following the same analysis procedure. Post-buckling

failure of welded aluminum panels was studied [342]. A global–local FE method was developed to resolve the stresses and strains in the welds of post-buckled stiffened panels subject to compression and shear. This method can be used to evaluate weld failure criteria. A similar approach can be used to investigate fracture mechanics-based approaches to the prediction of skin-stiffener separation. A 3D localized FE model was developed to predict likely conditions that could result in the generation of defects during FSW [343]. The workpiece was modeled using an Eulerian formulation, while the tool was modeled using a Lagrangian approach. The Coulomb's frictional contact model was adopted to define the interaction between the tool and the workpiece, while the welding speed was defined by material inflow and outflow velocities. The numerical results showed that the friction coefficient has a major effect on void formation. A lower friction coefficient results in larger void sizes. A lower welding speed results in smaller void sizes and a wider plastic zone which results in higher quality welds.

A new non-destructive testing (NDT) system focusing on micro size superficial defects in metallic joints was developed [344–346]. The innovative system uses a new type of eddy current probe, electronic devices for signal generation, conditioning and conversion and automated, mechanized, scanning and analysis software. The new probe provides enhanced lift-off immunity and improved sensitivity for micro size imperfections. The probe concept was studied using a FE method tool and verified experimentally using a standard defect. The testing results on some FSW specimens clearly showed that the system is able to detect superficial defects less than 60 μm deep, which significantly increases the actual state of the art in NDT reliability for detecting micro imperfections.

Analytical stress intensity factor and *J* integral solutions for resistance and FSSW with and without gap and bend in lap-shear specimens of different materials and thicknesses were developed [347]. The analytical stress intensity factor solutions were selectively validated by the results of 3D FE analyses for a spot weld with ideal geometry and for a FSSW with complex geometry, gap and bend. Sagar et al.'s paper [348] presented results on high-frequency ultrasonic imaging of the FSW joints between different materials. The unique feature of this paper is the use of high numerical aperture lenses that allow the excitation of leaky surface acoustic waves. These interact with weak joints, producing to produce interference patterns in incident and reflected waves at weak joint interfaces. The interference provides a vivid contrast, marking the weak interface joint as an easily recognizable feature. The authors presented a description of the high-frequency lenses, simulation of the contrast phenomenon and the application of the technique to FSW joints. The quality of FSW joints inferred from the images was correlated to the tensile fracture experiments. The comparisons showed that improperly bonded specimens had a relatively larger number of flaws. The results suggest that high-frequency acoustic microscopy is a useful method for the diagnostic evaluation of FSW joints.

4.3. Hardness

The hardness in the nugget zone is higher than that in HAZ and TMAZ, and an area of maximum hardness is located around the center of weld, whereas outside of this region, hardness reduces slightly in TMAZ and HAZ, and then rises sharply, moving towards base metal [349]. A mechanical and metallurgical characterization of FSW butt joints of aluminum alloy 6061-T6 with 6082-T6 was carried out [350]. For comparison, similar material joints made from each one of the two alloys were used. The work included an examination of microstructure, micro-hardness, tensile and bending tests for all joints. The results showed that in the hardness profile the lowest values were obtained in the AA6082-T6 alloy plate side where rupture occurred, and in the nugget all type of joints presented similar values. A fully coupled thermo-mechanical FE model was used to predict the FSW behaviors of AA5083 and AA2139 aluminum alloys [351]. In the case of non-age-hardenable AA5083, the dominant microstructure-evolution processes taking place during FSW are extensive plastic deformation and dynamic re-crystallization of highly deformed material subjected to elevated temperatures approaching the melting temperature. In the case of AA2139, in addition to plastic deformation and dynamic recrystallization, coarsening of precipitates, over-aging, dissolution, and re-precipitation also had to be considered. Limited data available in the open literature pertaining to the kinetics of the aforementioned microstructure-evolution processes were used to predict variation in the material hardness

throughout the various FSW zones of the two alloys. The computed results were found to be in reasonably good agreement with their experimental counterparts.

A real-time temperature measuring system can be used to measure the temperature change in the FSW process. Vickers hardness profiles were made on the cross-section of the joint after welding. The commercial software FlexPDE, a solver for partial difference equations with a FE method, was used to simulate the experimental FSW process [352]. The temperature distribution profile obtained from the simulation is symmetrical to the weld center and has a close correspondence with the hardness configuration. The region with the temperature over 300 °C is the zone of softening within the boundaries of base material and HAZ. The regions of 350 °C with minimum hardness are located near the boundary of HAZ and TMAZ. The maximum temperature about 500 °C distributes around the upper part of the weld center. However, the region above 400 °C only matches with the upper half of the weld nugget. Woo et al.'s paper [353] described a method that can predict the location of minimum hardness as a function of natural aging time in a heat-treatable 6061-T6 Al alloy plate subjected to FSW. The temperature distributions were simulated in the FSW plate by FE analysis. To determine the natural aging kinetics, hardness changes were measured as a function of natural aging time from a number of Al specimens that had been isothermally heat treated at different peak temperatures. The simulated temperature profiles and the kinetics of natural aging were correlated to predict the hardness profiles in the FSW plate. The predicted minimum hardness locations are consistent with the measured hardness profiles in that the hardness moves away from the weld centerline as the aging time increases. More interestingly, the predicted minimum hardness is located at a similar position of failure in cross-weld tensile samples.

Strain hardening and damage in 6005A-T6 aluminum alloy FSW joints were investigated using micro-hardness measurements, tensile testing and scanning electron microscopy (SEM) [354]. The locations of the various weld zones were determined by micro-hardness indentation measurements. The measured material properties and weld topology were then introduced into a fully coupled micro-mechanical FE model, accounting for nucleation and the growth of voids as well as the evolution of void shape. The model showed satisfactory preliminary results in predicting the tensile behavior of the weld and the true strain at fracture. Joint properties and thermal behaviors of FSW age hardenable 6061Al alloy were evaluated [355]. The surface bead width was observed to be gradually decreased with increasing welding speed and the hardness distribution of the welded zone showed lower value than that of the unaffected base metal, and tensile tests showed that the HAZ was the weakest region in the weld. A numerical simulation was executed against the FSW zone using a newly developed thermo-elastic–plastic finite analysis to examine thermal behaviors.

4.4. Static behavior

The asymmetric material flow, severe plastic deformation and thermal cycle imposed on the base material during FSW result in unique microstructural development, which causes a gradient in local mechanical properties in the weld region. Micro-tensile and indentation testing were used to determine the local mechanical properties in a FSW joint [356]. Experimental and numerical studies on the formability of FSW tailor welded blank sheets. Observations were based on hemispherical dome stretch tests carried out on five automotive sheets, 6111-T4, 5083-H18, 5083-O aluminum alloy, dual-phase steel (DP590) and AZ31 magnesium alloy [357]. The non-quadratic orthotropic yield function, Yld2000-2d, was used for the numerical analysis, of the mechanical properties of the aluminum alloy and DP590 sheets, while the Cazacu anisotropic/asymmetric yield function was used to investigate different hardening behavior in tension and compression for the AZ31 sheet. The local stress–strain curves exhibited a drastic change at the advancing side due to a steep gradient in mechanical properties. FE model predictions of the tensile performance of the joints, based on the local mechanical properties measured by micro-tensile testing, were in very good agreement with the macro-tensile test data. Numerical investigations focussed on the temperature distribution in the material during the FSW process were carried out by Fratini et al. [29] with the objective of improving the mechanical performance of FSW on aluminum alloy blanks of different thickness ratios. They derived a few simple process design rules and verified them through experiments. In particular a thickness ratio up to 2 was considered and a joint resistance of about 80% of the parent material's ultimate

tensile strength was observed. A multi-scale analysis based on macro- and micro-mechanical tests was conducted to determine and quantify the phenomena controlling the mechanical properties of joints made by using FSW on AA 6056 Al alloys in a T4 or T78 state and to construct a predictive model for plasticity and fracture [358]. Macro-tensile tests using samples machined transverse to the welding direction and strain maps obtained by digital image correlation (DIC), provided information about the overall strength, plastic strain localization, and fracture of the joint. 3D FE analysis of the deformation of the welded samples was used to quantify the effects of the geometrical, microstructural, and mechanical factors affecting the plastic flow localization process and the evolution of the constraint in the weak zone, which controls the damage rate. The ductility was addressed using a micromechanics-based damage model. The model was shown to capture very well, the drop in the overall ductility in the joints.

The properties of a wide range of FSW joints with dissimilar aluminum alloys or thicknesses were studied [359]. Two aluminum alloys, namely, 2024-T3 and 7075-T6, were selected for the study and were welded in ten different combinations of alloys and thicknesses. Dissimilar alloys are extruded into each other, the texture is heterogeneous in the weld zone, and that there is no significant diffusion of alloying elements between the alloys. For most configurations, the local and global mechanical properties decrease as the thickness ratio increases. The local yield strength and plasticity parameters substantially vary next to the weld centerline, hence requiring their implementation in FE models. The fracture mechanism was found to be a mixture of ductile and brittle fractures and to qualify as "quasi-cleavage." The objective of Pirondi's work [360] was to assess numerically the strength of cracked flat FSW panels for aerospace applications, by conducting simple experiments on small coupons of material (Kahn tear test). The transferability from one geometry to another, in particular the results obtained from Kahn tear tests to the prediction of the *R*-curve of cracked FSW M(T) panels was performed using the crack tip opening angle (CTOA). The Kahn tear test was reproduced first by means of FE analysis using a debond procedure based on the attainment of a critical CTOA as a function of crack length. The CTOA extracted from Kahn tests was then used to simulate the *R*-curve of M(T) panels of different widths. Two series of values of CTOA were determined: (i) considering the material as homogeneous with strength equal to that of the parent material; (ii) introducing different strengths locally for the weld TMAZ/HAZ and nugget.

Plastic flow localization and ductile failure during tensile testing of FSW aluminum specimens were investigated by Nielsen et al. [361] with a specific focus on modeling the local, finite train, hardening response. In the experimental part, FSW joints of 6005A-T6 aluminum alloy were prepared and analyzed using digital image correlation (DIC) during tensile testing as well as scanning electron microscopy (SEM) on polished samples and on fracture surfaces. The measured material properties and weld topology were introduced into a 3D FE model, fully coupled with the damage model. A Voce law hardening model involving a constant stage IV was used within an enhanced Gurson type micro-mechanical damage model, accounting for void nucleation, growth and coalescence, as well as void shape evolution. The stage IV hardening was found to increase the stiffness during plastic flow localization as well as to postpone the onset of fracture as determined by the void coalescence criterion. This modeling effort links the microstructure and process parameters to macroscopic parameters relevant to the optimization of the welds. Figs. 14 and 15 show the typical mesh and the Predicted localization and failure of macro-specimen separately.

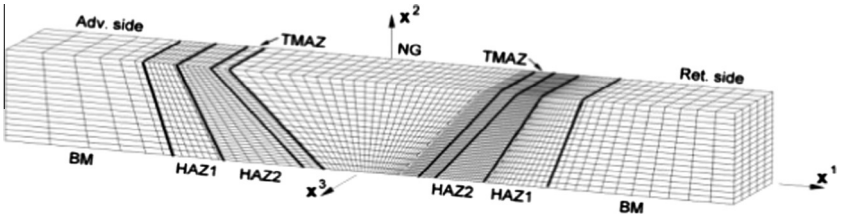

Fig. 14. Typical mesh used for the 3D analysis of a macro-specimen containing the welded joints (r = 1000 rpm, v = 1000 mm/min) [361].

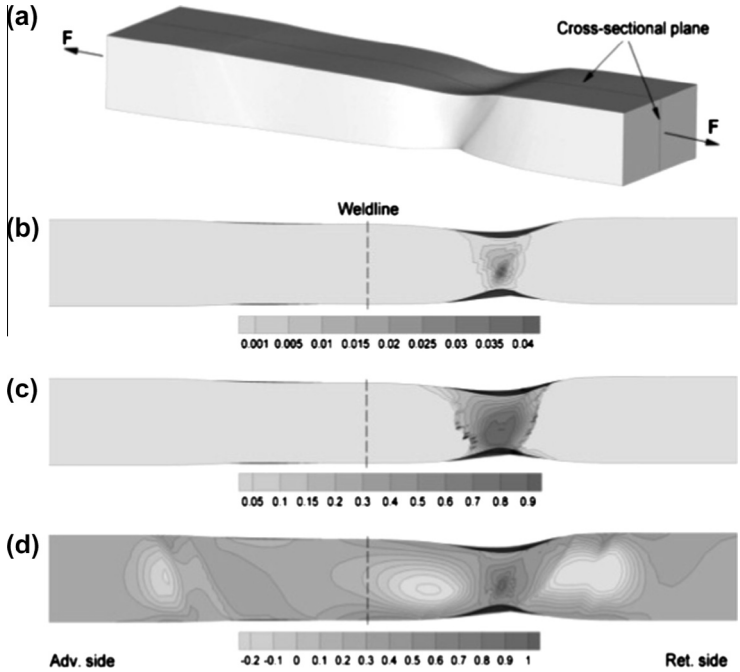

Fig. 15. Predicted localization and failure of macro-specimen containing the cold weld, here showing (a) the deformation at failure ($\varepsilon/\varepsilon u = 1.7$) as well as curves of constant (b) void volume fraction, f, (c) void aspect ratio, W, (d) stress triaxiality $\sigma_{kl}^{k}/(3\sigma_e)$, all plotted in the through thickness cross-sectional plane indicated in (a) [361].

Analysis methods were developed for the crippling failure of stiffened panels fabricated using laser beam and FSW [e.g. 362]. The work assesses modifications to conventional analysis methods and FE analysis methods for strength prediction. The experimental program has demonstrated the potential static strength of laser beam and FSW sheet-stiffener joints for post-buckling panel applications. The work undertaken has demonstrated that the crippling behavior of welded stiffened panels may be analyzed considering standard-buckling behavior. However, stiffened panel buckling analysis procedures must be altered to account for the weld joint geometry and the properties of process altered material. The aim of Tweedy et al.'s investigation [363] was to aid the development of performance specification data for subscale flat stiffened panels. The initial stiffened aluminum panels were fabricated with two hat-section stiffeners. Representative of a transport fuselage design, the skin panels were 0.040-in 2024-T3, and the stiffeners were 7075-T6 spaced on 8.0 in. centers. The 2-ft $\times$ 2-ft stiffened panels were tested statically in tension, compression, and shear. FE models were developed to evaluate the ability of modeling to predict the load carrying capacity of FSW structures. In the presentation, test results from riveted panels with identical geometry were compared with results from both the models and the FSW panels. The panels fabricated using FSW showed an increase in the overall performance including an increase in panel strength and axial displacement. The FSW shear panels failed less abruptly and with much less destruction than did the riveted panels, indicating an increase in the ability of the FSW panels to sustain damage.

The effect of FSW on the buckling behavior of an integrally stiffened panel (ISP) structure was investigated [364]. For proper consideration of the buckling modes, the Riks method based on geometric imperfection was introduced. The Ramberg–Osgood deformation plasticity model was used for the elasto-plastic material behavior. Buckling analyses with two different sectional shapes were conducted with buckling loads corresponding to 400 and 600 kN. After confirming that the predicted results without FSW were in excellent agreement with known analytical solutions, FE analyses for 2- and 3-stiffener ISP sections joined by FSW were performed. The simulated results with and without

FSW were compared to each other. The presence of the weld reduced the maximum buckling load from 3% to 10% depending on the sectional shape as a result of the reduction in material strength in the weld zone. To express the Swift hardening law in relation to FSW aluminum alloy 2017, tensile tests of FSW joints were carried out in relation to a face centered composite design [365]. Two types of identified models based on a least square method and a response surface method were used to assess the contribution of FSW-independent factors on the hardening parameters. These models were programmed into the FE code in ABAQUS to simulate tensile tests of FSW joints. These methods can be used to perform multi-criteria optimization for specific welds or for conducting numerical simulation of plastic deformation in the forming process of FSW parts such as hydroforming, bending and forging.

Three FE models were built in the ANSYS preprocessor to study the tensile stress state of aluminum alloy FSW sheets in airplanes [366]. In each model, a symmetrical constraint condition was acted on the left end surface while a tensile stress was loaded on the right. The stress concentrations of the welds depend on geometrical shapes. The eccentric bending caused by the tensile stress will affect the distribution of the stress when the model is concave or protrude. Hu et al. [367] investigated the bulging performance and circumferential thickness distribution of FSW tube with different strength matching coefficients by the hydro bulging experiment. The deformation behaviors and the stress and strain history of the welded tube during hydro-bulging were investigated by FE analysis and mechanics analysis. The equivalent stress of the weld is higher than that of the base material and the strain state of the weld is a biaxial tension for the FSW tube with a high strength matching coefficient. On the contrary, the equivalent stress of the weld is lower than that of the base material for the FSW tube with a low strength matching coefficient, and the tensile strain occurs in the circumferential of the weld, while the compressive strain firstly occurs in the axial direction of the weld and then gradually transforms to tensile strain. Local critical buckling stress of a FSW stiffened panel was calculated using a semi-empirical formula [368]. The axial compression tests on stiffened panel specimens were conducted to obtain the stability performance and carrying capacity of the structure. The FE software ABAQUS was applied to analyze the buckling behavior of the structure. The results indicated that the structure has a certain post-buckling carrying capacity and the FE method can be used to analyze the stability of the structure. This offers a referenced means for design optimization and engineering application of the structure.

The effect of heterogeneity in microstructure on the global and local tensile properties of FSW joints is significant. The strain distribution and the local stress–strain curves resulting from this heterogeneity can be mapped using the digital image correlation technique (DIC) during transverse tensile tests. This approach was used by Genevois et al. [369] in micro-tensile tests in the regions representative of the main microstructural zones parallel to the welding direction. A 3D FE model was developed to predict the weld behavior from the tensile curves of the individual regions of the weld. The tensile properties of the 5251 (O temper) welds are relatively homogeneous leading to high ductility and fracture in the base material. In contrast, the tensile properties of the various regions of the 2024 T351 and 2024 T6 welds are very heterogeneous and essentially controlled by the state of precipitation. Fanelli et al. [370] analyzed the FSSW joint by means of a complex 3D FE model which enabled an evaluation, in a parametric manner, the multifaceted internal geometry of the joint and the distribution of the mechanical characteristics of the material after welding. The authors concluded that it is possible to evaluate the structural behavior of the joint when new structural characteristics of the joint have been verified after the welding process. The aim of Pirondi and Fersini's work [371] was the assessment of the efficiency of the crack tip opening angle (CTOA) with respect to the transferability from one geometry to another, in particular the transferability obtained from Kahn tear tests on M(T) panels. The load–displacement behavior recorded during a Kahn tear test was reproduced by means of a FE analysis using a variable CTOA as a function of crack length. Experiments and simulations were run first on 6013-T6 aluminum alloy and then also on the FSBW joints of the same material.

During service conditions, Integrally Stiffened Panel (ISP) structures can be subjected to extreme compressive loading conditions and, due to their slenderness and low weight, ISP design must account for a reliable determination of buckling loads. In Valente et al.'s work [372], the structural performance of ISP structures was assessed, accounting for buckling in the elastoplastic range, by means of the FE method. Also, the buckling load-carrying capacity of multiple sets of reinforced structures, composed by a finite number of ISP and joined by FSW operations, was also studied. In doing so, it

is possible to numerically infer the influence of FSW zones in the overall stiffness and mechanical behavior of ISP structures with complex cross-section geometries. The distribution of stress and strain around the crack tip of 2A12 aluminum alloy FSW lap joints was calculated by a FE method under stretching forces [373]. The plastic deformation occurs first at the crack tip and the maximum plastic deformation is found in the crack tip region in the upper plate. The maximum plastic deformation leads to fracture of the heat-affected zone in the upper plate. Staud et al.'s article [374] focused on determining the constitutive material properties of FSW aluminum tailored blanks with regard to the FE simulation of sheet metal forming. While ordinary tensile tests can only determine the constitutive behavior of a simple tensile specimen, an optical strain measurement can be used to determine the flow stresses of the base and of the welded material with an adapted tensile specimen, respectively. By using the so-called rule of mixture, the advantage of this new approach was demonstrated by comparison of the tensile forces within FE simulations and experimental values.

A study on the mechanical characterization of FSWs between aluminum alloys 6061-T6 and 6082-T6 was carried out [375]. A comparison of single alloy joints made from each of the two alloys was also performed. The work included microstructure examination, micro-hardness tests, tensile tests and bending tests of all joint types. An approximate FE model of the joint, taking into account the spatial dependence of the tensile strength properties was made, modeling a bending test of the FSWs. Forcellese et al. [376] investigated the formability of FSW AZ31 magnesium alloy sheets by means of uniaxial tensile and hemispherical punch tests performed under different process conditions. The results of the tensile tests were analyzed in terms of flow stress and ductility at different temperature and strain rates. The hemispherical punch tests, carried out at different temperatures, provide the limiting dome height. The formability of FSW blanks was compared with that of the base material in order to evaluate the quality of the FSW joints. An in situ neutron diffraction technique was used to investigate the lattice strain distributions and micromechanical behavior in a FSW sheet of AA7475-T761 [377]. The lattice strain profiles around the weld center were measured as a function of the applied strain during tensile loading and unloading. The anisotropic elastic and plastic properties of the FSW aluminum alloy were simulated by elasto-plastic self-consistent (EPSC) model to predict the anisotropic deformation behaviors involving the grain-to-grain interactions.

A hybrid numerical and experimental study was undertaken to evaluate the performance of the FSW and super-plastically formed friction stir welded (SPF–FSW) titanium joints [378]. The simulation results were compared with the experimentally determined behavior of the joints to assess the validity of the modeling approach. This method adequately simulated the tensile behavior of a SPF–FSW joint, but due to geometrical influences, there were discrepancies between the numerical results and experimental observations. The formability of automotive FSW tailor-welded blank sheets was investigated experimentally and numerically for four automotive sheets, aluminum alloy 6111-T4, 5083-H18, 5083-O and DP590 steel sheets, each having one or two different thicknesses [379,380]. In particular, formability in three applications, including the simple tension test with various weld line directions, hemisphere dome stretching and cylindrical cup drawing tests was evaluated. For numerical simulation, mechanical properties previously characterized in literature were used. To represent the mechanical properties, the non-quadratic orthogonal anisotropic yield function was used along with the (full) isotropic hardening law, while the anisotropy of the weld zone was ignored for simplicity.

An attempt was made to develop a mathematical model for predicting the tensile strength of FSW AA6061 aluminum alloy by incorporating FSW process parameters [381]. Four factors, five levels and a central composite design were used to minimize number of experimental conditions. A response surface method (RSM) was used to develop the model. Statistical tools such as analysis of variance (ANOVA), Student's *t*-test, correlation co-efficient, etc. were used to validate the model. The mathematical model can be used to predict the tensile strength of FSW joints at 95% confidence level. Mun and Seo [382] proposed a faster method for analyzing extruded aluminum material that exploits the advantages of the inherent strain-based equivalent load.

The 3D thermal elastic–plastic FE analyses can be used to distinguish the strain induced by the thermal process from the total inherent strain in the FSW process [383]. The heat input per unit time was estimated by comparing the measured temperature distribution with the analytical equation. In the thermal analysis, serial computations were conducted by varying the heat input area and the heat

transfer coefficient of the back surface. It was found that the computed inherent strain produced by the thermal process alone, coincided with the measured strain in about 12 mm and larger range from the center of welding line while the radius of the shoulder is 7.75 mm. It was also found that the amount of compressive load might not be a dominant factor in determining the inherent strain near the weld line and that the temperature for releasing the tool would be important for estimating this inherent strain.

4.5. Fatigue behavior

Fatigue loading is a common cause of failure in the FSW joints. The fatigue life of a FSW joint results from a combination of crack initiation and propagation stages which are followed by the fast failure stage. Identifying and interpreting the locus of failure, crack initiation and propagation behavior are significant aspects in evaluating the mechanical characteristics of the FSW joints. Residual stresses play a key role on the mechanics underlying the propagation of fatigue cracks in FSW joints. It is widely accepted that compressive residual stresses may affect beneficially the fatigue life under loading condition, whereas tensile residual stresses may act to increase the stress distribution at the crack tip, resulting in a life-threatening condition in the FSW structure.

Al–Li alloys are characterized by strong anisotropy. The material microstructure and the different phases of 2198 Al–Li FSW joints were individuated by Cavaliere et al. [384] using TEM observations. Fig. 16 shows the geometry of the specimen and the associated FE mesh. Mechanical properties were evaluated by means of tensile and fatigue tests at room temperature. The fatigue tests were conducted in axial control mode with a stress ratio 0.33 for different welding conditions. Fig. 17 shows fatigue endurance curves. The initiation and propagation of cracks in the welded zone were also studied by applying thermo-elastic stress analysis (TSA) during cyclic fatigue tests, employing single edge notched specimens. All the results were validated by FE analysis. Fig. 18 shows Von Mises stress distribution and the stress field map obtained from FE simulation.

The propagation of a fatigue crack through a FSW joint of 2024-T351 Al alloy was investigated numerically [385]. Stress intensity was calculated based on a displacement correlation technique,

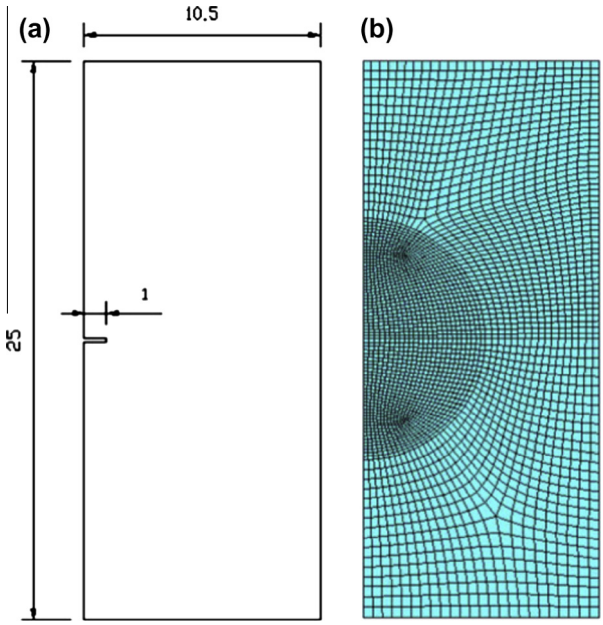

Fig. 16. Specimen geometry and the finite element mesh for small scale yielding problem solving for the single edge notch, all the units are in mm [394].

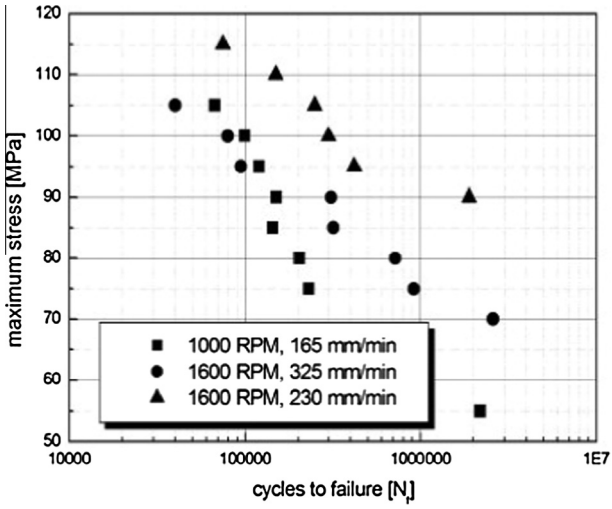

Fig. 17. Fatigue endurance curves for the joints welded with a rotatio n speed of the tool of 1600 RPM and travel speeds of 230 and 325 mm/min and 1000 RPM 165 mm/min [394].

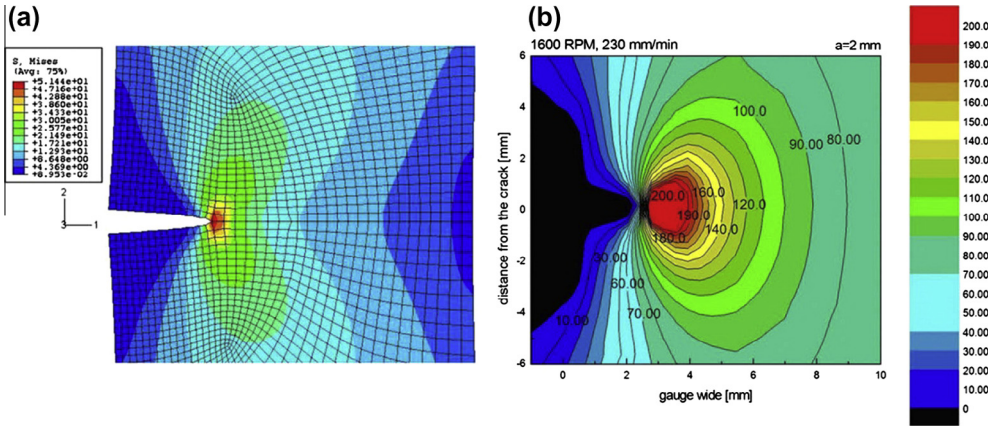

Fig. 18. Von Mises stress distribution (a) and stress field map for a crack length of 2 mm (b) obtained from ABAQUS calculations [394].

and fatigue crack growth through the FSW joint was investigated under linear elastic fracture mechanics (LEFM) using the Paris model. The concepts of crack closure, residual stress, and stress relaxation are incorporated into the Paris model to support the final results. The numerical approaches were applied to the high number of elements in the framework of Fracture Analysis Code (FRANC2D/L) to simulate the propagation of a fatigue crack through the FSW joint including various zones with different material properties. In a similar work, the fatigue life of a FSW joint in the 2024-T351 aluminum alloy was predicted [386]. The simulation was conducted using linear elastic fracture mechanics based on Paris' model. The entire crack growth process was investigated step by step through all of the FSW zones, and the fatigue lifetimes of the FSW joint under various loading conditions were predicted by implementing the same procedure. The numerical results were validated with experimental and analytical work. The fatigue crack growth in AA2024-T3 FSW butt joints was studied by a computational

approach based on a sequential usage of a FE method and a Dual Boundary Element (DBE) method [387]. The distribution of residual stress induced by the FSW process was mapped by means of a recently developed technique named contour method. The computed residual stress field was superimposed on the stress field produced by a remote fatigue traction load in a DBE environment. A two-parameter crack growth law was used for the assessment of the rate of crack propagation.

Fatigue tests under different stress ratios were performed on FSW samples of 2.0 mm thick Al–Li alloy 2198-T8 sheets [388–390]. Fatigue crack growth rates in the welded nugget were obtained and compared. There is no peculiar yielding process in the stress–strain curve of the welded nugget compared with the parent material. Yield strength and tensile strength have a "U" shape through the weld zone and have lower values in the weld zone. Unlike the parent material, fatigue crack growth rates in the welded nugget are not sensitive to stress ratios. The FE models were built and the crack closure method was used to calculate the effect of residual stress. Fracture surfaces were investigated to summarize the fracture feature of the welded nugget under fatigue load. Fatigue strength was investigated for FSW overlap and butt welded joints in different thicknesses based on concepts of nominal and effective notch stress [391]. The fatigue test results were compared with fatigue strength recommendations according to EN 1999-1-3 and International Institute of Welding (IIW). The results were also compared with published data and FE analysis was carried out to investigate the effect of plate thickness and nugget size on the fatigue strength of overlap joints. The slopes of the SN-curves for two different joint types differ from the slope recommended by IIW. The suggested fatigue design curves for the nominal and effective notch stress concept have a higher slope than given for fusion welds by IIW.

Due to design constraints, FSW components may include notches in the weld (friction stirred material), and there is a lack of information on the fatigue behavior of the weld in those conditions. In Moreira et al.'s work [392] the influence of FSW on the fatigue life of specimens of aluminum alloy 6063-T6, containing notches in the thermo-mechanically affected zone was studied. Welded and unwelded notched specimens were fatigue tested under load control at different stress levels. Compared to base material specimens, FSW specimens were found to have longer fatigue lives but of the same order of magnitude. The work included hardness, tensile and fatigue tests, and the FE analysis of the distribution of stress and strain. The notch-strain analysis was used for approximate modeling of the observed fatigue behavior. The use of residual K (Kres) approaches for the prediction of fatigue crack growth rates in residual stress fields was studied [393]. The FE models of the samples were built and the measured residual stress data were put into the models. The virtual crack closure technique (VCCT) was used to calculate Kres (stress intensity factor from residual stress) and how it changes with crack length. Local Kres values were used to calculate effective stress ratio values. The master curve approach was used to relate these to the corresponding values for crack growth rates. Predicted crack growth rates were compared with experimental results.

The thermo-elastic stress analysis (TSA) can be used to study the propagation characteristics of fatigue-cracks in FSW aluminum sheets. The TSA measurement system allowed crack evolution to be observed in real-time during fatigue cycles and allowed the stress fields to be derived from the measured variation in temperature. Fatigue tests were performed under tension with a load ratio of 0.1 and all the tests were conducted to failure point [394]. The thermo-elastic data were used to analyze principal stresses and principal strains on the specimen's surface and the crack growth rates during tests. The results were compared with those obtained by classical CCD camera monitoring of crack front propagation during cyclic loading. All results were validated by FE analysis performed using the ABAQUS software. The main aim of Ahmadi et al.'s study [395] was to investigate the fatigue behavior of single spot FSW using a strain-based, modified Morrow's damage equation. The correlation between the micro-hardness, cyclic material constants, and mechanical strength of different zones around the single spot FSW were assumed to be proportional to the hardness of the base material. Experimental fatigue tests of the single spot FSW specimens were carried out using a constant amplitude, load control, servo-hydraulic fatigue testing-machine. The ANSYS FE code was used to simulate a single tensile shear spot FSW joint. Non-linear elastic–plastic FE analysis was employed to obtain the values of local equivalent stress and strain near the notch roots of the joints.

The fatigue failure of FSW aluminum panels of alloy 6005A was analyzed by Shahri et al. [396]. These panels were produced with two main joint geometries: namely half overlap and hourglass.

The presence of crack like notches (interface between the welded work pieces) and blunt notches (corners and bends in the base metal) were studied with the FE method stress analysis combined with the critical distance method. It was shown that the location of failure and the fatigue limit could be predicted for three of the four types of profiles considered. The choice of the welding procedure (clamping condition) was found to influence significantly, the fatigue life and accuracy of prediction. It was also shown that local plastic deformation on the crack tip is induced by clamping, resulting in tensile residual stresses at the crack tip. The position of the failure can be explained by taking the stress intensity factor of the residual stress into account. The fatigue behavior of a FSW extruded aluminum alloy 6005A joint, which is used for train wall sides, was studied by Shahri and Sandström [397]. The structure used was a lap-butt joint with a sharp notch next to the weld nugget. Fatigue cracks and failure appeared at notches in the profile. In most profiles, cracks also started at the sharp notch at the weld, but the propagation was slow and complete fracture never took place there. FE stress analysis combined with the theory of critical distance was used to estimate the fatigue limit. The results from the analysis for the fatigue limit were within 3–28% of the observations. The stress analysis correctly predicted that failure would not occur in the welds. The fatigue strength of 2024-T3 aluminum alloy FSW single-lap joints in the presence of two crack-like unwelded zones at the overlap ends was studied [398]. A FE analysis was performed to predict the crack path and the stress intensity at the crack tip. The lifetime was estimated by examining the crack propagation behavior of the base material using the AFgrow software. The effect of an initial overload was also considered. The crack path was investigated optically and using the "fatigue failure mechanism map". Fig. 19 shows deformed joint and predicted crack path on the advancing side of 2024-T3 aluminum alloy FSW single-lap joint.

In Kang et al.'s research project [399], a front shock tower of a passenger vehicle was developed with various magnesium alloys and joining methods. Fatigue tests of various joint specimens including linear FSW, self-piecing rivet joint with and without adhesive, and spot FSW were conducted to predict the fatigue life of the joints in the structure. The magnesium alloys used for the specimens are AM60 (cast), AM30 (extrusion), and AZ31 (sheet). A fatigue life prediction method for the joints was performed using the stress-life curve approach. The FE modeling technique and the fatigue prediction method will be verified with fatigue tests of the actual front shock tower structure subjected to variable amplitude loadings in near future. An enhancement of a pseudo-numerical tool for investigations of fatigue crack growth in integrally stiffened metal panels was presented [400]. The model is based on an analytical approach that demands compatibility of displacement between the skin sheet and the stiffener. The focus of the work is on the incorporation of residual stress effects, in order to improve the accuracy of the simulation results for welded panel configurations that are manufactured by laser beam welding or FSW and which exhibit a significant amount of residual stress. Simulation results were compared with results from FE simulations on a two stringer panel. These showed good agreement with the base model as well as the capability of the tool enhancements to account for the crack retarding effect of residual stresses.

The fatigue behavior of dissimilar spot FSW or spot friction welds in lap-shear and cross-tension specimens was investigated [401,402]. Optical micrographs of the welds after failure under quasi-static and cyclic loading conditions showed that the Al/Fe welds in both types of specimens mainly fail along the interface surfaces between the aluminum and steel sheets. 3D FE analyses based on the micrograph of the welds before testing were conducted to obtain stress intensity factor and J integral solutions for the crack fronts along the nugget circumferences of the welds in both types of specimens. The computational results were used to explain the experimental observations on the growth patterns of fatigue cracks in the welds. Sutton et al. [403] investigated the effect of weld residual stress on the propagation of fatigue cracks in 2024-T351 aluminum alloy FSW plate. They used a limited set of residual stress measurements acquired by neutron diffraction and an equilibrium-based, weighted least square algorithm to reconstruct the complete residual stress tensor field from the measured residual stress data. By incorporating a least squares, complete equilibrated residual stress field into a FE model of the FSW region, progressive crack growth along a direction perpendicular to the welding line was simulated as part of the analysis. Results showed that (a) incorporation of the complete, self-equilibrated residual stress field into a FE model of the specimen provides a robust, hybrid approach for assessing the importance of residual stress on fatigue crack propagation, (b) the calculated stress-intensity factor due to the residual stress field, Kres, has the same trend as measured experimentally

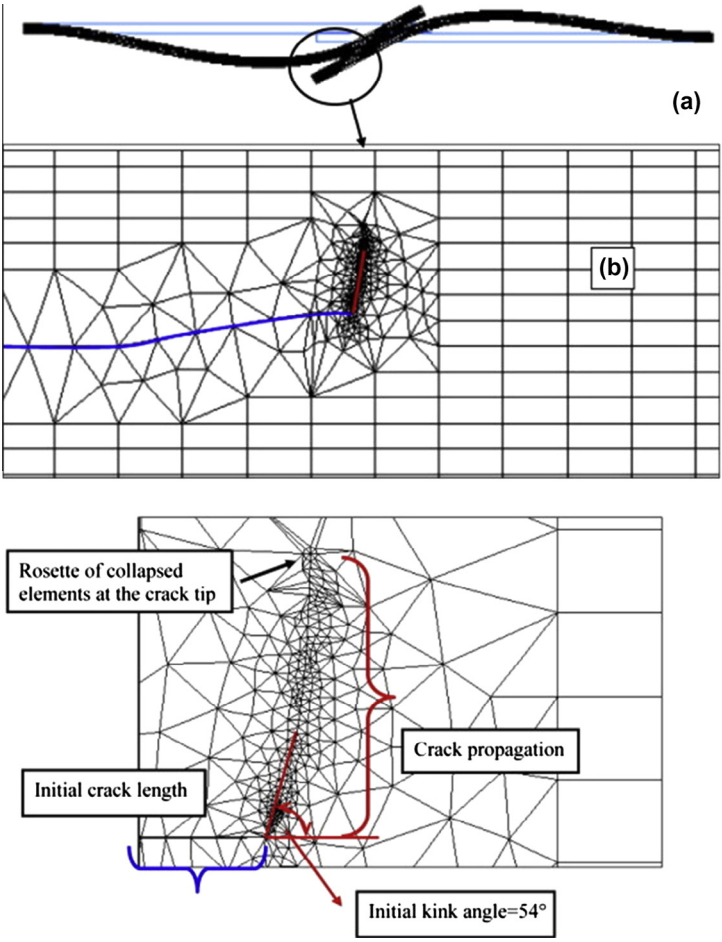

Fig. 19. (a) Deformed joint (magnified); (b) predicted crack path on the advancing side. In blue the initial defect, in red the crack propagation [398].

by the 'cut-compliance method' and (c) the da/dN results are readily explained with reference to the effect of the residual stress field on the applied stress intensity factor.

A continuous 3D FE model was used to simulate the FSW process of butt joints with a single block approach and to predict the residual stress field by considering both thermal and mechanical actions [404]. The residual stress effect on the fatigue life was estimated through fatigue crack propagation (FCP) tests in compact tension specimens. Encouraging results were found, leading to a few interesting conclusions that have to be properly verified in the future. The role of the residual stress on the propagation of fatigue cracks orthogonal to the weld direction in a FSW Ti–6Al–4V joint was investigated [405]. A numerical prediction of the fatigue crack growth rate in the presence of the residual stresses was carried out using AFGROW software. Reasonable correspondence between the model predictions and the experimental results were observed when the effects of residual stress were included in the simulation. Some new methods for enhancing the fatigue life and strength of FSSW joints were introduced recently using a localized plasticity process [406,407]. In the experimental section, the fatigue tests were carried out using a constant amplitude, load control, servo-hydraulic, fatigue testing machine on the as-welded and cold expanded FSSW joints with a cold expansion level of 3.3%. In

the numerical studies, 3D FE models were used to calculate stress and strain distributions in two batches of specimens using two multi-axial fatigue criteria: Smith-Watson-Topper and Fatemi-777Socie. The experimental and numerical S–N data revealed that the cold expansion method could improve the fatigue life of FSSW joints in all load ranges. In high cycle regimes, the fatigue life could be improved by up to 6 times.

4.6. Dynamic behavior

With the increase in the use of FSW joints in primary structures, such as aircraft and automotive structures, reliable and cost-effective techniques for structural health monitoring (SHM) of FSW are needed. Dynamic behavior analysis, when combined with validated FE analysis, can provide a key tool for SHM of FSW joints.

Investigations at the micro-mechanical level were reported for aluminum alloy 6111 spot FSW joints welded with different processing times [408,409]. Apart from microstructural studies and micro-hardness tests, a new approach to characterizing the distribution of the weld zone modulus using modal vibration tests on micron scale cantilever array specimens with a micro-scanning laser vibrometer and the corresponding FE simulations was developed. Micro-cantilever array samples were designed in such a way that each micro-cantilever represents one of the weld zones. Microscopic studies revealed a partial metallurgical bond formed in the direction of flow, which is governed by the tool used. The Vickers hardness numbers in those regions were found to be considerably lower than those of the base metal. Parametric studies to determine the effect of weld zone measurements on the modal frequencies have been carried out using FE models. Deformation and fracturing in impulsively loaded FSW sandwich panels were studied [410]. Micro-hardness and miniature tensile coupon testing revealed that FSW reduced the strength and ductility in the welds and in a narrow heat-affected zone on either side of the weld, by about 30%. To investigate the dynamic deformation and fracture processes, a particle-based method has been used to simulate the impulsive loading of the panels. This has been combined with a FE analysis utilizing a modified Johnson–Cook constitutive relation and a Cockcroft-Latham fracture criterion that accounted for local variation in material properties. This comprehensive study reveals the existence of a strong instability in the loading that results from changes in sand particle reflection during the dynamic evolution of the panel's surface topology.

A combination of experimental and modeling methods was used to investigate the mechanical response of edge-clamped sandwich panels subjected to the impact of explosively driven wet sand [411]. A porthole extrusion process followed by FSW was used to fabricate 6061-T6 aluminum sandwich panels with corrugated cores. The panels were edge clamped and subjected to localized high intensity dynamic loading by the detonation of spherical explosive charges encased in a concentric shell of wet sand placed at different standoff distances. A decoupled wet sand loading model was developed and incorporated into a parallel FE simulation capability. The model predictions for the remaining tests were found to be in close agreement with experimental observations for both sandwich panels and monolithic plates. It was found that the response of the sandwich panel to wet sand blast loading can be varied by redistributing the mass among the core webs and the face sheets. A computational fluid dynamic (CFD) model was presented to simulate the material flow and heat transfer in the FSW of 6061-T6 aluminum alloy (AA6061) [412]. The goal was to analyze the viscous and inertia loads applied to the FSW tool by varying the welding parameters, using a 3D model. A right-handed one-way thread on a tilted FSW tool pin with a smooth, concaved shoulder was considered to increase the accuracy of the numerical model. In addition, the viscous and frictional heating were assumed as the only sources of heat input. In the course of model verification, good agreement was found between the numerical results and the experimental observations.

5. Outlook

An adequate understanding of the behavior of the FSW joints is necessary to ensure the efficiency, safety and reliability of such joints. Numerical studies of the FSW process can provide realistic

predictions of the main variables of the process. This reduces the number of experimental tests, accelerates the design processes and reduces the cost of optimizing the variables. However, several important key problems and issues remain to be addressed. Approaches for the computational modeling of the FSW process are still under development and much work is still needed.

The most frequently used approach to the numerical analysis of FSW is the FE method. However, it is difficult or troublesome to calculate the advective term both for momentum and temperature using this method. It is also difficult to calculate large deformations of the materials. Moreover, a complex process is required to analyze substance transfer when considering joints between dissimilar materials. To avoid these difficult or troublesome processes, other numerical methods such as the finite difference method, particle method, fluid mechanics method etc., need to be adopted in the numerical analysis of the FSW processes. A suitable numerical method is useful for establishing computational FSW process models which are effective, reliable and bi-directional in nature.

The plunge stage in the FSW process is extremely critical since most of the initial thermo-mechanical conditions are generated then and the material undergoes significant transformation due to the high temperatures and stresses involved. There are few experimental studies that focus on the plunge stage, and not many numerical models that focus on the thermo-mechanical conditions developed during the plunge phase. One of the primary difficulties in simulating the plunge stage is the excessive mesh distortion of the FE model leading to premature termination of the program. On the other hand, the tool target depth is also important for producing sound welds. Shallow target depth results in generation of welds with inner channels or surface grooves. Deep target depths result in excessive flash. A significantly concave weld is produced, leading to localized thinning of the welded plates. Little work has been performed on the plunge stage.

One of the most significant differences between FSW and conventional fusion welding is that the formation of the FSW seam is affected by both the thermal and mechanical loads of the FSW tool. However, the definitive functions of mechanical loads of the FSW tool are not clearly described. Most numerical simulations of the FSW process neglect mechanical loads and so cannot describe this characteristic of FSW. This warrants more experimental and numerical research to investigate material processes during this stage.

Numerical modeling of the microstructure of the FSW joints needs a delicate compromise between accuracy and feasibility. On one hand, there are different zones with significantly different mechanical properties in a FSW joint. The mechanical and geometrical properties of these zones make numerical models complicated and computationally expensive. On the other hand, the incorporation of the different zones in numerical model might make a significant contribution to the accuracy of the simulation results. It is very important to validate the microstructure behavior of the FSW joints predicted by numerical analysis against experimental test results. Very limited numerical studies have been performed in this area.

Considerable residual stress and distortion can be produced by the FSW process, impeding industrial implementation. The ability to accurately predict residual stresses and the resultant distortions is a key product from simulations of assembly processes. Assembly processes necessarily consider large structural components potentially making simulations computationally expensive. It is very important to develop a greater understanding of the influence of the FSW process idealization on the prediction of residual stresses and distortion and thus determine the minimum required modeling fidelity for future assembly simulations. Little work has been undertaken in this area.

In the design of mechanical systems, which incorporate the FSW jointed components, for minimum vibration response, a specific knowledge of the dynamic behavior of the component materials and joints is important. Compared with developments in numerical analysis of process and strength behavior, research of dynamic behavior of the FSW joints is relatively unexplored.

It is also important for FSW process to benefit from the advantages of other joining techniques, such as adhesive bonding, ultrasonic welding, etc. These can be done by combining FSW process with other joining techniques and are referred to as hybrid joining processes. It is widely accepted that these produce much stronger joints in both static and fatigue tests. A simulative approach is useful for predicting the structural behavior and to improve the quality of hybrid joins. As such, it contributes to reduce process adjustments in the early stage of the product life cycle, and therefore helps to save time and costs. But until now there is no efficient numerical model of hybrid joint has been reported.

In order to make FSW joints more reliable and practical, it is important to develop non-destructive testing techniques (NDT) for detecting damage during the operation of FSW structures before the damage can propagate and cause catastrophic failure of the components. It is generally believed that nonlinear ultrasonic testing would be a useful technique to detect and estimate the size of both planar and volumetric defects. The development of reliable procedures for nonlinear ultrasonic FSW inspection requires an understanding of the interaction of ultrasonic waves with the various types of FSW defects and complex geometries. Although FE analysis is well suited to model almost any geometrical shape, traditional finite elements are not the best ones for correctly resolving the ultrasonic wave state at junctions of dissimilar materials. To avoid any adverse effects, alternative numerical approaches need to be sought.

6. Summary

Although FSW has been successfully used to join materials that are difficult-to-weld, it is still at an early stage. So far, the development of the FSW process for each new application has remained largely empirical. Scientific knowledge-based numerical studies are of significant help in understanding the FSW process.

In this paper, the research activities and progress to date in the development of numerical analysis of FSW are reviewed and their applicability to the manufacturing of components is emphasized. Firstly, different types of numerical methods and modeling techniques are considered; then the variables involved in numerical modeling of the FSW process are discussed. The microstructure behavior modeling of the FSW is described. Finally, advances in numerical analysis of mechanical characteristics of the FSW joints are presented.

Many challenges remain in numerical analysis of FSW. As FSW comprises complex phenomena involving many interrelated mechanisms and thermal processes, it is clear that a complete characterization of joint behavior is impossible. Accurate and reliable numerical analysis of the FSW is still a very difficult task as the behavior of the FSW joints is influenced by different factors in combination.

The references presented in this paper are by no means complete but they comprehensively represent the application of different numerical methods on the subject area. The main goal of the paper is to review recent progress in numerical analysis of FSW and to provide a basis for further research.

Acknowledgements

This study is partially supported by National Natural Science Foundation of China (Grant No. 50965009) and Special Program of the Ministry of Science and Technology, China (Grant No. 2012ZX04012-031).

References

[1] He X, Gu F, Ball A. Recent development in finite element analysis of self-piercing riveted joints. Int J Adv Manuf Technol 2012;58:643–9.
[2] He X. Finite element analysis of laser welding: a state of art review. Mater Manuf Process 2012;27:1354–65.
[3] He X. A review of finite element analysis of adhesively bonded joints. Int J Adhe Adhe 2011;31:248–64.
[4] He X. Recent development in finite element analysis of clinched joints. Int J Adv Manuf Technol 2010;48:607–12.
[5] He X, Pearson I, Young K. Self-pierce riveting for sheet materials: state of the art. J Mater Process Technol 2008;199:27–36.
[6] Thomas WM, Nicholas ED, Needham JC, Murch MG, Temple-Smith P, Dawes CJ. Friction stir butt welding. International Patent Application No. PCT/GB92/02203; 1991.
[7] Gemme F, Verreman Y, Dubourg L, Jahazi M. Numerical analysis of the dwell phase in friction stir welding and comparison with experimental data. Mater Sci Eng A 2010;527:4152–60.
[8] Mishra RS, Ma ZY. Friction stir welding and processing. Mater Sci Eng R: Rep 2005;50:1–78.
[9] El-Danaf EA, El-Rayes MM. Microstructure and mechanical properties of friction stir welded 6082 AA in as welded and post weld heat treated conditions. Mater Des 2013;46:561–72.
[10] Sonne MR, Tutum CC, Hattel JH, Simar A, De Meester B. The effect of hardening laws and thermal softening on modeling residual stresses in FSW of aluminum alloy 2024-T3. J Mater Process Technol 2013;213:477–86.
[11] Cao X, Jahazi M. Effect of tool rotational speed and probe length on lap joint quality of a friction stir welded magnesium alloy. Mater Des 2011;32:1–11.
[12] Chowdhury SM, Chen DL, Bhole SD, Cao X. Tensile properties of a friction stir welded magnesium alloy: effect of pin tool thread orientation and weld pitch. Mater Sci Eng A 2010;527:6064–75.

[13] Kitamura K, Fujii H, Iwata Y, Sun YS, Morisada Y. Flexible control of the microstructure and mechanical properties of friction stir welded Ti–6Al–4V joints. Mater Des 2013;46:348–54.
[14] Buffa G, Fratini L, Micari F. Mechanical and microstructural properties prediction by artificial neural networks in FSW processes of dual phase titanium alloys. J Manuf Process 2012;14:289–96.
[15] Sharifitabar M, Nami H. Microstructures of dissimilar friction stir welded joints between 2024-T4 aluminum alloy and Al/Mg2Si metal matrix cast composite. Compos Part B: Eng 2011;42:2004–12.
[16] Bozkurt Y, Uzun H, Salman S. Microstructure and mechanical properties of friction stir welded particulate reinforced AA2124/SiC/25p-T4 composite. J Compos Mater 2011;45:2237–45.
[17] The Welding Institute TWI. <www.twi.co.uk>.
[18] Nandan R, DebRoy T, Bhadeshia HKDH. Recent advances in friction-stir welding – process, weldment structure and properties. Prog Mater Sci 2008;53:980–1023.
[19] Threadgilll PL, Leonard AJ, Shercliff HR, Withers PJ. Friction stir welding of aluminum alloys. Int Mater Rev 2009;54:49–93.
[20] Çam G. Friction stir welded structural materials: beyond Al-alloys. Int Mater Rev 2011;56:1–48.
[21] Chao YJ, Qi X. Thermal and thermo-mechanical modeling of friction stir welding of aluminum alloy 6061-T6. J Mater Process Manuf Sci 1998;7:215–33.
[22] Lockwood WD, Tomaz B, Reynolds AP. Mechanical response of friction stir welded AA2024: experiment and modeling. Mater Sci Eng A 2002;323:348–53.
[23] Lockwood WD, Reynolds AP. Simulation of the global response of a friction stir weld using local constitutive behavior. Mater Sci Eng A 2003;339:35–42.
[24] Zhu XK, Chao YJ. Numerical simulation of transient temperature and residual stresses in friction stir welding of 304L stainless steel. J Mater Process Technol 2004;146:263–72.
[25] Khandkar MZH, Khan JA, Reynolds AP, Sutton MA. Predicting residual thermal stresses in friction stir welded metals. J Mater Process Technol 2006;174:195–203.
[26] Fratini L, Buffa G. CDRX modelling in friction stir welding of aluminium alloys. Int J Machine Tool Manuf 2005;45:1188–94.
[27] Fratini L, Beccari S, Buffa G. Friction stir welding fem model improvement through inverse thermal characterization. Trans North Am Manuf Res Inst SME 2005;33:259–66.
[28] Buffa G, Donati L, Fratini L, Tomesani L. Solid state bonding in extrusion and FSW: process mechanics and analogies. J Mater Process Technol 2006;177:344–7.
[29] Fratini L, Buffa G, Shivpuri R. Improving friction stir welding of blanks of different thicknesses. Mater Sci Eng A 2007;459:209–15.
[30] Buffa G, Fratini L, Shivpuri R. CDRX modelling in friction stir welding of AA7075-T6 aluminum alloy: analytical approaches. J Mater Process Technol 2007;191:356–9.
[31] Zhang Z, Zhang HW. Mechanical analysis of pin in friction stir welding process. J Mech Strength 2006;28:857–62 [in Chinese].
[32] Zhang Z, Zhang HW. Numerical simulation of dynamic recrystallization and hardness distribution in friction stir welding process. Acta Metall Sinica 2006;42:998–1002 [in Chinese].
[33] Zhang H, Zhang Z, Bie J, Zhou L, Chen J. Effect of viscosity on material behavior in friction stir welding process. Trans Nonferr Met Soc China (Engl Ed) 2006;16:1045–52.
[34] Zhang HW, Zhang Z. Numerical modeling of friction stir welding process by using rate-dependent constitutive model. J Mater Sci Technol 2007;23:73–80.
[35] Zhang Z, Zhang HW. Material behaviors and mechanical features in friction stir welding process. Int J Adv Manuf Technol 2007;35:86–100.
[36] Azimzadegan T, Serajzadeh S. Thermo-mechanical modeling of friction stir welding. Int J Mater Res 2010;101:390–7.
[37] Jamshidi Aval H, Serajzadeh S, Kokabi AH. The influence of tool geometry on the thermo-mechanical and microstructural behaviour in friction stir welding of AA5086. Proc Inst Mech Eng Part C 2011;225:1–16.
[38] Jamshidi Aval H, Serajzadeh S, Kokabi AH. Thermo-mechanical and microstructural issues in dissimilar friction stir welding of AA5086–AA6061. J Mater Sci 2011;46:3258–68.
[39] Jamshidi Aval H, Serajzadeh S, Kokabi AH. Evolution of microstructures and mechanical properties in similar and dissimilar friction stir welding of AA5086 and AA6061. Mater Sci Eng A 2011;528:8071–83.
[40] Jamshidi Aval H, Serajzadeh S, Kokabi AH. Experimental and theoretical evaluations of thermal histories and residual stresses in dissimilar friction stir welding of AA5086–AA6061. Int J Adv Manuf Technol 2012;61:149–60.
[41] He X. Numerical studies on friction stir welding of lightweight materials. Adv Mater Res 2013;743:118–22.
[42] Neto DM, Neto P. Numerical modeling of friction stir welding process: a literature review. Int J Adv Manuf Technol 2013;65:115–26.
[43] Tutum CC, Hattel JH. Numerical optimisation of friction stir welding: review of future challenges. Sci Technol Weld Join 2011;16:318–24.
[44] Gould JE, Feng ZL. Heat flow model for friction stir welding of aluminum alloys. Mater Process Manuf Sci 1998;7:185–94.
[45] Schmidt H, Hattel J, Wert J. An analytical model for the heat generation in friction stir welding. Model Simul Mater Sci Eng 2004;12:143–57.
[46] Colligan K. Material flow behavior during friction stir welding of aluminum. Weld J (Miami, Fla) 1999;78:229s–37s.
[47] Xu S, Deng X, Reynolds AP, Seidel TU. Finite element simulation of material flow in friction stir welding. Sci Technol Weld Join 2001;6:191–3.
[48] Seidel TU, Reynolds AP. Two-dimensional friction stir welding process model based on fluid mechanics. Sci Technol Weld Join 2003;8:175–83.
[49] Schmidt HNB, Dickerson TL, Hattel JH. Material flow in butt friction stir welds in AA2024-T3. Acta Mater 2006;54:1199–209.
[50] Khandkar MZH, Khan JA, Reynolds AP. Prediction of temperature distribution and thermal history during friction stir welding: input torque based model. Sci Technol Weld Join 2003;8:165–74.

[51] Nandan R, Roy GG, Lienert TJ. Numerical modelling of 3D plastic flow and heat transfer during friction stir welding of stainless steel. Sci Technol Weld Join 2006;11:526–37.
[52] Kang SW, Jang BS. A study on computational fluid dynamics simulation of friction stir welding. In: Analysis and design of marine structures – proceedings of the 4th international conference on marine structures, MARSTRUCT; 2013, p. 433–9.
[53] Dong P, Lu F, Hong JK, Cao Z. Coupled thermomechanical analysis of friction stir welding process using simplified models. Sci Technol Weld Join 2001;6:281–7.
[54] Shercliff HR, Colegrove PA. Modelling of friction stir welding. In: Cerjak H, editor. Mathematical modeling of weld phenomena, vol. 6. London: Maney; 2002. p. 927–74.
[55] Colegrove PA, Shercliff HR. Development of Trivex friction stir welding tool Part 1 – two-dimensional flow modelling and experimental validation. Sci Technol Weld Join 2004;9:345–51.
[56] Colegrove PA, Shercliff HR. Development of Trivex friction stir welding tool Part 2 – three-dimensional flow modeling. Sci Technol Weld Join 2004;9:352–61.
[57] Tello K, Duman U, Mendez P. Scaling laws for the welding arc, weld penetration and friction stir welding. In: ASM proceedings of the international conference: trends in welding research; 2009. p. 172–81.
[58] Tello K, Duman U, Mendez P. Advanced scaling techniques for the modeling of materials processing. In: Proceedings of the ASME summer heat transfer conference, vol. 3; 2009; p. 607–16.
[59] Tello K, Gerlich A, Mendez P. Constants for hot deformation constitutive models for recent experimental data. Sci Technol Weld Join 2010;15:260–6.
[60] Mendez P, Tello K, Lienert T. Scaling of coupled heat transfer and plastic deformation around the pin in friction stir welding. Acta Mater 2010;58:6012–26.
[61] Roy GG, Nandan R, DebRoy T. Dimensionless correlation to estimate peak temperature during friction stir welding. Sci Technol Weld Join 2006;11:606–8.
[62] Reynolds AP, Tang W, Khandkar Z, Khan JA, Lindner K. Relationships between weld parameters, hardness distribution and temperature history in alloy 7050 friction stir welds. Sci Technol Weld Join 2005;10:190–9.
[63] Buck GA, Langerman M. Non-dimensional characterization of the friction stir/spot welding process using a simple Couette flow model. Part I: constant property Bingham plastic solution. In: Ghosh S, Castro JC, Lee JK, editors. American institute of physics conference series, vol. 712; 2004. p. 1283–8.
[64] Krzyzanowski M, Davies PS, Rainforth WM, Wynne BP. Combined discrete/finite element multiscale approach for modelling of the tool/workpiece interface during high shear processing: hot rolling and friction stir welding applications. Mater Sci Forum 2010;638–642:2622–7.
[65] Krzyzanowski M, Rainforth MW. Advances on modelling of the tool/workpiece interface during high shear processing. Mater Sci Forum 2010;654–656:1634–7.
[66] Li WY, Yu M, Li JL. Effects of mass scaling factor on the plunge stage of friction stir welding. Trans Chin Weld Inst 2010;31:1–4 [in Chinese].
[67] Avettand-Fènoël M, Taillard R, Herbelot C, Imad A. Structure and mechanical properties of friction stirred beads of 6082-T6 Al alloy and pure copper. Mater Sci Forum 2010;638–642:1209–14.
[68] Khosa SU, Weinberger T, Enzinger N. Thermo-mechanical investigations during Friction Stir Spot Welding (FSSW) of AA6082-T6. Weld World 2010;54:R134–46.
[69] Hamilton R, Mackenzie D, Li HJ. Multi-physics simulation of friction stir welding process. Eng Comput (Swansea, Wales) 2010;27:967–85.
[70] Jang CD, Jang YJ. Welding deformation analysis of friction stir welded aluminum alloy structures using equivalent load method based on inherent strain. In: Proceedings of the international offshore and polar engineering conference, vol. 4; 2010. p. 290–7.
[71] Arora A, Nandan R, Reynolds AP, DebRoy T. Torque, power requirement and stir zone geometry in friction stir welding through modeling and experiments. Scr Mater 2009;60:13–6.
[72] Arora A, Debroy T, Bhadeshia HKDH. Back-of-the-envelope calculations in friction stir welding – velocities, peak temperature, torque, and hardness. Acta Mater 2011;59:2020–8.
[73] Chiumenti M, Cervera M, Agelet de Saracibar C. A novel stress-accurate FE technology for highly non-linear analysis with incompressibility constraint. In: AIP conference proceedings, vol. 1532; 2013. p. 45–56.
[74] Uyyuru RK, Kallas SV. Numerical analysis of friction stir welding process. J Mater Eng Perform 2006;15:505–18.
[75] Feulvarch E, Roux JC, Bergheau JM. A simple and robust moving mesh technique for the finite element simulation of Friction Stir Welding. J Comput Appl Math 2013;246:269–77.
[76] Chiumenti M, Cervera M, Agelet de Saracibar C, Dialami N. Numerical modeling of friction stir welding processes. Comput Method Appl Mech Eng 2013;254:353–69.
[77] Zhou MZ, Lei DG, Liang N, Yang JH. 3D coupled thermo-mechanical visco-plastic finite element simulation of friction stir welding process. Trans Chin Weld Inst 2010;31:5–9 [in Chinese].
[78] Wang H, Colegrove PA, dos Santos J. Hybrid modelling of 7449-T7 aluminium alloy friction stir welded joints. Sci Technol Weld Join 2013;18:147–53.
[79] Shojaeefard MH, Behnagh RA, Akbari M, Besharati Givi MK, Farhani F. Modelling and pareto optimization of mechanical properties of friction stir welded AA7075/AA5083 butt joints using neural network and particle swarm algorithm. Mater Des 2013;44:190–8.
[80] Dialami N, Chiumenti M, Cervera M, Agelet De Saracibar C. An apropos kinematic framework for the numerical modeling of friction stir welding. Comput Struct 2013;117:48–57.
[81] Pan WX, Li DS, Tartakovsky AM, Ahzi S, Khraisheh M, Khaleel M. A new smoothed particle hydrodynamics non-Newtonian model for friction stir welding: process modeling and simulation of microstructure evolution in a magnesium alloy. Int J Plast 2013;48:189–204.
[82] Cho JH, Boyce DE, Dawson PR. Modelling of strain hardening during friction stir welding of stainless steel. Model Simul Mater Sci Eng 2007;15:469–86.
[83] Cho JH, Dawson PR. Investigation on texture evolution during friction stir welding of stainless steel. Metall Mater Trans A 2006;37:1147–64.

[84] Ma NS, Kunugi A, Hirashima T, Okubo K, Kamioka M. Fem simulation for friction spot joining process. Weld Int 2009;23:9–14.
[85] Zhang Z, Chen JT. Computational investigations on reliable finite element-based thermo-mechanical coupled simulations of friction stir welding. Int J Adv Manuf Technol 2012;60:959–75.
[86] Assidi M, Fourment L, Guerdoux S, Nelson T. Friction model for friction stir welding process simulation: calibrations from welding experiments. Int J Mach Tools Manuf 2010;50:143–55.
[87] Terreros I, Iordanoff I, Charles JL, Coupard D, Tcherniaieff S. Discrete element method, a tool to investigate complex thermo mechanical behaviour: application to friction stir welding. Int J Mater Form 2009;2:573–6.
[88] Moraitis GA, Labeas GN. Investigation of friction stir welding process with emphasis on calculation of heat generated due to material stirring. Sci Technol Weld Join 2010;15:177–84.
[89] Hattel JH, Nielsen KL, Tutum CC. The effect of post-welding conditions in friction stir welds: from weld simulation to ductile failure. Eur J Mech, A/Solid 2012;33:67–74.
[90] Hattel JH, Schmidt HNB, Tutum C. Thermomechanical modelling of friction stir welding. In: ASM proceedings of the international conference: trends in welding research; 2009. p. 1–10.
[91] Boyce DE, Dawson PR, Sidle B, Gnäupel-Herold T. A multiscale methodology for deformation modeling applied to friction stir welded steel. Comput Mater Sci 2006;38:158–75.
[92] D'Urso G, Longo M, Giardini C, Ceretti E. Quality analysis of friction stir welded butt joints by means of experiments and simulations. Key Eng Mater 2012;504–506:759–64.
[93] D'Urso G, Longo M, Giardini C. Microstructure and mechanical properties of Friction Stir Welded AA6060-T6 tubes. Key Eng Mater 2013;554–557:977–84.
[94] D'Urso G, Longo M, Giardini C. Friction Stir Spot Welding (FSSW) of aluminum sheets: experimental and simulative analysis. Key Eng Mater 2013;549:477–83.
[95] Cho J, Kim HW, Kang SB. Overview of modeling strength evolution during friction stir welding. Mater Mater Sci Forum 2008;575–578:805–10.
[96] Buffa G, Fratini L. Towards tool path numerical simulation in modified friction stir spot welding processes. Adv Mater Res 2010;83–86:1220–7.
[97] Leitao C, Zhang BK, Padmanabhan R, Rodrigues DM. Influence of weld geometry and mismatch on formability of aluminium tailor welded blanks: numerical and experimental analysis. Sci Technol Weld Join 2011;16:662–8.
[98] Schmidt H, Hattel J. A local model for the thermomechanical conditions in friction stir welding. Model Simul Mater Sci Eng 2005;13:77–93.
[99] Alfaro I, Fratini L, Cueto E, Chinesta F. Numerical simulation of friction stir welding by natural element methods. Int J Mater Form 2008;1:1079–82.
[100] Grujicic M, Pandurangan B, Yen CF, Cheeseman BA. Modifications in the AA5083 Johnson–Cook material model for use in friction stir welding computational analyses. J Mater Eng Perform 2012;21:2207–17.
[101] Chenot JL, Massoni E. Finite element modelling and control of new metal forming processes. Int J Mach Tools Manuf 2006;46:1194–200.
[102] Zaeh MF, Schober A. Approach for modelling process effects during friction stir welding of composite extruded profiles. Adv Mater Res 2008;43:105–10.
[103] Van Der Stelt AA, Bor TC, Geijselaers HJM, Akkerman R, Huétink J. Free surface modeling of contacting solid metal flows employing the ALE formulation. Key Eng Mater 2012;504–506:431–6.
[104] Butan D, Monaghan J. Thermomechanical modelling friction stir welding aluminium 2024-T3. Int J Comput Mater Sci Surf Eng 2009;2:63–72.
[105] Yoshikawa G, Miyasaka F, Hirata Y, Katayama Y, Fuse T. Development of numerical simulation model for FSW employing particle method. Sci Technol Weld Join 2012;17:225–63.
[106] Zhao YH, Lin SB, He ZQ, Wu L. Numerical simulation of 2014 aluminum alloy friction stir welding process. Chin J Mech Eng 2006;42:92–7 [in Chinese].
[107] Zhang Z, Zhang HW. Effect of contact model on numerical simulation of friction stir welding. Acta Metall Sinica 2008;44:85–90 [in Chinese].
[108] Ferro P, Bonollo F. A semianalytical thermal model for fiction stir welding. Metall Mater Trans A 2010;41:440–9.
[109] Santos T, Vilaça P, Quintino L, Dos Santos J. Computational tools for modelling FSW and an improved tool for NDT. Weld World 2009;53:R99–R108.
[110] Assidi M, Fourment L. Accurate 3D Friction Stir Welding simulation tool based on friction model calibration. Int J Mater Form 2009;2:327–30.
[111] Zhou X, Pan W, MacKenzie D. Identifying friction stir welding process parameters through coupled numerical and experimental analysis. Int J Pressure Vessels Piping 2013;108–109:2–6.
[112] Perivilli S, Peddieson J, Cui J. Friction stir welding heat transfer: quasisteady modeling and its validation. J Manuf Sci Eng, Trans ASME 2009;131:0110071–78.
[113] Yan DY, Shi QY, Wu AP, Juergen S. A high-efficiency welding simulation method based on welding temperature. Trans Chin Weld Inst 2009;30:77–80 [in Chinese].
[114] Rai R, De A, Bhadeshia HKDH, DebRoy T. Review: friction stir welding tools. Sci Technol Weld Join 2011;16:325–42.
[115] Buffa G, Fratini L, Shivpuri R. Finite element studies on friction stir welding processes of tailored blanks. Comput Struct 2008;86:181–9.
[116] Arora A, De A, Debroy T. Toward optimum friction stir welding tool shoulder diameter. Scr Mater 2011;64:9–12.
[117] Mehta M, Arora A, De A, Debroy T. Tool geometry for friction stir welding – optimum shoulder diameter. Metall Mater Trans A 2011;42:2716–22.
[118] Biswas P, Mandal NR. Effect of tool geometries on thermal history of FSW of AA1100. Weld J 2011;90:129s–35s.
[119] Li H, MacKenzie D, Hamilton R. Parametric finite-element studies on the effect of tool shape in friction stir welding. Proc Inst Mech Eng Part B 2010;224:1161–73.
[120] Buffa G, Campanile G, Fratini L, Prisco A. Friction stir welding of lap joints: influence of process parameters on the metallurgical and mechanical properties. Mater Sci Eng A 2009;519:19–26.

[121] Buffa G, Forcellese A, Fratini L, Simoncini M. Experimental and numerical analysis on FSWed magnesium alloy thin sheets obtained using "pin" and "pinless" tool. Key Eng Mater 2012;504–506:747–52.
[122] Bruni C, Buffa G, D'Apolito L, Forcellese A, Fratini L. Tool geometry in friction stir welding of magnesium alloy sheets. Key Eng Mater 2009;410–411:555–62.
[123] Bruni C, Buffa G, Fratini L, Simoncini M. Friction stir welding of magnesium alloys under different process parameters. Mater Sci Forum 2010;638–642:3954–9.
[124] Manvatkar VD, Arora A, De A, DebRoy T. Neural network models of peak temperature, torque, traverse force, bending stress and maximum shear stress during friction stir welding. Sci Technol Weld Join 2012;17:460–6.
[125] Debroy T, De A, Bhadeshia HKDH, Manvatkar VD, Arora A. Tool durability maps for friction stir welding of an aluminium alloy. Proc Roy Soc A 2012;468:3552–70.
[126] Zhang Z, Liu YL, Chen JT. Effect of shoulder size on the temperature rise and the material deformation in friction stir welding. Int J Adv Manuf Technol 2009;45:889–95.
[127] Zhang Z, Liu HJ. Effect of pin shapes on material deformation and temperature field in friction stir welding. Trans Chin Weld Inst 2011;32:5–8 [in Chinese].
[128] Mukherjee S, Ghosh AK. Simulation of a new solid state joining process using single-shoulder two-pin tool. J Manuf Sci Eng, Trans ASME 2008;130:0410151–59.
[129] Lacki P, Kucharczyk Z, Sliwa RE, Gaaczynski T. Effect of tool shape on temperature field in friction stir spot welding. Arch Metall Mater 2013;58:595–9.
[130] Chang HT, Wang CJ, Cheng CP. Friction stir lap welded low carbon steel and ductile iron: microstructure and mechanical properties. Sci Technol Weld Joint 2013;18:688–96.
[131] Cox CD, Gibson BT, Strauss AM, Cook GE. The application of a rotating anvil in friction stir spot welding: a numerical and experimental study. In: ASM proceedings of the international conference: trends in welding research; 2013. p. 941–96.
[132] Zhang LG, Ji SD, Luan GH, Dong CL, Fu L. Friction stir welding of al alloy thin plate by rotational tool without pin. J Mater Sci Technol 2011;27:647–52.
[133] Ji SD, Zhang LG, Jin YY, Luan GH. Numerical simulation of rotational tool shoulder shape's effect on transfer behavior of welding plastic metal in friction stir welding. Mater Sci Forum 2012;704–705:1167–74.
[134] Fourment L, Guerdoux S. 3D numerical simulation of the three stages of Friction Stir Welding based on friction parameters calibration. Int J Mater Form 2008;1:1287–90.
[135] Buffa G, Hua J, Shivpuri R, Fratini L. Design of the friction stir welding tool using the continuum based FEM model. Mater Sci Eng A 2006;419:381–8.
[136] Zhang Z, Zhang HW. Effect of process parameters on quality of friction stir welds. Chin J Mater Res 2006;20:504–12 [in Chinese].
[137] Ganesh P, Senthil Kumar VS. Numerical analysis on superplastic forming of friction stir welded AA6061-T6 alloy sheet. Adv Mater Res 2012;488-489:753–8.
[138] Li WY, Yu M, Li JL, Gao DL. Explicit finite element analysis of the plunge stage of tool in friction stir welding. Mater Sci Forum 2009;620–622:233–6.
[139] Jabbari M. Elucidating of rotation speed in friction stir welding of pure copper: thermal modeling. Comput Mater Sci 2014;81:296–302.
[140] Michopoulos JG, Lambrakos S, Iliopoulos A. Friction stir welding process parameter effects on workpiece warpage due to residual strains. In: Proc ASME des eng technol conf; 2011; v2, Parts A and B. p. 233–40.
[141] Alimoradi A, Loh-Mousavi M, Salekrostam R. Finite element simulation of friction stir welding process of non similar aluminum–copper sheets. Defect Diffus Forum 2011;312–315:953–8.
[142] Zhang Z, Zhang HW. Numerical studies on controlling of process parameters in friction stir welding. J Mater Process Technol 2009;209:241–70.
[143] Zhang H, Huang JH, Lin SB, Wu L, Zhang JG. Temperature simulation of the preheating period in friction stir welding based on the finite element method. Proc Inst Mech Eng Part B 2006;220:1097–106.
[144] Zhao X, Kalya P, Landers RG, Krishnamurthy K. Empirical dynamic modeling of friction stir welding processes. J Manuf Sci Eng, Trans ASME 2009;131:0210011–19.
[145] Buffa G, Campanella D, Fratini L. On tool stirring action in friction stir welding of work hardenable aluminium alloys. Sci Technol Weld Join 2013;18:161–8.
[146] Carlone P, Palazzo GS. A numerical and experimental analysis of microstructural aspects in AA2024-T3 friction stir welding. Key Eng Mater 2013;554–557:1022–30.
[147] Rajamanickam N, Balusamy V, Madhusudhanna Reddy G, Natarajan K. Effect of process parameters on thermal history and mechanical properties of friction stir welds. Mater Des 2009;30:2726–31.
[148] Gök K, Aydin M. Investigations of friction stir welding process using finite element method. Int J Adv Manuf Technol 2013;68:775–80.
[149] Zhang Z, Wan ZY. Predictions of tool forces in friction stir welding of AZ91 magnesium alloy. Sci Technol Weld Join 2012;17:495–500.
[150] Veljic DM, Rakin MP, Perovic MM. Heat generation during plunge stage in friction stir welding. Thermal Sci 2013;17:489–96.
[151] Dubourg L, Doran P, Larose S, Gharghouri MA, Jahazi M. Prediction and measurements of thermal residual stresses in AA2024-T3 friction stir welds as a function of welding parameters. Mater Sci Forum 2010;638–642:1215–20.
[152] Roy BS, Saha SC, DebBarma J. 3-D modeling & numerical simulation of Friction Stir welding process. Adv Mater Res 2012;488–489:1189–93.
[153] Zhang JL, Li BZ, Zhang XC, Wang QX. A friction stir welding platform of thin plates. Adv Mater Res 2013;628:206–10.
[154] Al-Badour F, Merah N, Shuaib AN, Bazoune A. Experimental and finite element modeling of friction stir seal welding of tube–tubesheet joint. Adv Mater Res 2012;445:771–6.
[155] Zhao Y, Wu AP, Ren JL, Sato YS, Kokawa H, Miyake M, et al. Temperature and force response characteristics of friction stir welding on invar 36 alloy. Sci Technol Weld Join 2013;18:232–8.

[156] Carlone P, Palazzo GS. Influence of process parameters on microstructure and mechanical properties in AA2024-T3 friction stir welding. Metall Microstruct Anal 2013;2:213–22.
[157] Li WY, Zhang ZH, Li JL, Chao YJ. Numerical analysis of joint temperature evolution during friction stir welding based on sticking contact. J Mater Eng Perform 2012;21:1849–56.
[158] Zhang ZH, Li WY, Han J, Li JL. Numerical analysis of joint temperature evolution during friction stir welding based on plastic deformation heat. Chin Weld (Engl Ed) 2011;20:76–80.
[159] Zhang LG, Ji SD, Liu ZL, Gao SS. Effect of welding parameters on welding temperature field of friction stir welding of curved structure's overlap joint. Rev Adv Mater Sci 2013;33:175–9.
[160] Wang XJ, Lu YX, Zhang ZK, Liang JL, Guo TK. The temperature field test and numerical simulation of steel's friction stir welding process. Adv Mater Res 2013;706–708:370–4.
[161] Yan DY, Shi QY, Wu AP. Numerical analysis on the functions of stir tool's mechanical loads during friction stir welding. Acta Metall Sinica 2009;45:994–9 [in Chinese].
[162] Yan DY, Shi QY, Wu AP, Silvanus J, Liu Y, Zhang ZL. Numerical analysis on the residual distortion of al alloy sheet after friction stir welding. Acta Metall Sinica 2009;45:183–8 [in Chinese].
[163] Su P, Gerlich A, North TH, Bendzsak GJ. Intermixing in dissimilar friction stir spot welds. Metall Mater Trans A 2007;38:584–95.
[164] Su P, Gerlich A, North TH, Bendzsak GJ. Material flow during friction stir spot welding. Sci Technol Weld Join 2006;11:61–71.
[165] García-Arribas A, Feutchwanger J, Fernández E, Penalva M, Arregi B. Reluctance sensor for penetration depth control in friction stir welding. Sensor Lett 2013;11:62–5.
[166] Mandal S, Rice JM, Elmustafa AA. A numerical study of the plunge stage in friction stir welding using abaqus. In: Proc frict stir weld process IV – TMS 2007 annual meet exhibit; 2007. p. 127–33.
[167] Mandal S, Rice JM, Elmustafa AA. Experimental and numerical investigation of the plunge stage in friction stir welding. J Mater Process Technol 2008;203:411–9.
[168] Gan W, Li ZT, Khurana S. Tool mushrooming in friction stir welding of L80 steel. In: Proc frict stir weld process IV – TMS 2007 annual meet exhibit; 2007. p. 279–83.
[169] Rice JM, Mandal S, Elmustafa AA. Investigation of a donor material in friction stir welding. In: Proc frict stir weld process V – TMS 2009 annual meet exhibit; 2009. p. 337–42.
[170] Rice JM, Mandal S, Elmustafa AA. Microstructural investigation of donor material experiments in friction stir welding. Int J Mater Form; in press.
[171] Arora A, Mehta M, De A, Debroy T. Load bearing capacity of tool pin during friction stir welding. Int J Adv Manuf Technol 2012;61:911–20.
[172] Buffa G, Fratini L, Micari F, Settineri L. On the choice of tool material in friction stir welding of titanium alloys. Trans North Am Manuf Res Inst SME 2012;40:785–94.
[173] Scutelnicu E, Birsan D, Cojocaru R. Research on friction stir welding and tungsten inert gas assisted friction stir welding of copper. In: Proc 4th int conf manuf eng, quality product syst, MEQAPS'11; 2011. p. 97–102.
[174] Able N, Pfefferkorn F. Laser-assisted friction stir lap welding of aluminum. In: Proc ASME summer heat transfer conf, vol. 4; 2005. p. 425–9.
[175] Mandal S, Rice J, Hou G, Williamson KM, Elmustafa AA. Modeling and simulation of a donor material concept to reduce tool wear in friction stir welding of high-strength materials. J Mater Eng Perform 2013;22:1558–64.
[176] He X. Thermo-mechanical modelling of friction stir welding process. Adv Mater Res 2013;774–776:1155–9.
[177] Nandan R, Prabu B, De A, Debroy T. Improving reliability of heat transfer and materials flow calculations during friction stir welding of dissimilar aluminum alloys. Weld J (Miami, Fla) 2007;86:313–22.
[178] Nandan R, Lienert TJ, DebRoy T. Toward reliable calculations of heat and plastic flow during friction stir welding of Ti–6Al–4V alloy. Int J Mater Res 2008;99:434–44.
[179] Seidel TU, Reynolds AP. Visualization of the material flow in AA2195 friction-stir welds using a marker insert technique. Metall Mater Trans A 2001;32:2879–84.
[180] Schneider JR, Beshears R, Nunes Jr AC. Interfacial sticking and slipping in the friction stir welding process. Mater Sci Eng A 2006;435-436:297–304.
[181] Guerra M, Schmidt C, McClure JC, Murr LE, Nunes AC. Flow patterns during friction stir welding. Mater Charact 2002;49:95–101.
[182] Tutunchilar S, Haghpanahi M, Besharati Givi MK, Asadi P, Bahemmat P. Simulation of material flow in friction stir processing of a cast Al–Si alloy. Mater Des 2012;40:415–26.
[183] Colegrove PA. Modelling and development of the Trivex friction stir welding tool. Welding World 2004;48:10–26.
[184] Hyoe T, Colegrove PA, Shercliff HR. Thermal and microstructure modelling in thick plate aluminium alloy 7075 friction stir welds. In: TMS annual meeting; 2003. p. 33–42.
[185] Colegrove PA, Shercliff HR. Two-dimensional CFD modelling of flow round profiled FSW tooling. Sci Technol Weld Join 2004;9:483–92.
[186] Colegrove PA, Shercliff HR. 3-Dimensional CFD modelling of flow round a threaded friction stir welding tool profile. J Mater Process Technol 2005;169:320–7.
[187] Colegrove PA, Shercliff HR. Experimental and numerical analysis of aluminium alloy 7075-T7351 friction stir welds. Sci Technol Weld Join 2003;8:360–8.
[188] Idagawa HS, Torres EA, Ramirez AJ. CFD modeling of dissimilar aluminum-steel friction stir welds. In: ASM proceedings of the international conference: trends in welding research; 2013. p. 604–10.
[189] Zhang HW, Zhang Z, Chen JT. The finite element simulation of the friction stir welding process. Mater Sci Eng A 2005;403:340–8.
[190] Zhang HW, Zhang Z, Chen JT. Finite element analysis of friction stir welding process. Trans Chin Weld Inst 2005;26:13–8 [in Chinese].
[191] Wang GX, Zhu LL, Zhang Z. Modeling of material flow in friction stir welding process. Chin Weld (Engl Ed) 2007;16:63–70.

[192] Santiago D, Urquiza S, Lombera G, de Vedia L. 3D Modeling of material flow and temperature in friction stir welding. Soldagem e Inspecao 2009;14:248–56 [in Portuguese].
[193] Song M, Kovacevic R. Thermal modeling of friction stir welding in a moving coordinate system and its validation. Int J Mach Tool Manuf 2003;43:605–15.
[194] Song M, Kovacevic R. Numerical and experimental study of the heat transfer process in friction stir welding. Proc Inst Mech Eng Part B 2003;217:73–85.
[195] Song M, Kovacevic R. Heat transfer modelling for both workpiece and tool in the friction stir welding process: a coupled model. Proc Inst Mech Eng Part B 2004;218:17–33.
[196] Zhang HW, Zhang Z, Chen JT. 3D modeling of material flow in friction stir welding under different process parameters. J Mater Process Technol 2007;183:62–70.
[197] Zhang Z, Chen JT, Zhang HW. Modeling of the friction stir process under different pressures on the shoulder. J Aeronaut Mater 2005;25:33–7 [in Chinese].
[198] Zhang HW, Zhang Z, Chen JT. Analysis of 3D flow in friction stir welding process. China Mech Eng 2006;17:719–23 [in Chinese].
[199] Zhang Z, Liu YL, Chen JT, Zhang HW. Material flow patterns in friction stir welding. Trans China Weld Inst 2007;28:17–21 [in Chinese].
[200] Cho JH, Dawson PR. Modeling texture evolution during friction stir welding of stainless steel with comparison to experiments. J Eng Mater Technol, Trans ASME 2008;130:0110071–01100712.
[201] Cho JH, Boyce DE, Dawson PR. Modeling strain hardening and texture evolution in friction stir welding of stainless steel. Mater Sci Eng A 2005;398:146–63.
[202] Zhang Z, Zhang HW. A fully coupled thermo-mechanical model of friction stir welding. Int J Adv Manuf Technol 2008;37:279–93.
[203] Zhang Z, Liu YL. Effect of preheating time on friction stir welding. Chin J Mech Eng 2009;45:13–8 [in Chinese].
[204] Zhang Z, Chen JT, Zhang ZW, Zhang HW. Coupled thermo-mechanical model based comparison of friction stir welding processes of AA2024-T3 in different thicknesses. J Mater Sci 2011;46:5815–21.
[205] Zhang HW, Zhang Z, Chen JT. Effect of angular velocity of the pin on material flow during friction stir welding. Acta Metall Sinica 2005;41:853–9 [in Chinese].
[206] Zhang HW, Zhang Z, Chen JT. Effect of translational velocity on material flow in friction stir welding. Acta Aeronaut Astronaut Sinica 2006;27:949–56 [in Chinese].
[207] Zhang Z, Zhang HW. Simulation of 3D material flow in friction stir welding of AA6061-T6. Chin Weld (Engl Ed) 2008;17:57–63.
[208] Shimoda Y, Tsubaki M, Yasui T, Fukumoto M. Experimental and numerical studies of material flow during welding by friction stirring. Quart J Jpn Weld Soc 2011;29:114s–8s.
[209] Zhang Z, Zhang HW. Material behavior analysis in joining non straight line weld by using friction stir welding. J Plast Eng 2006;13:108–14 [in Chinese].
[210] Fratini L, Buffa G, Micari F, Shivpuri R. On the material flow in FSW of T-joints: influence of geometrical and tecnological parameters. Int J Adv Manuf Technol 2009;44:570–8.
[211] Guo ZH, Zhao GY, Ke LM, Xing L, Zhu SF. Finite element analysis of materials flow behavior in friction stir welding of 7075 aluminum alloy plate. Appl Mech Mater 2012;117–119:1621–4.
[212] Gao Z, Krumphals F, Sherstnev P, Enzinger N, Niu JT, Sommitsch C. Analysis of plastic flow during friction stir spot welding using finite element modeling. Key Eng Mater 2012;504–506:419–24.
[213] Hamilton C, Kopyscianski M, Senkov O, Dymek S. A coupled thermal/material flow model of friction stir welding applied to Sc-modified aluminum alloys. Metall Mater Trans A 2013;44:1730–40.
[214] Grujicic M, Arakere G, Pandurangan B, Ochterbeck JM, Yen CF, Cheeseman BA, et al. Computational analysis of material flow during friction stir welding of AA5059 aluminum alloys. J Mater Eng Perform 2012;21:1824–40.
[215] Ji SD, Shi QY, Zhang LG, Zou AL, Gao SS, Zan LV. Numerical simulation of material flow behavior of friction stir welding influenced by rotational tool geometry. Comput Mater Sci 2012;63:218–26.
[216] Ji SD, Zou AL, Yue YM, Luan GH, Jin YY, Li F. Numerical simulation of effect of rotational tool with screw on material flow behavior of friction stir welding of Ti6Al4V alloy. Acta Metall Sinica (Engl Lett) 2012;25:365–73.
[217] Wang H, Colegrove PA, Dos Santos JF. Numerical investigation of the tool contact condition during friction stir welding of aerospace aluminium alloy. Comput Mater Sci 2013;71:101–8.
[218] Kim D, Badarinarayan H, Ryu I, Kim J, Kim C, Okamoto K, et al. Numerical simulation of friction stir welding process. Int J Mater Form 2009;2:383–6.
[219] Kim D, Chung K, Badarinarayan H. An experimental and numerical approach to evaluate the effect of welding conditions on temperature during friction stir spot welding. In: ASM proceedings of the international conference: trends in welding research; 2009. p. 60–6.
[220] Su H, Wu C, Chen M. Analysis of material flow and heat transfer in friction stir welding of aluminium alloys. China Weld (Engl Ed) 2013;22:6–10.
[221] Nandan R, Roy GG, Lienert TJ, Debroy T. Three-dimensional heat and material flow during friction stir welding of mild steel. Acta Mater 2007;55:883–95.
[222] Zhang Z, Chen JT. The simulation of material behaviors in friction stir welding process by using rate-dependent constitutive model. J Mater Sci 2008;43:222–32.
[223] Shercliff HR, Russell MJ, Taylor A, Dickerson TL. Microstructural modelling in friction stir welding of 2000 series aluminium alloys. Mecanique et Ind 2005;6:25–35.
[224] Frigaard Ø, Grong Ø, Midling OT. A process model for friction stir welding of age hardening aluminum alloys. Metall Mater Trans A 2001;32:1189–200.
[225] Schmidt H, Hattel J. Heat source models in simulation of heat flow in friction stir welding International. J Offshore Polar Eng 2004;14:296–304.
[226] Schmidt H, Hattel J. Modelling heat flow around tool probe in friction stir welding. Sci Technol Weld Join 2005;10:176–86.

[227] Long T, Tang W, Reynolds AP. Process response parameter relationships in aluminium alloy friction stir welds. Sci Technol Weld Join 2007;12:311–7.
[228] Khandkar MZH, Khan JA. Thermal modeling of overlap friction stir welding for Al-alloys. J Mater Process Manuf Sci 2001;10:91–105.
[229] Ulysse P. Three-dimensional modeling of the friction stir-welding process. Int J Mach Tools Manuf 2002;42:1549–57.
[230] Kiral BG, Tabanoglu M, Serindag HT. Finite element modeling of friction stir welding in aluminum alloys joint. Math Comput Appl 2013;18:122–31.
[231] Chao YJ, Qi X, Tang W. Heat transfer in friction stir welding – experimental and numerical studies. J Manuf Sci Eng, Trans ASME 2003;125:138–45.
[232] Chao YJ, Liu S, Chien CH. Friction stir welding of AL 6061-T6 thick plates: Part II – numerical modeling of the thermal and heat transfer phenomena. J Chin Inst Eng 2008;31:769–79.
[233] Yin PF, Zhang R, Xiong JT, Zhao K, Li JL. An effective numerical simulation of temperature distribution of friction stir welding in quasi-steady-state. J Northwestern Polytech Univ 2012;30:622–7 [in Chinese].
[234] Larsen A, Stolpe M, Hattel JH. Estimating the workpiece-backingplate heat transfer coefficient in friction stir welding. Eng Comput (Swansea, Wales) 2012;29:65–82.
[235] Prasanna P, Rao BS, Rao GKM. Finite element modeling for maximum temperature in friction stir welding and its validation. Int J Adv Manuf Technol 2010;51:925–33.
[236] Shi QY, Wang XB, Kang X, Sun YJ. Temperature fields during friction stir welding. J Tsinghua Univ 2010;50:980–3 [in Chinese].
[237] Yan DY, Shi QY, Wu AP, Juergen S, Zhang ZL. Developmental thermal-mechanical coupled analysis model for friction stir welding. J Mech Eng 2010;46:106–12 [in Chinese].
[238] Muci-Küchler KH, Kalagara S, Arbegast WJ. Simulation of a refill friction stir spot welding process using a fully coupled thermo-mechanical FEM model. J Manuf Sci Eng, Trans ASME 2010;132:0145031–35.
[239] Xu WF, Liu JH, Zhu HQ. Numerical simulation of thermal field of friction stir welded 2219 aluminum alloy thick plate. Trans Chin Weld Inst 2010;31:63–6 [in Chinese].
[240] Buffa G, Fratini L. Friction stir welding of steels: process design through continuum based FEM model. Sci Technol Weld Join 2009;14:239–46.
[241] Xu JD, Vaze SP, Ritter RJ, Colligan KJ, Pickens JR. Experimental and numerical study of thermal process in friction stir welding. In: ASM conf proc: join adv special mater; 2004. p. 10–9.
[242] Dong XW, Li XF, Zuo DW, Wang JS, Dong CL, Li G. Simulation of the optimization of aluminum alloy friction stir welding sequence based on coupled thermo-mechanical model. J Funct Mater 2012;43:767–70 [in Chinese].
[243] Zhu WF, Xu C. Numerical simulation of friction stir welding for aluminum alloy railway carriage manufacturing. Trans Chin Weld Inst 2008;29:45–9 [in Chinese].
[244] Awang M, Mucino VH. Energy generation during friction stir spot welding (FSSW) of Al 6061-T6 plates. Mater Manuf Process 2010;25:167–74.
[245] Lu SX, Yan JC, Li WG, Yang SQ. Simulation on temperature field of friction stir welded joints of 2024-T4 Al. Acta Metall Sinica (Engl Lett) 2005;18:552–6.
[246] Kim DG, Badarinarayan H, Kim JH, Kim CM, Okamoto K, Wagoner RH, et al. Numerical simulation of friction stir butt welding process for AA5083-H18 sheets. Eur J Mech, A/Solid 2010;29:204–15.
[247] Bie J, Liu YL, Zhang Z. Effect of processing parameters on temperature distributions in friction stir welding. J Plast Eng 2008;15:212–7 [in Chinese].
[248] Rajesh SR, Bang HS, Kim HJ, Bang HS. Analysis of complex heat flow phenomena with friction stir welding using 3D-analytical model. Adv Mater Res 2007;15–17:339–44.
[249] Jiang ML, Wang M, Chen D. The overview of modeling the thermo-mechanical three dimensional friction stir welding process. Adv Mater Res 2011;189–193:2129–33.
[250] Wang L, Zhu JJ, Yin KY, You H. Temperature numerical simulation of friction stir welding process of radar cooling board. Appl Mech Mater 2012;155–156:1180–3.
[251] Cox C, Lammlein D, Strauss A, Cook G. Modeling the control of an elevated tool temperature and the effects on axial force during friction stir welding. Mater Manuf Process 2010;25:1278–82.
[252] Zhang Z, Bie J. Fully coupled thermo-mechanical model for numerical simulation of friction stir welding process. Chin Mech Eng 2008;19:1240–5 [in Chinese].
[253] Rangel Pacheco M, Paul Kabche J, Thesi I, Nunes Diesel F. Temperature distribution analysis in plates joined by Friction Stir Welding. In: ASME int mech eng congress exposit, proceedings, vol. 11; 2010. p. 163–9.
[254] Rangel Pacheco M, Calas Lopes Pacheco PM. Analysis of the temperature distribution in friction stir welding using the finite element method. Mater Sci Forum 2013;758:11–9.
[255] Zhang ZH, Li WY, Li JL, Chao YJ. Numerical analysis of effect of backplate diffusivity on the transient temperature in friction stir welding. J Mater Eng Perform 2013;22:2446–50.
[256] Kastelic S, Tusek J, Kobecar D, Medved J, Mrvar P. AA413.0 and AA1050 joined with friction stir welding. Materiali Tehnologije 2013;47:195–8.
[257] McNelley TR, Swaminathan S, Su JQ. Recrystallization mechanisms during friction stir welding/processing of aluminum alloys. Scr Mater 2008;58:349–54.
[258] Murr LE. A review of FSW research on dissimilar metal and alloy systems. J Mater Eng Perform 2010;19:1071–89.
[259] Imam M, Biswas K, Racherla V. On use of weld zone temperatures for online monitoring of weld quality in friction stir welding of naturally aged aluminium alloys. Mater Des 2013;52:730–9.
[260] Imam M, Biswas K, Racherla V. Effect of weld morphology on mechanical response and failure of friction stir welds in a naturally aged aluminium alloy. Mater Des 2013;44:23–34.
[261] Fratini L, Buffa G. Metallurgical phenomena modeling in friction stir welding of aluminum alloys: analytical versus neural network based approaches. J Eng Mater Technol, Trans ASME 2008;130:0310011–16.
[262] Fratini L, Buffa G. Continuous dynamic recrystallization phenomena modeling in friction stir welding of aluminum alloys: a neural-network-based approach. Proc Inst Mech Eng Part B 2007;221:857–64.

[263] Buffa G, Fratini L, Micari F. A neural network based approach for the design of FSW processes. Key Eng Mater 2009;410–411:413–20.
[264] Fratini L, Buffa G, Palmeri D. Using a neural network for predicting the average grain size in friction stir welding processes. Comput Struct 2009;87:1166–74.
[265] Saluja RS, Ganesh Narayanan R, Das S. Cellular automata finite element (CAFE) model to predict the forming of friction stir welded blanks. Comput Mater Sci 2012;58:87–100.
[266] Patel C, Das S, Narayanan RG. CAFE modeling, neural network modeling, and experimental investigation of friction stir welding. Proc Inst Mech Eng Part C 2013;227:1164–76.
[267] Yuan SJ, Hu ZL, Wang XS. Evaluation of formability and material characteristics of aluminum alloy friction stir welded tube produced by a novel process. Mater Sci Eng A 2012;543:210–6.
[268] McWilliams BA, Yu JH, Yen CF. Numerical simulation and experimental characterization of friction stir welding on thick aluminum alloy AA2139-T8 plates. Mater Sci Eng A 2013;585:243–52.
[269] Kamp N, Sullivan A, Tomasi R, Robson JD. Modelling of heterogeneous precipitate distribution evolution during friction stir welding process. Acta Mater 2006;54:2003–14.
[270] Kamp N, Sullivan A, Tomasi R, Robson JD. Modelling heterogeneous precipitation in 7xxx aluminium alloys during complex processing. Mater Sci Forum 2006;519–521:1435–40.
[271] Fanelli P, Montanari R, Rovatti L, Ucciardello N, Vivio F, Vullo V. Microstructural characterization and modelling of Friction Stir Spot Welded joints in 6082 aluminium alloy. Metall Italiana 2011;103:43–9 [in Spanish].
[272] Yang BC, Yan JH, Sutton MA, Reynolds AP. Banded microstructure in AA2024-T351 and AA2524-T351 aluminum friction stir welds. Part I. Metallurgical studies. Mater Sci Eng A 2004;364:55–65.
[273] Xu SW, Deng XM. A study of texture patterns in friction stir welds. Acta Mater 2008;56:1326–41.
[274] Buffa G, Fratini L, Schneider M, Merklein M. Micro and macro mechanical characterization of friction stir welded Ti–6Al–4V lap joints through experiments and numerical simulation. J Mater Process Technol 2013;213:2312–22.
[275] Wang H, Colegrove PA, Mayer HM, Campbell L, Robson RD. Material constitutive behaviour and microstructure study on aluminium alloys for friction stir welding. Adv Mater Res 2010;89–91:615–20.
[276] Zhang Z, Zhang H. Effect of welding parameters on mixing of materials in nugget zone of friction stir welds. Acta Metall Sinica 2007;43:321–6 [in Chinese].
[277] Grujicic M, Arakere G, Yalavarthy HV, He T, Yen CF, Cheeseman BA. Modeling of AA5083 material-microstructure evolution during butt friction-stir welding. J Mater Eng Perform 2010;19:672–84.
[278] Eisazadeh H, Hamedi M, Rashad-S K. Numerical investigation of temperature distribution in friction stir welding. Weld World 2009;53:265–70.
[279] Zhang Z, Liu YL, Zhang HW. Effect of variation of axial load on material deformations and temperature distributions in friction stir welding. Acta Metall Sinica 2007;43:868–74 [in Chinese].
[280] Li K, Aidun D, Marzocca P. Time-varying functionally graded material thermal modeling of friction stir welding joint of dissimilar metals. In: ASM proc inter conf: trend weld res; 2009. p. 731–5.
[281] Li K, Aidun D, Marzocca P. 3-D thermo-mechanical analysis of Friction Stir Welding of dissimilar metals using functionally graded material concept. In: ASM proc inter conf: trend weld res; 2009. p. 726–30.
[282] Wu CS, Zhang WB, Shi L, Chen MA. Visualization and simulation of plastic material flow in friction stir welding of 2024 aluminium alloy plates. Trans Nonferr Met Soc Chin (Engl Ed) 2012;22:1445–51.
[283] Kalaiselvan K, Murugan N. Dry sliding wear behaviour of Friction Stir Welded aluminum (6061)-B 4C composite. Int J Microstruct Mater Propert 2013;8:239–51.
[284] Jamshidi Aval H, Serajzadeh S, Kokabi AH. Theoretical and experimental investigation into friction stir welding of AA 5086. Int J Adv Manuf Technol 2011;52:531–44.
[285] Mirjalili A, Serajzadeh S, Jamshidi Aval H, Kokabi AH. Modeling and experimental study on friction stir welding of artificially aged AA2017 plates. Mater Manuf Proc 2013;28:683–8.
[286] Chen H, Zhao YH, Zhang YK, Wu LN, Lin SB. Mechanistic study on friction stir welding of 2014 aluminium alloy. In: International astronautical federation – 58th international astronautical congress, vol. 8; 2007. p. 5400–11.
[287] Forrest D, Nguyen J, Posada M, DeLoach J, Boyce D, Cho J et al. Simulation of HSLA-65 friction stir welding. In: ASM proc inter conf: trend weld res; 2005. p. 279–86.
[288] Fratini L, Buffa G, Shivpuri R. Mechanical and metallurgical effects of in process cooling during friction stir welding of AA7075-T6 butt joints. Acta Mater 2010;58:2056–67.
[289] Simar A, Pardoen T, De Meester B. Modeling temperature histories in friction stir welding including material convection effects. In: ASM proc inter conf: trend weld res; 2005. p. 273–8.
[290] Cho HH, Hong ST, Roh JH, Choi HS, Kang SH, Steel RJ, et al. Three-dimensional numerical and experimental investigation on friction stir welding processes of ferritic stainless steel. Acta Mater 2013;61:2649–61.
[291] Nandan R, Roy GG, Debroy T. Numerical simulation of three dimensional heat transfer and plastic flow during friction stir welding. Metall Mater Trans A 2006;37:1247–59.
[292] Biagi R, Lim JY, Bart-Smith H. In-plane compression response of extruded aluminum 6061-T6 corrugated core sandwich columns. J Am Ceram Soc 2011;94:S76–84.
[293] Grujicic M, Arakere G, Pandurangan B, Hariharan A, Cheeseman BA, Yen CF, et al. Computational analysis and experimental validation of the friction-stir welding behaviour of Ti–6Al–4V. Proc Inst Mech Eng Part B 2011;225:208–23.
[294] Buffa G, Hua J, Shivpuri R, Fratini L. A continuum based fem model for friction stir welding – model development. Mater Sci Eng A 2006;419:389–96.
[295] Rajesh SR, Bang HS, Chang WS, Kim HJ, Bang HS, Oh CI, et al. Numerical determination of residual stress in friction stir weld using 3D-analytical model of stir zone. J Mater Process Technol 2007;187–188:224–6.
[296] Lewis AC, Fonda RW, Jones HN. Image-based finite element simulations of friction stir welds. In: Proc int offshore polar eng conf; 2011. p. 557–60.
[297] Simar A, Jonckheere C, Deplu K, Pardoen T, De Meester B. Comparing similar and dissimilar friction stir welds of 2017-6005A aluminum alloys. Sci Technol Weld Join 2010;15:254–9.

[298] Scialpi A, Troughton M, Andrews S, De Filippis LAC. Viblade: friction stir welding per materiali plastici. Rivista Italiana della Saldatura 2008;60:635–43 [in Italian].
[299] Zumpano G, Meo M. A new nonlinear elastic time reversal acoustic method for the identification and localisation of stress corrosion cracking in welded plate-like structures – a simulation study. Int J Solid Struct 2007;44:3666–84.
[300] Caseiro JF, Valente RAF, Andrade-Campos A, Yoon JW. On the elasto-plastic buckling of Integrally Stiffened Panels (ISP) joined by Friction Stir Welding (FSW): numerical simulation and optimization algorithms. Int J Mech Sci 2013;76:49–59.
[301] Biro AL, Chenelle BF, Lados DA. Processing, microstructure, and residual stress effects on strength and fatigue crack growth properties in friction stir welding: a review. Metall Mater Trans B 2012;43:1622–37.
[302] He X. Computational investigation of mechanical behaviour of FSW joints. Appl Mech Mater 2013;389:260–6.
[303] Buffa G, Ducato A, Fratini L. Numerical procedure for residual stresses prediction in friction stir welding. Finite Elem Anal Des 2011;47:470–6.
[304] Chen CM, Kovacevic R. Finite element modeling of friction stir welding – thermal and thermomechanical analysis. Int J Mach Tools Manuf 2003;43:1319–26.
[305] Chen C, Kovacevic R. Thermomechanical modelling and force analysis of friction stir welding by the finite element method. Proc Inst Mech Eng Part C 2004;218:509–20.
[306] Chen CM, Kovacevic R. Parametric finite element analysis of stress evolution during friction stir welding. Proc Inst Mech Eng Part B 2006;220:1359–71.
[307] McCune RW, Murphy A, Price M, Butterfield J. The influence of friction stir welding process idealization on residual stress and distortion predictions for future airframe assembly simulations. J Manuf Sci Eng, Trans ASME 2012;134:031011-1–1-9.
[308] Zhang HW, Zhang Z, Chen JT. Effect of process parameters on material flow and residual stress in friction stir welding. Chin J Mech Eng 2006;42:103–8 [in Chinese].
[309] Zhang Z, Chen JT, Zhang HW. Scale effect of pin on friction stir welding. J Mater Eng 2006;1:19–23 [in Chinese].
[310] Soundararajan V, Zekovic S, Kovacevic R. Thermo-mechanical model with adaptive boundary conditions for friction stir welding of Al 6061. Inter J Mach Tools Manuf 2005;45:1577–87.
[311] Murphy A, McCune W, Quinn D, Price M. The characterization of friction stir welding process effects on stiffened panel buckling performance. Thin-Wall Struct 2007;45:339–51.
[312] Paulo RMF, Carlone P, Valente RAF, Teixeira-Dias F, Palazzo GS. Integrated design and numerical simulation of stiffened panels including friction stir welding effects. Key Eng Mater 2013;554–557:2237–42.
[313] Yan DY, Wu AP, Silvanus J, Shi QY. Predicting residual distortion of aluminum alloy stiffened sheet after friction stir welding by numerical simulation. Mater Des 2011;32:2284–91.
[314] Fratini L, Pasta S. Residual stresses in friction stir welded parts of complex geometry. Int J Adv Manuf Technol 2012;59:547–57.
[315] Liu C, Yi X. Residual stress measurement on AA6061-T6 aluminum alloy friction stir butt welds using contour method. Mater Des 2013;46:366–71.
[316] Wen SW, Colegrove PA, Williams SW, Morgan SA, Wescott A, Poad M. Rolling to control residual stress and distortion in friction stir welds. Sci Technol Weld Join 2010;15:440–7.
[317] Jin LZ, Sandström R. Numerical simulation of residual stresses for friction stir welds in copper canisters. J Manuf Process 2012;14:71–81.
[318] Richards DG, Prangnell PB, Withers PJ, Williams SW, Nagy T, Morgan S. Efficacy of active cooling for controlling residual stresses in friction stir welds. Sci Technol Weld Join 2010;15:156–65.
[319] Lévesque D, Dubourg L, Blouin A. Laser ultrasonics for defect detection and residual stress measurement of friction stir welds. Nondestruct Test Evaluat 2011;26:319–33.
[320] Carney KS, Hatamleh O, Smith J, Matrka T, Gilat A, Hill M, et al. A numerical simulation of the residual stresses in laser-peened friction stir-welded aluminum 2195 joints. Int J Struct Integrity 2011;2:62–73.
[321] Wang XJ, Li N, Zhang ZK, Li CR. FSW residual stress of aluminum alloy LY12. Trans Chin Weld Inst 2012;33:81–4 [in Chinese].
[322] Ya M, Dai FL, Xie HM, Lu J. Measurement of non-uniform residual stresses by combined moire interferometry and hole-drilling method: theory, experimental method and applications. Acta Mech Sinica 2003;19:567–74.
[323] Bastier A, Maitournam MH, Roger F, Dang Van K. Modelling of the residual state of friction stir welded plates. J Mater Process Technol 2008;200:25–37.
[324] Richards DG, Prangnell PB, Williams SW, Withers PJ. Global mechanical tensioning for the management of residual stresses in welds. Mater Sci Eng A 2008;489:351–62.
[325] Ge YZ, Sutton MA, Deng X, Reynolds AP. Limited weld residual stress measurements in fatigue crack propagation: Part I. Complete field representation through least-squares finite-element smoothing. Fatigue Fract Eng Mater Struct 2006;29:524–36.
[326] Lawrjaniec D, Abisror A, Decker C, Koçak M, Dos Santos J. Numerical simulation of friction stir welding. Mater Sci Forum 2003;426–432:2993–8.
[327] Richards DG, Prangneil PB, Withers PJ, Williams SW, Wescot A, Oliver EC. Geometry effects when controlling residual stresses in friction stir welds by mechanical tensioning. Mater Sci Forum 2006;524–525:71–6.
[328] Deplus K, Simar A, Haver WV, De Meester B. Residual stresses in aluminium alloy friction stir welds. Int J Adv Manuf Technol 2011;56:493–504.
[329] Riahi M, Nazari H. Analysis of transient temperature and residual thermal stresses in friction stir welding of aluminum alloy 6061-T6 via numerical simulation. Inter J Adv Manuf Technol 2011;55:143–52.
[330] Zaeh MF, Tekkaya AE, Langhorst M, Ruhstorfer M, Schober A, Pietzka D. Experimental and numerical investigation of the process chain from composite extrusion to friction stir welding regarding the residual stresses in composite extruded profiles. Prod Eng 2009;3:353–60.
[331] Li HK, Shi QY, Wang X, Li T, Liu Y. Residual stress and distortion of Al alloy panels welded by FSW. Trans Chin Weld Inst 2008;29:81–4 [in Chinese].

[332] Sadeghi S, Najafabadi MA, Javadi Y, Mohammadisefat M. Using ultrasonic waves and finite element method to evaluate through-thickness residual stresses distribution in the friction stir welding of aluminum plates. Mater Des 2013;52:870–80.
[333] He YL, Dawson PR, Boyce DE. Modeling damage evolution in friction stir welding process. J Eng Mater Technol, Trans ASME 2008;130:0210061–02100610.
[334] Borino G, Fratini L, Parrinello F. Mode i failure modeling of friction stir welding joints. Int J Adv Manuf Technol 2009;41:498–503.
[335] Nielsen KL. Ductile damage development in friction stir welded aluminum (AA2024) joints. Eng Fract Mech 2008;75:2795–811.
[336] Yu M, Li WY, Li JL, Chao YJ. Modelling of entire friction stir welding process by explicit finite element method. Mater Sci Technol (United Kingdom) 2012;28:812–7.
[337] Fratini L, Buffa G, Monaco LL. Improved FE model for simulation of friction stir welding of different materials. Sci Technol Weld Join 2010;15:199–207.
[338] Trimble D, Monaghan J, O'Donnell GE. Force generation during friction stir welding of AA2024-T3. CIRP Ann Manuf Technol 2012;61:9–12.
[339] Zadpoor AA, Sinke J, Benedictus R. Theoretical prediction of failure in forming of friction stir welded blanks. Int J Mater Form 2008;1:305–8.
[340] Zadpoor AA, Sinke J, Benedictus R. Finite element modeling and failure prediction of friction stir welded blanks. Mater Des 2009;30:1423–34.
[341] Nguyen NT, Kim DY, Kim HY. Assessment of the failure load for an AA6061-T6 friction stir spot welding joint. Proc Inst Mech Eng Part B 2011;225:1746–56.
[342] Van Der Veen IS, Murphy A, Benedictus R. Post-buckling failure of welded aluminium panels. Collection of technical papers – AIAA/ASME/ASCE/AHS/ASC structures, struct dyn mater conf, vol. 11; 2006. p. 8044–60.
[343] Al-Badour F, Merah N, Shuaib A, Bazoune A. Coupled Eulerian Lagrangian finite element modeling of friction stir welding processes. J Mater Process Technol 2013;213:1433–9.
[344] Rosado LS, Santos TG, Piedade M, Ramos PM, Vilaça P. New non-destructive test technique on metal inspection. In: Proc 19th IMEKO world congress, vol. 1; 2009. p. 11–6.
[345] Rosado LS, Santos TG, Piedade M, Ramos PM, Vilaça P. Advanced technique for non-destructive testing of friction stir welding of metals. Measure: J Int Measure Confed 2010;43:1021–30.
[346] Rosado LS, Santos TG, Ramos PM, Vilaça P, Piedade M. A differential planar eddy currents probe: fundamentals, modeling and experimental evaluation. NDT E Int 2012;51:85–93.
[347] Tran VX, Pan J. Analytical stress intensity factor solutions for resistance and friction stir spot welds in lap-shear specimens of different materials and thicknesses. Eng Fract Mech 2010;77:2611–39.
[348] Sagar SP, Miyasaka C, Ghosh M, Tittmann BR. NDE of friction stir welds of Al alloys using high-frequency acoustic microscopy. Nondestruct Test Eval 2012;27:375–89.
[349] Pashazadeh H, Masoumi A, Teimournezhad J. Numerical modelling for the hardness evaluation of friction stir welded copper metals. Mater Des 2013;49:913–21.
[350] Moreira PMGP, Santos T, Tavares SMO, Richter-Trummer V, Vilaça P, de Castro PMST. Mechanical and metallurgical characterization of friction stir welding joints of AA6061-T6 with AA6082-T6. Mater Des 2009;30:180–7.
[351] Grujicic M, Arakere G, Yen CF, Cheeseman BA. Computational investigation of hardness evolution during friction-stir welding of AA5083 and AA2139 aluminum alloys. J Mater Eng Perform 2011;20:1097–108.
[352] Lin BY, Yuan P, Liu JJ. Temperature distribution of aluminum alloys under friction stir welding. Adv Mater Res 2011;264–265:217–22.
[353] Woo W, Choo H, Withers PJ, Feng Z. Prediction of hardness minimum locations during natural aging in an aluminum alloy 6061-T6 friction stir weld. J Mater Sci 2009;44:6302–9.
[354] Simar A, Nielsen KL, De Meester B, Pardoen T, Tvergaard V. Strain hardening and damage in 6xxx series aluminum alloy friction stir welds. Mater Sci Forum 2009;638–642:333–8.
[355] Chang WS, Bang HS, Jung SB, Yeon YM, Kim HJ, Lee WB. Joint properties and thermal behaviors of friction stir welded age hardenable 6061Al alloy. Mater Sci Forum 2003;426–432:2953–8.
[356] Rao D, Huber K, Heerens J, dos Santos JF, Huber N. Asymmetric mechanical properties and tensile behavior prediction of aluminum alloy 5083 friction stir welding joints. Mater Sci Eng A 2013;565:44–50.
[357] Lee W, Chung K-H, Kim D, Kim J, Kim C, Okamoto K, et al. Experimental and numerical study on formability of friction stir welded TWB sheets based on hemispherical dome stretch tests. Int J Plast 2009;25:1626–54.
[358] Gallais C, Simar A, Fabregue D, Denquin A, Lapasset G, De Meester B, et al. Multiscale analysis of the strength and ductility of AA 6056 aluminum friction stir welds. Metall Mater Trans A 2007;38:964–81.
[359] Zadpoor AA, Sinke J, Benedictus R. Global and local mechanical properties and microstructure of friction stir welds with dissimilar materials and/or thicknesses. Metall Mater Trans A 2010;41:3365–78.
[360] Pirondi A. Modelling strength of cracked friction stir welded panels by means of the crack tip opening angle (CTOA). Eng Fract Mech 2010;77:2091–9.
[361] Nielsen KL, Pardoen T, Tvergaard V, De Meester B, Simar A. Modeling of plastic flow localization and damage development in friction stir welded 6005A aluminum alloy using physics based strain hardening law. Int J Solid Struct 2010;47:2359–70.
[362] Murphy A, Lynch F, Price M, Gibson A. Modified stiffened panel analysis methods for laser beam and friction stir welded aircraft panels. Proc Inst Mech Eng Part G 2006;220:267–78.
[363] Tweedy B, Sellmeyer S, Jahn A, Burford D. Static strength comparison of riveted versus friction stir welded stiffened panels. In: Collection of technical papers – AIAA/ASME/ASCE/AHS/ASC structures, struct dyn mater conf, vol. 11; 2006. p. 7959–73.
[364] Yoon JW, Bray GH, Valente RAF, Childs TER. Buckling analysis for an integrally stiffened panel structure with a friction stir weld. Thin-Wall Struct 2009;47:1608–22.

[365] Bouzaiene H, Rezgui MA, Ayadi M, Zghal A. Correlation between welding and hardening parameters of friction stir welded joints of 2017 aluminum alloy. Trans Nonferr Met Soc Chin (Engl Ed) 2012;22:1064–72.
[366] Yang FP, Sun Q. Analysis of stress concentration in weld of sheets welded by friction stir welding using finite element method. Trans Chin Weld Inst 2007;28:109–12 [in Chinese].
[367] Hu ZL, Wang XS, Yuan SJ. Plastic deformation of 2024 aluminum alloy friction stir welded tube during hydro bulging. Rare Met Mater Eng 2012;41:2113–7 [in Chinese].
[368] Shao Q, He YT, Zhang T, Wu LM. Study on stability performance of friction stir welded stiffened panel under uniaxial compress load. J Mech Eng 2012;48:64–8 [in Chinese].
[369] Genevois C, Deschamps A, Vacher P. Comparative study on local and global mechanical properties of 2024 T351, 2024 T6 and 5251 O friction stir welds. Mater Sci Eng A 2006;415:162–70.
[370] Fanelli P, Vivio F, Vullo V. Experimental and numerical characterization of Friction Stir Spot Welded joints. Eng Fract Mech 2012;81:17–25.
[371] Pirondi A, Fersini D. Simulation of ductile crack growth in thin panels using the crack tip opening angle. Eng Fract Mech 2009;76:88–100.
[372] Valente RAF, Yoon RAF, Bray GH, Childs TER. On the influence of fsw in the elastoplastic buckling load-carrying capacity of extruded integrally stiffened panels for aeronautic applications. Int J Mater Form 2010;3:1019–22.
[373] Zhou YL, Liu T, Zhang YH. Numerical simulation of tensile deformation on aluminum alloy FSW lap joints. Trans Chin Weld Inst 2009;30:57–60 [in Chinese].
[374] Staud D, Giera A, Merklein M, Geiger M. Enhanced numerical results on friction stir welded aluminium butt joints. Key Eng Mater 2007;344:759–66.
[375] Moreira PMGP, Santos T, Tavares SMO, Richter-Trummer V, Vilaça P, De Castro PMST. Mechanical characterization of friction stir welds of two dissimilar aluminium alloys of the 6xxx series. Mater Sci Forum 2008;587–588:430–4.
[376] Forcellese A, Fratini L, Gabrielli F, Simoncini M. Formability of friction stir welded AZ31 magnesium alloy sheets. Mater Sci Forum 2010;638–642:1249–54.
[377] Liu XP, Lin PR, Hofmann M, Johansson S, Wang YD. In-situ neutron diffraction studies of micromechanical behavior in a friction stir welded AA7475-T761. Metall Mater Trans A 2011;42:89–94.
[378] Edwards PD, Sanders DG, Ramulu M. Simulation of tensile behavior in friction stir welded and superplastically formed-titanium 6Al–4V alloy. J Mater Eng Perform 2010;19:510–4.
[379] Kim DY, Lee W, Kim JY, Chung KH, Kim CM, Okamoto K, et al. Macro-performance evaluation of friction stir welded automotive tailor-welded blank sheets: Part II – formability. Int J Solid Struct 2010;47:1063–81.
[380] Kim DY, Lee W, Kim JY, Kim CM, Chung KS. Formability evaluation of friction stir welded 6111-T4 sheet with respect to joining material direction. Int J Mech Sci 2010;52:612–25.
[381] Elangovan K, Balasubramanian V, Babu S. Predicting tensile strength of friction stir welded AA6061 aluminium alloy joints by a mathematical model. Mater Des 2009;30:188–93.
[382] Mun HS, Seo SI. Welding strain analysis of friction stir-welded aluminum alloy structures using inherent strain-based equivalent loads. J Mech Sci Technol 2013;27:2775–82.
[383] Serizawa H, Murakawa H, Shimazaki J. Numerical study of factors for generating inherent strain in friction stir welding. In: ASM proceedings of the international conference: trends in welding research; 2013. p. 922–9.
[384] Cavaliere P, Cabibbo M, Panella F, Squillace A. 2198 Al–Li plates joined by Friction Stir Welding: mechanical and microstructural behavior. Mater Des 2009;30:3622–31.
[385] Golestaneh AF, Ali A. Application of numerical method to investigation of fatigue crack behavior through friction stir welding. J Failure Anal Prevent 2009;9:147–58.
[386] Golestaneh AF, Ali A, Voon Wong S, Mustapha F, Zadeh M. Computational investigation of crack behavior in friction stir welding. Simulation 2009;85:45–59.
[387] Citarella RG, Carlone P, Lepore M, Palazzo GS. A FEM-DBEM investigation of the influence of process parameters on crack growth in aluminum friction stir welded butt joints. Key Eng Mater 2013;554–557:2118–26.
[388] Ma YE, Zhao ZQ, Liu BQ, Li WY. Mechanical properties and fatigue crack growth rates in friction stir welded nugget of 2198–T8 Al–Li alloy joints. Mater Sci Eng A 2013;569:41–7.
[389] Ma YE, Liu BQ, Zhao ZQ. Fatigue properties of Al–Li 2198-T8 friction stir welded integral panel. J Northwestern Polytech Univ 2013;31:98–102 [in Chinese].
[390] Ma YE, Liu BQ, Zhao ZQ. Crack paths in a friction stir-welded pad-up for fuselage applications. J Aircraft 2013;50:879–85.
[391] Barsoum Z, Khurshid M, Barsoum I. Fatigue strength evaluation of friction stir welded aluminium joints using the nominal and notch stress concepts. Mater Des 2012;41:231–8.
[392] Moreira PMGP, de Oliveira FMF, de Castro PMST. Fatigue behaviour of notched specimens of friction stir welded aluminum alloy 6063-T6. J Mater Process Technol 2008;207:283–92.
[393] Ma YE, Staron P, Fischer T, Irving PE. Size effects on residual stress and fatigue crack growth in friction stir welded 2195-T8 aluminium – Part II: modelling. Int J Fatigue 2011;33:1426–34.
[394] Cavaliere P, De Santis A, Panella F, Squillace A. Thermoelasticity and CCD analysis of crack propagation in AA6082 friction stir welded joints. Int J Fatigue 2009;31:385–92.
[395] Ahmadi SR, Hassanifard SP, Pour MM. Fatigue life prediction of friction stir spot welds based on cyclic strain range with hardness distribution and finite element analysis. Acta Mech 2012;223:829–39.
[396] Shahri MM, Sandström R, Osikowicz W. Critical distance method to estimate the fatigue life time of friction stir welded profiles. Int J Fatigue 2012;37:60–8.
[397] Shahri MM, Sandström R. Fatigue analysis of friction stir welded aluminium profile using critical distance. Int J Fatigue 2010;32:302–9.
[398] Fersini D, Pirondi A. Analysis and modelling of fatigue failure of friction stir welded aluminum alloy single-lap joints. Eng Fract Mech 2008;75:790–803.
[399] Kang H, Kari K, Getti A, Khosrovaneh AK, Su X, Zhang L et al. Fatigue predictions of various joints of magnesium alloys. In: Proc mater sci technol conf exhibit, vol. 2; 2012. p. 1322–37.

[400] Häusler SM, Horst P. Fast analytical algorithm for fatigue crack life estimations of integrally stiffened metallic panels. Key Eng Mater 2008;385–387:529–32.
[401] Tran VX, Pan J. Fatigue behavior of dissimilar spot friction welds in lap-shear and cross-tension specimens of aluminum and steel sheets. Int J Fatigue 2010;32:1167–79.
[402] Tran VX, Pan J, Pan T. Fatigue behavior of spot friction welds in lap-shear and cross-tension specimens of dissimilar aluminum sheets. Int J Fatigue 2010;32:1022–41.
[403] Sutton MA, Reynolds AP, Ge YZ, Deng X. Limited weld residual stress measurements in fatigue crack propagation: Part II. FEM-based fatigue crack propagation with complete residual stress fields. Fatigue Fract Eng Mater Struct 2006;29:537–45.
[404] Fratini L, Macaluso G, Pasta S. Residual stresses and FCP prediction in FSW through a continuous FE model. J Mater Process Technol 2009;209:5465–74.
[405] Pasta S, Reynolds AP. Residual stress effects on fatigue crack growth in a Ti–6Al–4V friction stir weld. Fatigue Fract Eng Mater Struct 2008;31:569–80.
[406] Hassanifard S, Mohammad Pour M, Rashid HA. A novel method for improving fatigue life of friction stir spot welded joints using localized plasticity. Mater Des 2014;53:962–71.
[407] Hassanifard S, Rash Ahmadi S, Mohammad Pour M. Weld arrangement effects on the fatigue behavior of multi friction stir spot welded joints. Mater Des 2013;44:291–302.
[408] Thoppul SD, Gibson RF. Mechanical characterization of spot friction stir welded joints in aluminum alloys by combined experimental/numerical approaches. Part I: micromechanical studies. Mater Charact 2009;60:1342–51.
[409] Thoppul SD, Gibson RF. Mechanical characterization of spot friction stir welded joints in aluminum alloys by combined experimental/numerical approaches. Part II: macromechanical studies. Mater Charact 2009;60:1352–60.
[410] Wadley HNG, Borvik T, Olovsson L, Wetzel JJ, Dharmasena KP, Hopperstad OS, et al. Deformation and fracture of impulsively loaded sandwich panels. J Mech Phys Solids 2013;61:674–99.
[411] Rimoli JJ, Talamini B, Wetzel JJ, Dharmasena KP, Radovitzky R, Wadley HNG. Wet-sand impulse loading of metallic plates and corrugated core sandwich panels. Int J Impact Eng 2011;38:837–48.
[412] Atharifar H, Lin DC, Kovacevic R. Numerical and experimental investigations on the loads carried by the tool during friction stir welding. J Mater Eng Perform 2009;18:339–50.